

Copyright
by
Gregory Michael Glass
2007

**Performance of Tension Lap Splices with MMFX High Strength
Reinforcing Bars**

by

Gregory Michael Glass, B.S.E.

Thesis

Presented to the Faculty of the Graduate School of

The University of Texas at Austin

in Partial Fulfillment

of the Requirements

for the Degree of

Master of Science in Engineering

The University of Texas at Austin

May 2007

**Performance of Tension Lap Splices with MMFX High Strength
Reinforcing Bars**

**Approved by
Supervising Committee:**

James O. Jirsa

John E. Breen

Acknowledgements

I would like to thank everyone who has made this research process and this thesis enjoyable, rewarding, and possible. Thank you to Dr. Jim Jirsa for his guidance and patience during the past two years. Thank you also for your trust and confidence in my work. I enjoyed working closely with you during the past two years.

Thank you to my family for the support you have always provided for me. Your encouragement in everything that I have done has allowed me to achieve my goals. Thank you for believing in me and supporting me in every decision that I have made, no matter where it has taken me.

Thank you to my fellow students at Ferguson Lab. I would have never completed this research program within two years without your help. Thank you especially to Katie Hoyt, Brian Graves, and Kristin Donnelly for your efforts on this project.

Thank you to the researchers at the University of Kansas and North Carolina State University. The data from your research greatly increased the database of results for my analyses and provided confirmation of the results found at the University of Texas.

Finally, thank you to our sponsor, MMFX Steel Corporation of America, for funding this project.

May 4, 2007

Abstract

Performance of Tension Lap Splices with MMFX High Strength Reinforcing Bars

Gregory Michael Glass, M.S.E.

The University of Texas at Austin, 2007

Supervisor: James O. Jirsa

The specialized microstructure and chemical composition of MMFX reinforcement results in a material that possesses both corrosion resistance and high tensile strength. MMFX Steel Corporation of America guarantees for its reinforcement a minimum ultimate tensile capacity of 150 ksi and a minimum yield strength of 100 ksi when measured using the 0.2% elongation method. To safely utilize the high strength of MMFX steel in design, proper anchorage of the reinforcement must be provided.

Development length equations included in the ACI 318-05 building design code and the 4th edition of the AASHTO LRFD bridge design code are based on data obtained from splice tests failing primarily at bar stresses less than their respective maximum allowable design yield strengths for tensile reinforcement of 80 ksi and 75 ksi. Limited data exists for splices failing at bar stresses greater than 75-80 ksi, and no data exists for

splices failing at bar stresses greater than 120 ksi — a stress attainable by MMFX reinforcement.

To determine the adequacy of the development length equations in the ACI 318 and AASHTO LRFD design codes and a development length equation proposed by ACI Committee 408 at high bar stresses, the University of Texas, the University of Kansas, and North Carolina State University are each testing 22 beam-splice specimens designed to fail at bar stresses between 80 ksi and 140 ksi. Test variables include bar size, concrete compressive strength, splice length, concrete cover, and amount of transverse reinforcement (confinement). The results of 45 tests completed by the researchers are reported in this thesis. Splice design recommendations are presented for bars spliced at high stress, and general design considerations are outlined for flexural members reinforced with high strength reinforcing bars.

Table of Contents

List of Tables	x
List of Figures	xi
CHAPTER 1	1
Introduction.....	1
1.1 MMFX Reinforcement.....	1
1.2 Project Scope and Objectives.....	2
CHAPTER 2	5
Bond Failure Mechanism.....	5
2.1 Bond Force Transfer	5
2.2 Governing Parameters.....	9
2.2.1 Development/Splice Length.....	9
2.2.2 Concrete Compressive Strength.....	10
2.2.3 Bar Size.....	11
2.2.4 Concrete Cover and Bar Spacing.....	11
2.2.5 Transverse Reinforcement	13
2.2.6 Reinforcing Bar Relative Rib Area.....	13
2.2.7 Bar Casting Position	14
CHAPTER 3	15
Previous Research.....	15
3.1 Testing Methods.....	15
3.1.1 Pullout Test	15
3.1.2 Beam-End Test.....	16
3.1.3 Beam-Splice Test.....	17
3.2 Descriptive Equations	18
3.2.1 Orangun, Jirsa, and Breen (1977)	18
3.2.2 Darwin, <i>et al.</i> (1996a)	20

3.2.3 Zuo and Darwin (2000).....	22
3.3 United States Design Code Equations	23
3.3.1 ACI 318-05	23
3.3.2 ACI 408R-03 Recommendations.....	25
3.3.3 AASHTO LRFD 4 th Edition	26
3.3.4 Comparison of Development Length Equations.....	28
3.4 MMFX Bond Research.....	34
CHAPTER 4	37
Experimental Program	37
4.1 Beam-Splice Tests	37
4.1.1 Test Matrix.....	37
4.1.2 Specimen Design	40
4.1.3 Specimen Fabrication and Instrumentation	43
4.1.4 Laboratory Test Setup and Testing Procedure.....	46
4.2 Reinforcement Tests	49
4.2.1 Specimen Description	49
4.2.2 Laboratory Test Setup and Testing Procedure.....	50
CHAPTER 5	52
Experimental Results	52
5.1 Reinforcement Tests	52
5.1.1 #5 Bars	52
5.1.2 #8 Bars	55
5.1.3 #11 Bars	57
5.2 Beam-Splice Tests	60
5.2.1 Tests Conducted at the University of Texas	60
5.2.2 Tests Conducted at Other Participating Research Universities ..	84
CHAPTER 6	86
Evaluation of Test Results	86
6.1 Comparison of Duplicate Tests.....	86

6.2	Performance of Development Length Equations.....	87
6.2.1	All Specimens	88
6.2.2	Splices not Confined by Transverse Reinforcement.....	89
6.2.3	Splices Confined by Transverse Reinforcement.....	91
6.3	Effect of Splice Length.....	92
6.4	Effect of Confinement.....	100
6.5	Crack Widths	108
CHAPTER 7		113
	Implementation of Results	113
7.1	Introduction to Design Considerations	113
7.2	Splice Design Recommendations	113
7.3	Requirements for Transverse Reinforcement	118
7.4	General Design Considerations.....	119
7.4.2	Ultimate Behavior.....	121
7.4.3	Deflections	124
7.4.4	Crack Widths	125
7.4.5	General Design Overview and Future Research.....	127
CHAPTER 8		129
	Conclusions.....	129
8.1	Research Summary	129
8.2	Conclusions.....	131
APPENDIX		133
	Beam-Splice Specimen Details.....	133
REFERENCES		138
VITA		141

List of Tables

Table 3-1: Distribution of test/calculated failure stress ratios for design code equations (data from ACI 408 database 10-2001).....	30
Table 3-2: Performance of ACI 318 and AASHTO LRFD design code equations within the range of allowable design stresses and concrete strengths.....	34
Table 3-3: Performance of ACI 318 and AASHTO LRFD design code equations outside the range of acceptable design stresses ($f_c' \leq 10,000$ psi).....	34
Table 4-1: Experimental test matrix (duplicate tests bolded, tests not included in original matrix italicized).....	39
Table 4-2: Beam-splice specimen design details.....	42
Table 4-3: Concrete mix proportions (per cubic yard).....	46
Table 5-1: Summary of results for #5 MMFX tension tests.....	53
Table 5-2: Summary of results for #8 MMFX tension tests.....	56
Table 5-3: Summary of results for #11 MMFX tension tests.....	59
Table 5-4: Summary of results for UT unconfined tests.....	71
Table 5-5: Summary of results for UT confined tests.....	84
Table 5-6: Summary of results for non-UT unconfined tests.....	85
Table 5-7: Summary of results for non-UT confined tests.....	85
Table 6-1: Comparison of duplicate tests.....	87
Table 6-2: Distribution of test/calculated failure stress ratios for all specimens.....	89
Table 6-3: Distribution of test/calculated failure stress ratios for unconfined specimens.....	90
Table 6-4: Distribution of test/calculated failure stress ratios for confined specimens....	92
Table 6-5: Expected increases in failure stresses over unconfined C0 specimens for C1 and C2 specimens based on ACI 408 calculated failure stress predictions – UT specimens.....	105
Table 6-6: Actual increases in failure stresses over unconfined C0 specimens for C1 and C2 splices – UT specimens.....	105
Table 6-7: Comparison of deflection increases over unconfined C0 specimens for pairs of C1 and C2 beams – UT specimens.....	107
Table 7-1: Distribution of MMFX test/calculated failure stress ratios when using the ACI 408 development length equation with $\phi = 0.82$	116
Table 7-2: Distribution of test/calculated failure stress ratios when using the ACI 408 development length equation with $\phi = 0.82$ (Data includes all bond tests in the ACI 408 database 10-2001 and the MMFX research program failing at bar stresses > 75 ksi).....	117
Table A-1: Splice details for specimens tested at the University of Texas.....	135
Table A-2: Splice details for specimens tested at North Carolina State University and the University of Kansas.....	136
Table A-3: Cross-section, reinforcement, and failure load details for specimens tested at the University of Texas.....	137

List of Figures

Figure 2-1: Bond force transfer (adapted from ACI 408).....	6
Figure 2-2: Formation of Goto cracks (adapted from ACI 408).....	7
Figure 2-3: Radial cracking due to hoop tensile stresses (adapted from ACI 408)	7
Figure 2-4: Splitting failure (adapted from ACI 408).....	8
Figure 2-5: Pullout failure (adapted from ACI 408).....	8
Figure 2-6: Types of splitting failure (adapted from Orangun, Jirsa, Breen 1977)	12
Figure 3-1: Schematic of pullout test (adapted from ACI 408).....	15
Figure 3-2: Schematic of beam-end test (adapted from ACI 408).....	17
Figure 3-3: Schematic of beam-splice test (adapted from ACI 408R-03).....	18
Figure 3-4: Definition of A_{rr} and n for different failure planes.....	20
Figure 3-5: Test vs. calculated stresses using ACI 408 equation with $\phi = 1.00$ (data from ACI 408 database 10-2001).....	31
Figure 3-6: Test vs. calculated stresses using ACI 408 equation with $\phi = 0.82$ (data from ACI 408 database 10-2001).....	32
Figure 3-7: Test vs. calculated stresses using ACI 318 equation (data from ACI 408 database 10-2001, f_s and f_c' limits not applied).....	32
Figure 3-8: Test vs. calculated stresses using AASHTO LRFD equation (data from ACI 408 database 10-2001, f_s and f_c' limits not applied).....	33
Figure 4-1: General cross-section for beam specimens (#8 and #11).....	42
Figure 4-2: General cross-section for slab specimens (#5).....	43
Figure 4-3: Elevation of test specimens and loading schematic	43
Figure 4-4: Varying levels of transverse reinforcement among a group of three specimens containing #8 bars	44
Figure 4-5: Varying splice length among a pair of specimens containing #5 bars.....	45
Figure 4-6: Confined #8 splices with strain gauges at the ends of the splices.....	45
Figure 4-7: Typical laboratory test setup for narrow splice specimens	48
Figure 4-8: Typical laboratory test setup for wide splice specimens.....	48
Figure 4-9: Typical test setup for reinforcement tension tests.....	50
Figure 5-1: Stress-strain relationship for #5 MMFX bars (End of plot indicates removal of extensometer).....	53
Figure 5-2: Comparison of MMFX and Grade 60 stress-strain behavior.....	54
Figure 5-3: 0.2% offset yield - #5 MMFX bars.....	54
Figure 5-4: #5 MMFX reinforcement specimens after testing	55
Figure 5-5: Stress-strain relationship for #8 MMFX bars (End of plot indicates removal of extensometer).....	56
Figure 5-6: 0.2% offset yield - #8 MMFX bars.....	57
Figure 5-7: #8 MMFX reinforcement specimens after testing	57
Figure 5-8: Stress-strain relationship for #11 MMFX bars (End of plot indicates removal of extensometer).....	58
Figure 5-9: 0.2% offset yield - #11 MMFX bars.....	59
Figure 5-10: #11 MMFX reinforcement specimens after testing	60
Figure 5-11: Typical bar stress-load plot for unconfined specimen (8-8-XC0-1.5).....	62

Figure 5-12: Typical load-deflection plot for unconfined specimen (8-8-XC0-1.5)	62
Figure 5-13: Cracking of typical unconfined specimen at early loading stages	63
Figure 5-14: Cracking of typical unconfined splice at onset of longitudinal splitting	64
Figure 5-15: Cracking of typical unconfined splice near failure	65
Figure 5-16: Measured crack widths for typical unconfined splice (8-8-XC0-1.5)	66
Figure 5-17: Unconfined splice at failure	67
Figure 5-18: Unconfined splice after failure.....	67
Figure 5-19: Bar strain vs. load for 5-5-OC0-1.25 highlighting initiation of failure by exterior splices (Gauges on bar 4 malfunctioned during this test)	68
Figure 5-20: 5-5-OC0-2 after failure	69
Figure 5-21: Measured end-of-splice crack widths for UT unconfined specimens	72
Figure 5-22: Comparison of cracking of unconfined and confined specimens near the failure load of the unconfined specimen	73
Figure 5-23: Effect of stirrups on arresting splitting cracks	75
Figure 5-24: Cracking at the end of typical confined splice at 80% of failure load.....	76
Figure 5-25: Formation of inclined side splitting cracks	76
Figure 5-26: 0.08 in. crack at the end of a splice in specimen 11-5-XC2-3. Applied load is 68% of failure load.	77
Figure 5-27: Increased cracking and deflections at failure for varying levels of confinement	78
Figure 5-28: Nonlinear load-deflection plot for a highly confined specimen (8-5-XC2-1.5).....	79
Figure 5-29: Comparison of measured crack widths for two confined specimens (8-8-XC1-1.5 and 8-8-XC2-1.5)	80
Figure 5-30: Load-deflection of confined specimens experiencing concrete crushing prior to splice failure	81
Figure 5-31: Ruptured #8 bar in specimen 8-5-OC2-1.5	82
Figure 5-32: Failure sequence for specimen 8-5-OC2-1.5	82
Figure 5-33: Failure sequence of specimen 8-5-OC2-1.5 demonstrated through load-deflection behavior	83
Figure 5-34: Measured end-of-splice crack widths for UT confined specimens.....	84
Figure 6-1: Distribution of test/calculated failure stress ratios for all specimens.....	89
Figure 6-2: Distribution of test/calculated failure stress ratios for unconfined specimens.....	90
Figure 6-3: Distribution of test/calculated failure stress ratios for confined specimens.....	92
Figure 6-4: Effect of l_s/d_b on ACI 408 test/calculated failure stress ratios	94
Figure 6-5: Effect of l_s/d_b on ACI 318 test/calculated failure stress ratios	94
Figure 6-6: Effect of l_s/d_b on AASHTO LRFD test/calculated failure stress ratios	95
Figure 6-7: Comparison of ACI 408 test/calculated failure stress ratios for pairs of specimens containing shorter (OC) and longer (XC) splices	96
Figure 6-8: Comparison of ACI 318 test/calculated failure stress ratios for pairs of specimens containing shorter (OC) and longer (XC) splices	96
Figure 6-9: Comparison of AASHTO LRFD test/calculated failure stress ratios for pairs of specimens containing shorter (OC) and longer (XC) splices.....	97
Figure 6-10: Effect of l_s/d_b on ACI 408 test/calculated failure stress ratios (data from ACI 408 database 10-2001).....	98

Figure 6-11: Effect of l_s/d_b on ACI 318 test/calculated failure stress ratios (data from ACI 408 database 10-2001, bar stress and concrete strength limits not applied) .	99
Figure 6-12: Effect of l_s/d_b on AASHTO test/calculated failure stress ratios (data from ACI 408 database 10-2001, bar stress and concrete strength limits not applied).....	99
Figure 6-13: Load-deflection for a group of three splices with varying levels of transverse reinforcement.....	100
Figure 6-14: Increases in failure stresses and deflections relative to unconfined splice – UT tests.....	101
Figure 6-15: Test/calculated failure stress ratios versus cover/confinement term in ACI 318 equation (bar stress and concrete strength limits not applied)	103
Figure 6-16: Test/calculated failure stress ratios versus cover/confinement term in ACI 408 equation	103
Figure 6-17: Test/calculated failure stress ratios versus cover/confinement term in ACI 318 equation (limit changed to 4.0, bar stress and concrete strength limits not applied).....	104
Figure 6-18: Increasing nonlinearity of MMFX stress-stress behavior between C1 and C2 failure stresses	106
Figure 6-19: Reduction in the efficiency of confinement with increasing failure stress	107
Figure 6-20: End-of-splice crack widths for UT #5 specimens (load at or below 60% of failure load)	109
Figure 6-21: End-of-splice crack widths for UT #8 specimens (load at or below 60% of failure load)	111
Figure 6-22: End-of-splice crack widths for UT #11 specimens (load at or below 60% of failure load)	112
Figure 7-1: Distribution of MMFX test/calculated failure stress ratios when using the ACI 408 development length equation with $\phi = 0.82$	116
Figure 7-2: Distribution of test/calculated failure stress ratios when using the ACI 408 development length equation with $\phi = 0.82$ (Data includes all bond tests in the ACI 408 database 10-2001 and the MMFX research program failing at bar stresses > 75 ksi)	118
Figure 7-3: Span and loading of example beam	120
Figure 7-4: Details of example beam.....	120
Figure 7-5: Calculated load-deflection for example beam assuming varying design yield strengths for the MMFX reinforcement	122
Figure 7-6: Calculated service load deflections for the example beam assuming varying design yield strengths for the MMFX reinforcement	125
Figure 7-7: Calculated crack widths for the example beam assuming varying design yield strengths for the MMFX reinforcement	127

CHAPTER 1

Introduction

1.1 MMFX REINFORCEMENT

MMFX microcomposite steel reinforcement is manufactured using a patented proprietary process which results in a high strength material that is reported to have corrosion resistance. A high chromium content of 9-10% — a percentage nearing that of stainless steel — is partially responsible for the corrosion resistance of the material. A specialized microstructure also provides a means of corrosion resistance.

Ordinary black steel is composed of a two phased microstructure of ferrite and iron-carbide. Macrogalvanic electrochemical cells between the two phases of the steel microstructure lead to a reaction in which electrons flow from the ferrite anode to the iron-carbide cathode where corrosion byproducts are produced. In contrast to ordinary black steel, the microstructure of MMFX reinforcement is composed of 100% packet martensite between untransformed sheets of austenite. MMFX steel is nearly devoid of carbide so the development of macrogalvanic cells is greatly reduced; consequently, the production of corrosion products is also greatly reduced (Zia 2003, Dawood, *et al.* 2004).

The corrosion resistance of MMFX steel has been tested in laboratories in order to evaluate the claims made by MMFX Steel Corporation of America — the manufacturers of MMFX reinforcement. A report compiled by the Concrete Innovation Appraisal Service examined the results of several independent research studies related to the corrosion resistance of MMFX steel. The authors found that that there is sufficient evidence that MMFX steel exhibits improved corrosion resistance over conventional ASTM A 615 reinforcing steel

and that this corrosion resistance can lead to longer service lives and lower life-cycle costs (Zia 2003).

In addition to corrosion resistance, MMFX steel possesses a very high tensile strength due to its low average carbon content of 0.08%. The producers of MMFX steel guarantee a minimum ultimate tensile strength of 150 ksi and a minimum yield strength of 100 ksi when measured using the 0.2% offset method (MMFX 2004). Previous research has indicated that the actual ultimate tensile strength of MMFX reinforcement can be as high as 177 ksi and the actual 0.2% offset yield strength may be closer to 120 ksi (El-Hacha and Rizkalla 2002). As with many high strength steels, MMFX reinforcement does not display a clearly defined yield point or a yield plateau. However, the steel still displays a reasonable amount of ductility with a minimum elongation of 7% for #11 and smaller bars (MMFX 2004).

MMFX steel has been approved for use in structural concrete design subject to the 80 ksi limitation on tensile yield strength given in the ACI 318-05 building code. The material conforms to the provisions of ASTM A1035-04, ASTM A 615 Grade 75, and AASHTO M31 Grade 75 (MMFX 2004).

1.2 PROJECT SCOPE AND OBJECTIVES

MMFX reinforcement is most efficient when a design utilizes both its corrosion resistant and high strength attributes. However, design yield strengths for reinforcing steel in flexural concrete members are currently limited to 75 ksi in the AASTHO LRFD bridge design code and 80 ksi in the ACI 318-05 building design code. These limits are imposed since many design equations have been developed on empirical data. The applicability of these equations beyond the limits of the variables included in the empirical data cannot be guaranteed without additional laboratory tests on specimens that expand the breadth of variables in the experimental database.

Development length equations are examples of equations produced from empirical data. Due to such factors as the non-homogeneity of concrete and the large variation in stresses between cracked and uncracked portions of a member, the bond failure mechanism is difficult to accurately characterize through purely theoretical expressions. For this reason, development length equations have been developed based on the average behavior displayed by a large database of experimental bond tests.

The development length equation included in the ACI 318-05 building code is based on the experimental results of bond tests failing primarily at bar stresses less than the code limit of 80 ksi. The AASHTO LRFD development length equation is a semi-theoretical equation that has limits imposed on it based on experimental data. A development length equation recently proposed by ACI Committee 408 is based on a larger database of tests than those used in the development of the ACI 318 and AASHTO LRFD code equations, but the data are still limited in the very high stress range. The expanded database includes only 12 tests failing at bar stresses greater than 100 ksi and does not include any tests failing at bar stresses greater than 120 ksi.

The research program reported herein is a joint effort between the University of Texas, the University of Kansas, and North Carolina State University. In this study, each research group will test 22 beam-splice specimens to evaluate the bond capacity of MMFX steel spliced at high stresses. Test variables include bar size, concrete compressive strength, splice length, concrete cover, and amount of transverse reinforcement (confinement). All splices will be designed to fail at stresses between 80 ksi and 140 ksi. To accurately relate bar strains to bar stresses, a series of tension tests will also be performed on the MMFX bars.

The results of this research program will significantly increase the number of tests in the ACI 408 database failing at high stress levels. Data from these tests will be

compared with the current ACI 408, ACI 38-05, and AASHTO LRFD development length equations to determine their adequacy at high strengths. Based on these evaluations, design recommendations will be proposed for the splicing and anchorage of high strength bars.

Crack widths and deflections will also be monitored to evaluate the serviceability performance of members reinforced with MMFX bars at very high stress levels. Based on these observations, general design recommendations will be presented for members reinforced with high strength bars.

CHAPTER 2

Bond Failure Mechanism

2.1 BOND FORCE TRANSFER

The basic principles of reinforced concrete design require proper anchorage of reinforcing bars. Without sufficient anchorage, reinforcement cannot develop the stresses required to reach the ultimate capacity of a member. Current design codes require that a minimum embedment length of a reinforcing bar be provided beyond a point of high tensile stress. Adequate lengths are also required at all locations where reinforcement is spliced. The evolution of the current design code requirements for development length of reinforcement will be discussed in Chapter 3. In this chapter, bond failure mechanisms are discussed. Unless otherwise noted, information provided in the remainder of this chapter has been derived from a 2003 report compiled by ACI Committee 408 entitled *Bond and Development of Straight Reinforcing Bars in Tension* (ACI 408R-03). This report summarizes the bond failure mechanism and the major research efforts that have led to the current descriptive and design code equations.

Development length provisions are based on expressions for the bond forces between reinforcing bars in tension and the surrounding concrete. At low stresses, chemical adhesion between the bar and the concrete is sufficient to transfer forces between the two materials. As stress increases, chemical adhesion can no longer maintain force transfer; and the reinforcing bar begins to slip relative to the surrounding concrete.

After the initial slip of the bar, force transfer is obtained primarily through bearing between the bar deformations and the concrete. Friction provides a smaller, yet

significant, amount of force transfer. As slip continues, friction on the barrel of the bar reduces; and force is transferred to the concrete entirely by the bar deformations. Compressive bearing forces on the bar ribs increase along with friction forces along the surface of the deformations. The bond force transfer mechanism is shown in Figure 2-1.

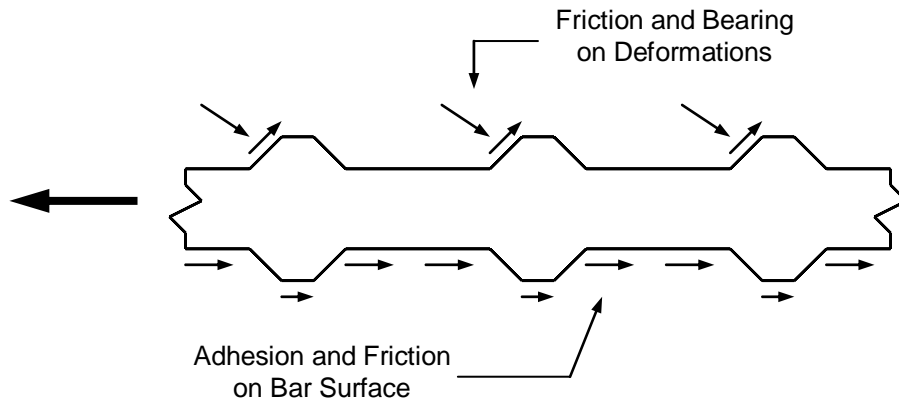


Figure 2-1: Bond force transfer (adapted from ACI 408)

Compressive and shear stresses in the concrete surrounding the bar balance the forces applied by the reinforcing bar. Local compressive stresses immediately ahead of the bar deformations result in principle tensile stresses that may cause cracking perpendicular to lug on the reinforcing bar. These cracks, first identified by Goto, rarely play a major role in bond failure. Hoop tensile stresses in the concrete surrounding the bar caused by the wedging action of the bar deformations produce more serious cracks which extend radially from the reinforcing bar. Depictions of Goto and radial crack formations are shown in Figure 2-2 and Figure 2-3, respectively.

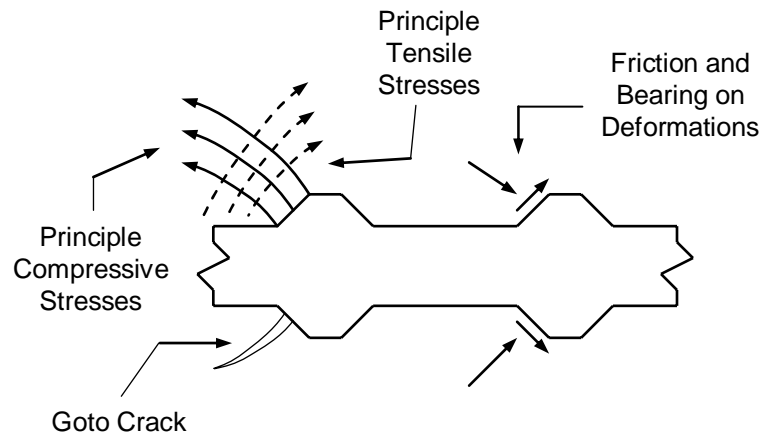


Figure 2-2: Formation of Goto cracks (adapted from ACI 408)

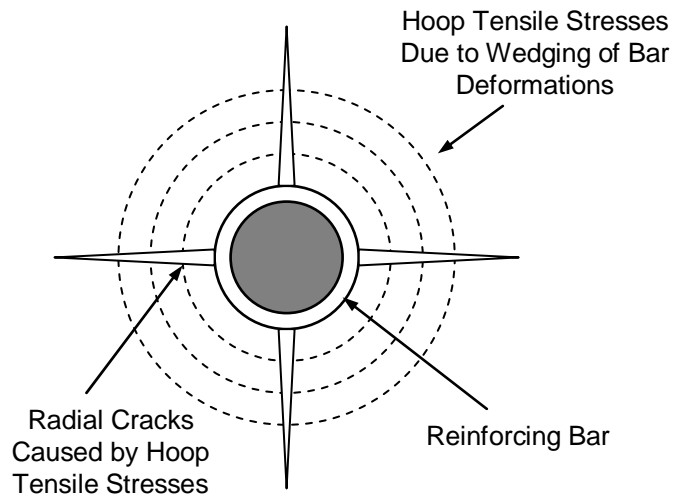


Figure 2-3: Radial cracking due to hoop tensile stresses (adapted from ACI 408)

Radial cracks initially form near the loaded end of an anchored or spliced bar since this portion is the most highly stressed region of the bar. As load is increased, radial cracks progress longitudinally down the length of the bar. Bond failure occurs when these radial cracks progress fully through the concrete cover along the full development or splice length. The surrounding concrete is no longer capable of providing anchorage for the reinforcing bar, and the bar can no longer carry load. This

mode of failure is referred to as splitting failure. A splitting failure is demonstrated in Figure 2-4.

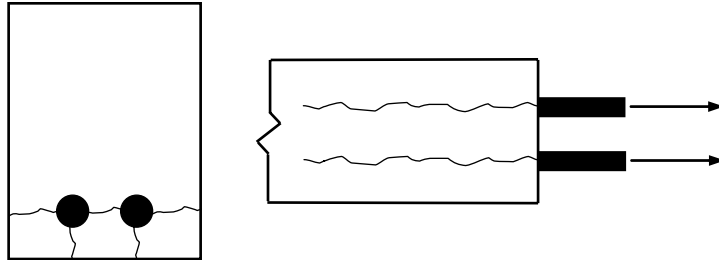


Figure 2-4: Splitting failure (adapted from ACI 408)

If the surrounding concrete has sufficient strength such that it can prevent the extension of splitting cracks, failure may occur due to the shearing of concrete immediately surrounding the bar. This mode of failure is referred to as a pullout failure. The increased strength necessary to obtain a pullout failure may be obtained by using concrete with a higher compressive strength, increasing the concrete cover provided around the reinforcing bar, and/or providing a high level of transverse reinforcement. A schematic of a pullout failure is given in Figure 2-5 .

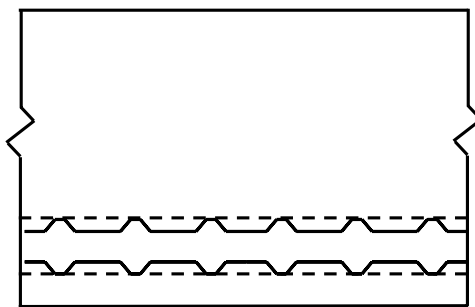


Figure 2-5: Pullout failure (adapted from ACI 408)

2.2 GOVERNING PARAMETERS

Research on laboratory specimens failing in bond has highlighted the most influential parameters related to bond strength of uncoated reinforcing bars. These parameters are development/splice length, concrete compressive strength, bar size, concrete cover and bar spacing, transverse reinforcement, relative rib area of the reinforcing bar, and bar casting position.

2.2.1 Development/Splice Length

An increase in development/splice length will result in a higher bond capacity. Mathey and Watstein (1961) indicated that bond stress and the ratio of bar diameter to bonded length are approximately linearly related. Research by Darwin, *et al.* (1996b) confirms that the relationship between bond force and bonded length is nearly linear but not proportional. Therefore, an increase in bond force by a given percentage will require a higher percentage increase in development length.

The non-proportional relationship between bond force and bonded length is a result of the non-uniform participation in force transfer by the tensioned and non-tensioned ends of the bar. Bond failure is incremental, with slip first occurring at the loaded end where bond stresses are highest. Splitting also initiates at the loaded end and progresses down the length of the bar. Post failure examinations of concrete surrounding spliced bars indicate that localized crushing in front of the bar ribs varies along the length of the splice due to the incremental failure mode. More crushing is observed near the non-tensioned end of the bar than at the loaded end where crushing is minimal or non-existent. This suggests a failure sequence initiated by splitting at the loaded end followed by a rapid slip of the bar at the non-loaded end. Therefore, the non-loaded end is less effective in transferring bond forces than the loaded end.

Despite the non-proportional relationship, current design equations for development length assume a linear and proportional relationship between bond force and bonded length for simplicity. The design equations like those found in the ACI 318 building code are conservative for most bonded lengths with typical bar stresses but become less conservative as the bonded length and bar stress increase. Eventually, these equations can become unconservative if applied to relatively long bonded lengths with high stresses in the reinforcing bars.

2.2.2 Concrete Compressive Strength

The contribution of concrete compressive strength to the bond strength of reinforcing bars in tension has traditionally been represented using the term $\sqrt{f_c'}$. Below $f_c' = 8000$ psi, this assumption is reasonably accurate; however, the implications of using this relationship at higher strengths have been debated among researchers. Many (Azizinamini *et al.* 1993, Azizinamini, Chisala, and Ghosh 1995, Zuo and Darwin 1998, 2000, Hamad and Itani, 1998) have found that the average bond strength normalized with respect to $\sqrt{f_c'}$ decreases with increased concrete strength because not all bar lugs contribute equally in bond force transfer in higher strength concrete. However, Esfahani and Rangan (1998) found the opposite relationship to be true.

The consensus of ACI Committee 408 is that bond strength is best represented by $f_c'^{1/4}$. Statistical analyses conducted by Darwin, *et al.* (1996a) and Zuo and Darwin (2000) showed that $f_c'^{1/4}$ provided the best representation of the contribution of concrete to bond strength when compared to a database of 367 bond tests. Zuo and Darwin also found that concrete strength affects the contribution of transverse reinforcement to bond strength. Their analyses showed that the optimal factor for relating these two parameters falls between $f_c'^{3/4}$ and f_c' .

2.2.3 Bar Size

Larger diameter bars require larger forces to be developed in order to cause splitting failure for a given bonded length. This is due to the increased surface area associated with larger bars. For a given force within a bar, the bond stresses developed on the surface of the bar will be lower as the surface area increases. However, the area of a bar increases at a higher rate than the surface area of a bar as the bar diameter increases. Therefore, although larger bars can maintain higher forces than smaller bars for a given bonded length, the stress developed in the bars at that bonded length will be higher in the smaller bars. As a result, the required development length to develop a given stress increases with bar diameter.

Bar size also affects the contribution of transverse reinforcement to bond strength. Slip of larger bars mobilizes higher strains in the transverse reinforcement than slip of smaller bars. The higher strains in the confining reinforcement provide an increase in the confining force.

2.2.4 Concrete Cover and Bar Spacing

When bond failure is governed by the splitting mode, the relative values of bottom cover, side cover, and $\frac{1}{2}$ the clear spacing between bars play a significant role in bond failure. The minimum of these values is a principle factor in the determination of bond strength. An increase in the minimum value results in an increase in overall bond strength. Research by Orangun, Jirsa, and Breen (1977) and Darwin, *et al.* (1996a) has also suggested that the relative values of the maximum and minimum of the bar cover and spacing terms play a secondary role in bond strength. For large variations in maximum and minimum cover (i.e. – widely spaced bars with small bottom covers), the increase in bond strength may be as large as 25% over that of a situation where all three cover and spacing values were equal (Darwin, *et al.* 1996a).

The minimum value of bottom cover, side cover, and $\frac{1}{2}$ the clear spacing between bars also determines the failure plane on which splitting will occur. Failure will tend to occur through the plane of least cover. If bottom cover, side cover, and $\frac{1}{2}$ the bar clear spacing are equal, splitting will occur along both a horizontal and a vertical plane through the bars. This is known as a face and side split failure. If bottom cover is the smallest of the governing cover/spacing values, splitting will initiate through a vertical plane toward the bottom face of the member. When bottom cover is significantly smaller than side cover or $\frac{1}{2}$ the bar clear spacing, several splitting planes will form toward the bottom face in a 'V' pattern. This is known as a V-notch failure. In other cases, a horizontal side splitting failure plane will eventually form; and failure will occur due to a face and side split mode. When the side cover and $\frac{1}{2}$ the bar clear spacing are less than the bottom cover, failure will occur through a horizontal splitting plane through the bars. This is known as a side split failure. These three types of splitting failure are depicted in Figure 2-6.

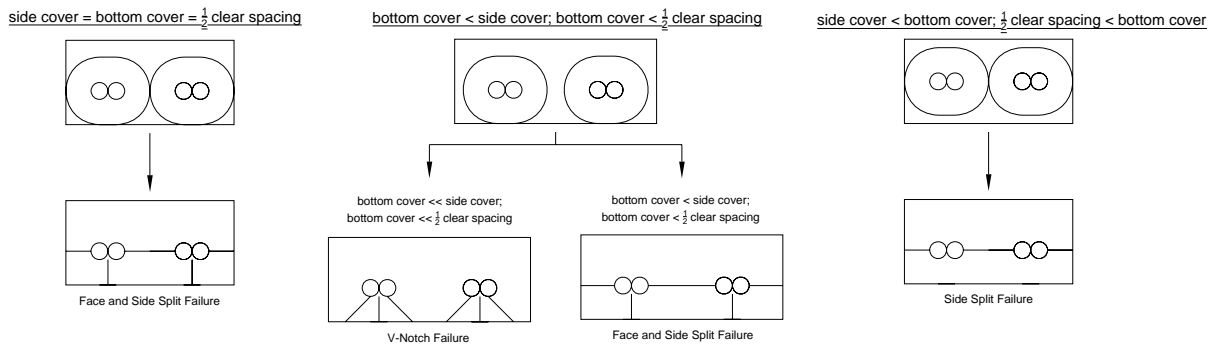


Figure 2-6: Types of splitting failure (adapted from Orangun, Jirsa, Breen 1977)

An increase in concrete cover and spacing values above those required to transition failure from the splitting mode to the pullout mode will provide little or no increase in bond strength.

2.2.5 Transverse Reinforcement

Transverse reinforcement increases overall bond strength by limiting the progression of splitting cracks. Its effectiveness is governed not only by the amount of transverse reinforcement provided but also by the properties of the bar being developed and the strength of the concrete surrounding the bar.

When bond failure is governed by the splitting mode, an increase in the area of transverse reinforcement crossing the potential crack planes will result in an increase in bond strength. However, an increase in the tensile strength of the transverse reinforcement will not provide additional bond capacity since the transverse reinforcement rarely yields (Maeda, Otani and Aoyama 1991; Sakurada, Moohasi and Tanaka 1993; Azizinamini, Chisala, and Ghosh 1995).

As discussed in Section 2.2.2, the contribution of transverse steel to total bond strength is related to a factor between $f_c^{3/4}$ and f_c' . Therefore, an increase in concrete strength will result in a non-proportional increase in bond strength. An increase in bar size has also been shown to increase the effectiveness of transverse reinforcement as discussed in Section 2.2.3. In a similar way, bar deformation geometry affects the performance of transverse reinforcement. This will be discussed in Section 2.2.6.

An increase in transverse reinforcement above that necessary to transition from splitting failure to pullout failure will result in little or no increase in bond strength.

2.2.6 Reinforcing Bar Relative Rib Area

The effect of bar deformation geometry on bond strength is not governed strictly by deformation size or spacing alone. Rather, the ratio of bearing area to the shearing area of the bar — known as the relative rib area R_r — determines the contribution of bar geometry to bond strength. A detailed method for measuring R_r is provided in ACI 408.3 but the relationship may be expressed generally as

$$R_r = \frac{\text{projected rib area normal to bar axis}}{\text{nominal bar perimeter} \cdot \text{center - to - center rib spacing}}$$

Darwin, *et al.* (1996b) and Zuo and Darwin (2000) showed that an increase in R_r will produce an increase in bond strength for bars confined by transverse reinforcement. This effect is due to the increased wedging action provided by higher R_r rib patterns. The increased wedging mobilizes larger strains in the transverse reinforcement which results in higher confining forces. According to Darwin, *et al.* (1996b), the use of bars with $R_r = 0.1275$ (average $R_r = 0.0727$ for standard bars) could provide up to a 26% reduction in required splice length. This effect is most pronounced for bars with small covers and a large amount of transverse reinforcement.

Because the effect of R_r is related to increased strains in the transverse reinforcement, an increase in R_r does not provide an increase in bond strength for uncoated unconfined bars. However, Darwin, *et al.* concluded from laboratory tests that increased R_r did provide additional bond strength for unconfined epoxy-coated bars.

2.2.7 Bar Casting Position

Bottom cast bars display higher bond strength than top cast bars. This is due to the increased settlement and amount of bleed water at the location of a top cast bar in relation to a bottom cast bar. These factors reduce the efficiency of the surrounding concrete to prevent splitting cracks from developing. Although modern U.S. design codes (ACI 318, AASHTO LRFD) only begin to recognize this “top bar effect” when the amount of fresh concrete below a bar is greater than 12 in., any increase in depth of concrete below a bar will reduce the bond strength of the bar.

CHAPTER 3

Previous Research

3.1 TESTING METHODS

Current descriptive equations and design codes for bond strength are based on empirical knowledge gained from a multitude of laboratory experiments. Sections 3.1.1, 3.1.2, and 3.1.3 describe the three most common testing procedures used to determine bond strength. Information regarding these testing procedures was obtained from the ACI 408 report referred to in Chapter 2.

3.1.1 Pullout Test

Pullout tests are the easiest and least expensive bond tests to conduct; however, they provide the least realistic results of bond strength. In these tests, tension is applied directly to a bar which has been embedded in a block of concrete. A schematic of a pullout test is shown in Figure 3-1 .

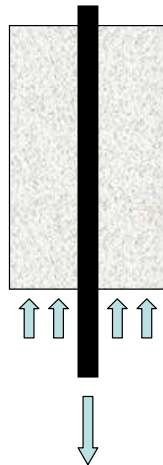


Figure 3-1: Schematic of pullout test (adapted from ACI 408)

Results of pullout tests are not a good indicator of actual bond strength because they do not represent realistic loading conditions found in structural members. The concrete block is placed in compression during the test while bars being anchored as tension reinforcement are usually surrounded by concrete in tension. Compression struts also form between the end reaction and the reinforcing bar which place the bar in lateral compression. In actual structural members, compression between the bar and the surrounding concrete is produced as the lugs of the bar bear on the concrete after adhesion is overcome and initial slip of the bar occurs. To prevent crushing failure of the concrete block, pullout specimens usually contain a high level of confining transverse reinforcement. As described previously, transverse reinforcement adds significantly to the bond strength by preventing the growth of splitting cracks. Due to these shortcomings, ACI Committee 408 does not recommend pullout tests as a sole indicator of bond strength.

3.1.2 Beam-End Test

Beam-end tests are the simplest tests that reflect realistic boundary conditions and bond strength results. In these tests, tension is applied to a reinforcing bar that has been eccentrically embedded in a block of concrete. A schematic of a beam-end test is shown in Figure 3-2.

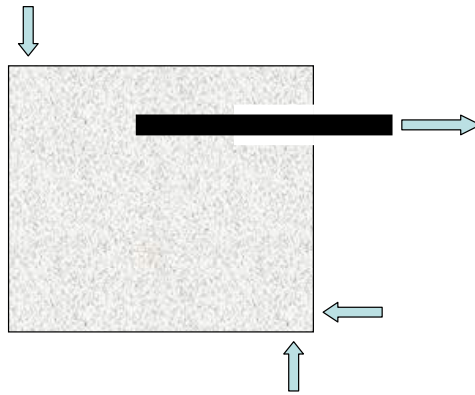


Figure 3-2: Schematic of beam-end test (adapted from ACI 408)

Unlike the pullout test, beam-end tests more accurately represent actual loading conditions in structural members. Both the bar and the surrounding concrete are placed in tension due to eccentric placement of the reinforcing bar in the concrete block. The effect of the end reactions can be negated if the supports are located at a distance of at least the embedment length of the bar from the end of the reinforcing bar. Shear reinforcement can be detailed such that it does not provide confinement to the bar being developed or it may enclose the reinforcing bar in order to study the effect of transverse reinforcement.

3.1.3 Beam-Splice Test

Full scale beam tests provide the most accurate results for bond strength since they best duplicate the actual stress state around the reinforcing bars being developed. A popular full scale test used for bond research is the beam-splice test. In these tests, bars are lap spliced within a constant moment region at the center of the beam span. A schematic of a beam splice test is shown in Figure 3-3. Because of its simplicity of design and fabrication and because of the accuracy of the test results, beam splice tests

have provided the majority of data for the development of descriptive and design code equations for bond and anchorage of reinforcement.

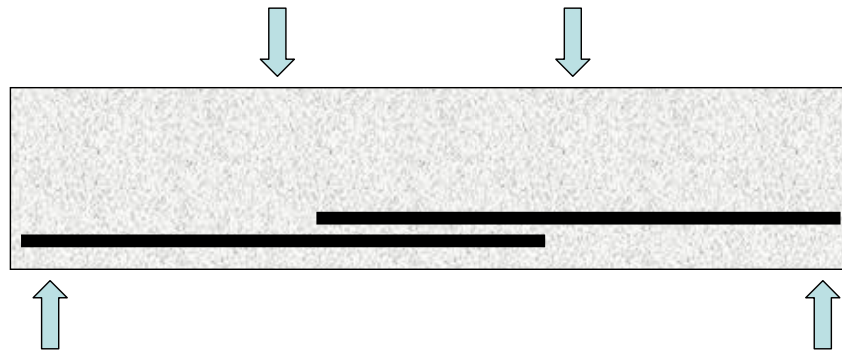


Figure 3-3: Schematic of beam-splice test (adapted from ACI 408R-03)

3.2 DESCRIPTIVE EQUATIONS

3.2.1 Orangun, Jirsa, and Breen (1977)

Orangun, Jirsa, and Breen developed descriptive equations for the bond strength of splices with and without confining transverse reinforcement that incorporated the most influential variables related to bond behavior. The researchers assumed a linear relationship between the average bond stress, u , and l_d/d_b . Bond strength was assumed to be proportional to $\sqrt{f'_c}$.

Nonlinear regression analysis of 62 beams — of which four contained side cast bars, one contained top cast bars, and 57 contained bottom cast bars — produced a best fit curve for the average bond stress, u_c^* , of bars without transverse reinforcement

$$\frac{u_c^*}{\sqrt{f'_c}} = 1.22 + 3.23 \frac{C}{d_b} + 53 \frac{d_b}{l_d} \quad (1)$$

where:

C = smaller of concrete clear cover or half of the clear spacing between bars (in)

$d_b = \text{bar diameter (in)}$

$l_d = \text{development or splice length (in)}$

$f_c' = \text{concrete compressive strength (psi)}$

$u_c^* = \text{average bond stress (psi)}$

Since the results were meant to be used as a basis for design, the coefficients of the best fit equation were conservatively rounded to produce an approximate average bond stress, u_c ,

$$\frac{u_c}{\sqrt{f_c'}} = 1.2 + 3\frac{C}{d_b} + 50\frac{d_b}{l_d} \quad (2)$$

An additional 27 splice tests and 27 development length tests containing confining transverse reinforcement were included in further analyses to determine the contribution of confining steel, u_s , to the total average bond stress, u_b . The best fit expression for total average bond stress was found to be

$$\frac{u_b}{\sqrt{f_c'}} = \frac{u_c + u_s}{\sqrt{f_c'}} = 1.2 + 3\frac{C}{d_b} + 50\frac{d_b}{l_d} + \frac{A_{tr}f_{yt}}{500snd_b} \quad (3)$$

where:

$A_{tr}^* = \text{area of transverse reinforcement crossing the plane of splitting (in}^2\text{)}$

$f_{yt} = \text{yield stress of transverse reinforcement (psi)}$

$n^* = \text{number of bars being developed or spliced in the plane of splitting}$

$s = \text{spacing of transverse reinforcement (in)}$

*See Figure 3-4 for examples

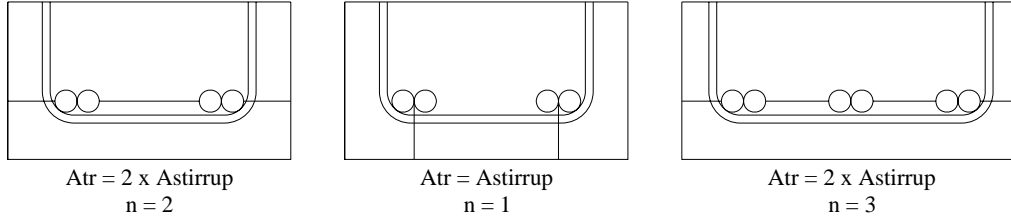


Figure 3-4: Definition of A_{tr} and n for different failure planes

This expression can be rewritten in terms of bar force by replacing the term u_b with $A_b f_s / \pi d_b l_d$ and substituting $A_b = \frac{\pi d_b^2}{4}$.

$$\frac{T_b}{\sqrt{f_c'}} = \frac{T_c + T_s}{\sqrt{f_c'}} = \frac{A_b f_s}{\sqrt{f_c'}} = 3\pi l_d (C + 0.4d_b) + 200A_b + \frac{\pi l_d A_{tr} f_{yt}}{500sn} \quad (4)$$

The previous equations are only applicable to cases in which splitting governs. To prevent cases of pullout failure, the following restriction applies.

$$\frac{1}{d_b} \left(C + 0.4d_b + \frac{A_{tr} f_{yt}}{1500sn} \right) \leq 2.5 \quad (5)$$

3.2.2 Darwin, *et al.* (1996a)

Darwin, *et al.* used a larger database of 133 unconfined and 166 confined bottom cast splice and development specimens to reevaluate the findings of Orangun, Jirsa, and Breen. The researchers found that normalizing bond forces with respect to $f_c'^{1/4}$ resulted in a better correlation of data than normalizing with respect to $\sqrt{f_c'}$. The resulting expressions also accounted for the ratio of maximum to minimum cover values and the beneficial effects of increased relative rib area, R_r , on the contribution of transverse reinforcement to total bond force.

Bond force provided by concrete alone was given as

$$\frac{T_c}{f_c^{1/4}} = \frac{A_b f_s}{f_c^{1/4}} = [63l_d(c_{\min} + 0.5d_b) + 2130A_b] \left(0.1 \frac{c_{\min}}{c_{\max}} + 0.9 \right) \quad (6)$$

where $\left(0.1 \frac{c_{\max}}{c_{\min}} + 0.9 \right) \leq 1.25$

where:

c_{\min} = minimum of c_s or c_b (in)

c_{\max} = maximum of c_s or c_b (in)

c_s = minimum of $c_{si} + 0.25$ in. or c_{so} (in)

c_{si} = one-half clear spacing between bars (in)

c_{so} = side cover of reinforcing bars (in)

c_b = bottom cover of reinforcing bars (in)

Total bond force was given as the sum of the contribution of concrete and the contribution due to confining transverse reinforcement.

$$\frac{T_b}{f_c^{1/4}} = \frac{T_c + T_s}{f_c^{1/4}} = \frac{A_b f_s}{f_c^{1/4}} = [63l_d(c_{\min} + 0.5d_b) + 2130A_b] \left(0.1 \frac{c_{\max}}{c_{\min}} + 0.9 \right) + 2226t_r t_d \frac{NA_{tr}}{n} + 66 \quad (7)$$

The previous restriction on $\left(0.1 \frac{c_{\max}}{c_{\min}} + 0.9 \right)$ still applies and:

N = number of transverse stirrups, or ties, within the development length

R_r = relative rib area of reinforcement as defined in Section 6.6 of ACI 408R-03

$t_d = 0.72d_b + 0.28$

$t_r = 9.6R_r + 0.28$

As with the expressions developed by Orangun, Jirsa, and Breen, the expressions from Darwin, *et al.* only apply to cases where splitting failure governs. To prevent pullout failures, the following restriction applies.

$$\frac{1}{d_b} \left((c_{\min} + 0.5d_b) \left(0.1 \frac{c_{\max}}{c_{\min}} + 0.9 \right) + \frac{35t_r t_d A_{tr}}{sn} \right) \leq 4.0 \quad (8)$$

3.2.3 Zuo and Darwin (2000)

Zuo and Darwin continued the research performed by Darwin, *et al.* using a database of experimental results larger than that considered in the previous research. The results of 171 unconfined and 196 confined bottom cast splice and development specimens were used. This database included a significantly larger population of specimens cast in high strength concrete ($f_c' > 8000$ psi). Analysis of the new database confirmed the finding of Darwin, *et al.* that $f_c'^{1/4}$ is a better indicator of the concrete contribution to bond strength than $\sqrt{f_c'}$. Therefore, the expression for the concrete contribution to bond force shown below includes only minor changes from that cited by Darwin, *et al.*

$$\frac{T_c}{f_c'^{1/4}} = \frac{A_b f_s}{f_c'^{1/4}} = [59.8l_d (c_{\min} + 0.5d_b) + 2350A_b] \left(0.1 \frac{c_{\max}}{c_{\min}} + 0.9 \right) \quad (9)$$

where $\left(0.1 \frac{c_{\max}}{c_{\min}} + 0.9 \right) \leq 1.25$

Zuo and Darwin found that the contribution of confining transverse reinforcement to the total bond force is related to the concrete compressive strength and is best represented by a value between $f_c'^{3/4}$ and f_c' . For simplicity, the researchers chose to conservatively use $f_c'^{3/4}$ in their descriptive equations. The expression for total bond force then becomes

$$\frac{T_b}{f_c'^{1/4}} = \frac{T_c + T_s}{f_c'^{1/4}} = \frac{A_b f_s}{f_c'^{1/4}} =$$

$$[59.8l_d(c_{\min} + 0.5d_b) + 2350A_b] \left(0.1 \frac{c_{\min}}{c_{\max}} + 0.9 \right) + \left(31.14t_r t_d \frac{NA_{tr}}{n} + 4 \right) \sqrt{f_c'} \quad (10)$$

where all variables remain as defined in Equation (7) except $t_d = 0.78d_b + 0.22$.

To exclude cases in which pullout failure governs, the following restriction applies.

$$\frac{1}{d_b} \left((c_{\min} + 0.5d_b) \left(0.1 \frac{c_{\max}}{c_{\min}} + 0.9 \right) + \left(\frac{0.52t_r t_d A_{tr}}{sn} \right) \sqrt{f_c'} \right) \leq 4.0 \quad (11)$$

3.3 UNITED STATES DESIGN CODE EQUATIONS

The previous descriptive equations were developed as best fit curves based on empirical data; therefore, they must be altered to provide conservatism before being used in design. Furthermore, current design codes no longer consider anchorage requirements in terms of average bond strength. Modern codes mandate a required development or splice length necessary to reach the desired stress — usually the material yield stress — in a given bar.

3.3.1 ACI 318-05

The development length requirements in the ACI 318-05 Building Code are based on the expressions given by Orangun, Jirsa, and Breen in Section 3.2.1. Solving Equation (3) for l_d and replacing $(C + 0.4d_b)$ with $c_b = (C + 0.5d_b)$ produces

$$l_d = \left(\frac{\frac{f_s}{\sqrt{f_c'}} - 200}{12 \left(\frac{c_b + K_{tr}}{d_b} \right)} \right) d_b \quad (12)$$

where $K_{tr} = \frac{A_{tr} f_{yt}}{1500sn}$.

Setting the stress in the bar at splitting failure, f_s , equal to the yield stress of the bar, f_y , removing the 200 from the numerator, and changing 1/12 to 3/40 results in the final development length equation

$$l_d = \left(\frac{3}{40} \frac{f_y}{\sqrt{f_c'}} \frac{\psi_t \psi_e \psi_s \lambda}{\left(\frac{c_b + K_{tr}}{d_b} \right)} \right) d_b \quad (13)$$

where:

$$f_y \leq 80,000 \text{ psi}$$

$$f_c' \leq 10,000 \text{ psi}$$

$\psi_t = 1.3$ where horizontal reinforcement is placed such that more than 12 in. of fresh concrete is cast below the developed length or splice
 $= 1.0$ for all other cases.

$\psi_e = 1.5$ for epoxy-coated bars or wires with covers less than $3d_b$ or clear spacing less than $6d_b$.

$= 1.2$ for all other epoxy-coated bars

$= 1.0$ for all uncoated bars

$\psi_t \psi_e$ need not exceed 1.7

$\psi_s = 0.8$ for No. 6 and smaller bars and deformed wires

$= 1.0$ for No. 7 and larger bars

$$\lambda = 1.3 \text{ or } 6.7\sqrt{f'_c}/f_{ct} \geq 1.0 \text{ for lightweight concrete}$$

$$= 1.0 \text{ for normalweight concrete}$$

To prevent situations where pullout failure governs,

$$\frac{c_b + K_{tr}}{d_b} \leq 2.5 \quad (14)$$

The limits placed on the concrete compressive strength, f'_c , and the bar yield stress, f_y , represent the limits of applicability for the ACI 318 design equation. The variables included in the empirical data used in the background research by Orangun, Jirsa, and Breen were limited to concrete strengths and bar stresses within this range. Given the empirical development of the equation, the ACI 318 expression should not be applied beyond the limits of the variables included in the supporting research.

3.3.2 ACI 408R-03 Recommendations

The ACI 408 Committee on Bond and Development of Straight Reinforcing Bars in Tension has produced a recommended design equation for development length that incorporates the recent research performed by Zuo and Darwin. Solving Equation (10) for the required development length, l_d , and setting f_s equal to f_y produces

$$l_d = \left(\frac{\left(\frac{f_y}{\phi f'_c} - 2400\omega \right) \psi_t \psi_e \lambda}{76.3 \left(\frac{c\omega + K_{tr}}{d_b} \right)} \right) d_b \quad (15)$$

where:

$$c = c_{min} + d_b/2 \text{ (in)}$$

$$K_{tr} = \frac{0.52t_r t_d A_{tr}}{sn} \sqrt{f'_c}$$

$t_r, t_d =$ as defined in Equation (10)

$\psi_b, \psi_e, \lambda =$ as defined in Equation (13)

$\phi^* =$ modification factor = 0.82 when using load factors given in ACI 318-05

$$\omega = \left(0.1 \frac{c_{\max}}{c_{\min}} + 0.9 \right) \leq 1.25$$

* See Section 3.3.4 for a discussion of the purpose of the modification factor.

The following restriction ensures that splitting, rather than bar pullout, governs.

$$\frac{c\omega + K_{tr}}{d_b} \leq 4.0 \quad (16)$$

3.3.3 AASHTO LRFD 4th Edition

The development length requirements given in the 4th edition of the AASHTO LRFD Bridge Design Specifications are not based on the research presented in Sections 3.2.1, 3.2.2, or 3.2.3. Rather, they are based on the requirements included in the ACI building code prior to 1989. The underlying assumption used to derive the required development length is that bond stress, u , is equal to the bond force per unit length, U , divided by the sum of the perimeters of the bars developed at a section, Σ_o .

$$u = \frac{U}{\Sigma_o} = \frac{\Delta f_s d_b}{4\Delta l} \quad (17)$$

For design purposes, the change in stress, Δf_s , is equal to the yield stress, f_y ; and the length, Δl , is equal to the development length, l_d . In the ACI 318-63 building code, the bond stress was subject to the limitation

$$u = 0.305 \frac{\sqrt{f'_c}}{d_b} \leq 0.800 \text{ksi} \quad (18)$$

where f_c' is given in ksi. Setting Equation (17) equal to Equation (18), solving for l_d , and multiplying by 1.2 to account for the negative effects of closely spaced bars results in the basic development length equation for #11 and smaller bars.

$$l_d = \frac{1.25A_b f_y}{\sqrt{f_c'}} \quad (19)$$

In this equation, f_c' and f_y are in ksi and are limited to 10 ksi and 75 ksi, respectively for similar reasons that stress limits are applied to the ACI 318 development length equation described in Section 3.3.1. The basic development length is subject to the restriction

$$l_d \geq 0.4d_b f_y$$

The basic development length is then increased or decreased by multiplying by the following factors where applicable.

- 1.4 – for horizontal reinforcement where more than 12.0 in. of fresh concrete is cast below the reinforcement
- $\frac{0.22\sqrt{f_c'}}{f_{ct}} \geq 1.0$ – for lightweight concrete where f_{ct} (ksi) is specified
- 1.3 – for all lightweight concrete where f_{ct} is not specified
- 1.2 – for sand lightweight concrete where f_{ct} is not specified
- 1.5 – for epoxy coated bars with cover less than $3d_b$ or with clear spacing between bars less than $6d_b$
- 1.2 – for all other epoxy coated bars
- 0.8 – for reinforcement spaced laterally not less than 6.0 in. center-to-center, with not less than 3.0 in. clear cover measured in the direction of the spacing

- $\frac{(A_s \text{ required})}{(A_s \text{ provided})}$ – where anchorage or development for the full yield strength of reinforcement is not required, or where reinforcement in flexural members is in excess of that required by analysis
- 0.75 – where reinforcement is enclosed within a spiral composed of bars of not less than 0.25 in. in diameter and spaced at not more than a 4.0 in. pitch

3.3.4 Comparison of Development Length Equations

ACI Committee 408 maintains a database of full scale development length beam tests dating from 1955. The current database — database 10-2001 — contains the results of 478 independent development length tests on bottom cast bars. This database is useful for the development of new descriptive equations related to bond strength and for evaluating the reliability of current and future design code equations for development length.

When comparing the performance of development length equations, one must consider the intended use of each equation. Predictive equations should provide reasonably accurate estimates of failure stresses. Therefore, the mean test/calculated failure stress ratio for a large sample of tests should ideally be near 1.0. Design equations are meant to provide conservative estimates of failure stresses. Traditionally, equations used in ultimate strength design have represented a reasonable lower bound on data often defined by the 5% fractile. The 5% fractile represents a curve on which there is 90% confidence that there is a 95% probability that the actual strength exceeds the nominal strength (ACI 318). Therefore, very few tests (less than 5-10%) should fail at stresses below those calculated by the design equation; and the mean tests/calculated failure stress ratio for a design equation should be significantly higher than 1.0. In both predictive and

design equations, coefficients of variation should be low. This indicates that the variables used in the equations correlate well with test data.

For the remainder of this thesis, the ACI 408 equation will be evaluated as a predictive equation and the modification factor, ϕ , will be taken as 1.0 unless otherwise noted. The ACI 318 and AASHTO equations will be evaluated as design equations. When appropriate, the ACI 408 equation will also be examined as a design equation with the modification factor, ϕ , set to 0.82 as recommended by ACI Committee 408. When this modification factor is applied, the ACI 408 equation is converted to a lower bound expression and an approximate 5% fractile. The modification factor should not be confused with a strength reduction factor typically used in strength design and ordinarily denoted by the symbol ϕ . The strength reduction factor accounts for material understrengths, geometry tolerances, and desired ductility. It is not meant to convert best fit expressions into lower bound equations.

The distributions of test/calculated failure stress ratios for the ACI 408, ACI 318, and AASHTO LRFD equations are compared in Table 3-1. Two rows of data are shown for the ACI 408 development length equation. The first includes data calculated with the modification factor $\phi = 1.00$ to demonstrate the capability of the equation to represent a best fit of current experimental data. The second row includes data calculated with the modification factor $\phi = 0.82$ to demonstrate the reliability of the equation as a design guideline. It is important to note that the code mandated limits on bar stresses and concrete compressive strengths have not been applied when calculating the failure stresses according to the ACI 318 and AASHTO equations. These limits have been omitted in order to evaluate the performance of the equations through the full range of variables. More specific analyses with the limits applied will follow.

<i>N = 478</i>	<i>Distribution of Test/Calculated Failure Stress Ratios</i>						
<i>Equation</i>	<i>Mean</i>	<i>Std. Dev.</i>	<i>COV</i>	<i>Max</i>	<i>Min</i>	<i># < 1.0</i>	<i>% < 1.0</i>
ACI 408 ($\phi = 1.00$)	1.01	0.14	0.13	1.64	0.62	252	53
ACI 408 ($\phi = 0.82$)	1.23	0.17	0.13	2.00	0.76	28	6
ACI 318 [†]	1.25	0.30	0.24	2.42	0.51	95	20
AASHTO [‡]	1.32	0.37	0.28	2.63	0.50	90	19

† limits $f_s \leq 80$ ksi and $f_c' \leq 10,000$ psi not applied

‡ limits $f_s \leq 75$ ksi and $f_c' \leq 10,000$ psi not applied

Table 3-1: Distribution of test/calculated failure stress ratios for design code equations (data from ACI 408 database 10-2001)

The data presented in Table 3-1 indicate that the proposed equation from ACI Committee 408 performs well as both a best fit predictive equation and as a design equation through the full range of bar stresses and concrete strengths included in the ACI 408 database. The predictive ACI 408 equation results in a mean test/calculated failure stress ratio of 1.01. When the modification factor of 0.82 is applied to the ACI 408 equation, the mean test/calculated failure stress ratio is significantly above 1.0 and less than 6% of tests fall below the minimum desired value of 1.0. The low coefficient of variation of 0.13 for both versions of the ACI 408 equation suggests that the variables in the equations are well correlated with the experimental data.

Data for the ACI 318 and AASHTO code equations shown in Table 3-1 suggest that the equations are not suitable for use through the full range of bar stresses and concrete strengths represented in the ACI 408 database of bond tests. While both equations produce mean test/calculated failure stress ratios that are significantly higher than 1.0, they both also result in nearly 20% of tests failing below the calculated failure stress. The coefficients of variation for both equations are also much greater than the coefficient of variation of 0.13 produced by the ACI 408 predictive and design equations.

The performance of the ACI 408 predictive and design equations, the ACI 318 design equation, and the AASHTO design equation through the full range of bar stresses and concrete strengths included in the ACI 408 database are shown in Figure 3-5 through Figure 3-8. For reference, data points are labeled as either within or outside the allowable bar stress and concrete strength limits for the ACI 318 and AASHTO plots.

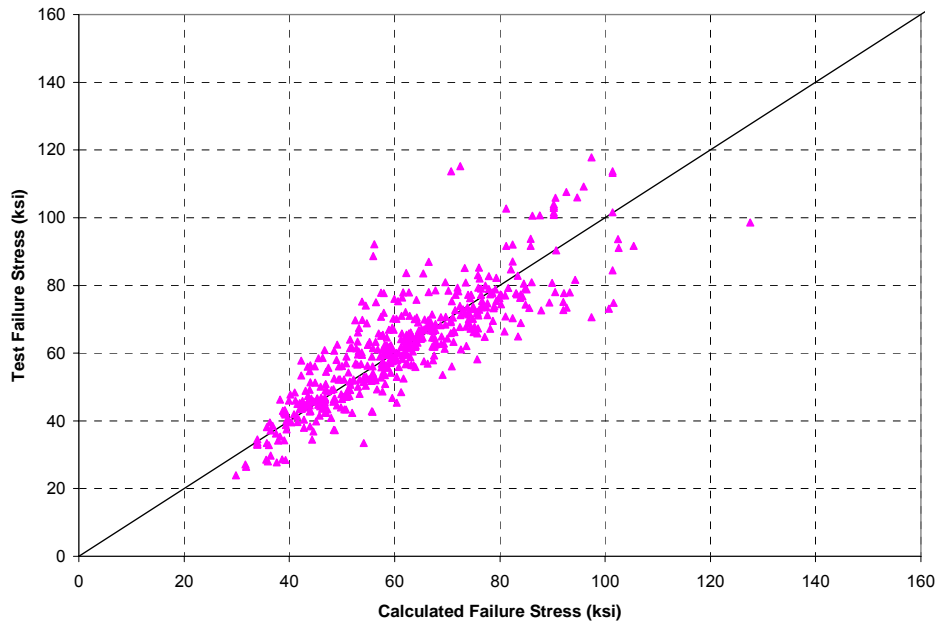


Figure 3-5: Test vs. calculated stresses using ACI 408 equation with $\phi = 1.00$ (data from ACI 408 database 10-2001)

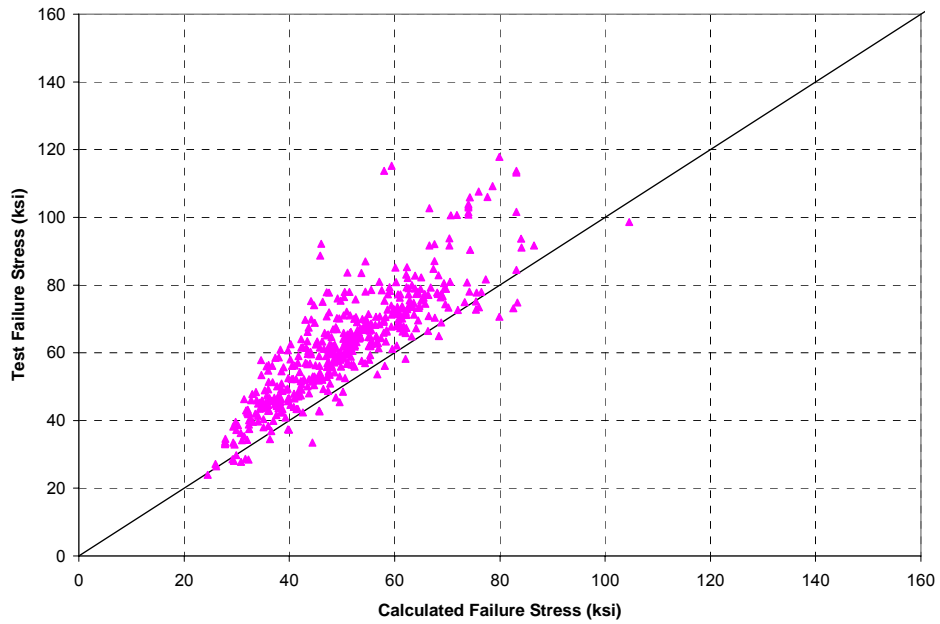


Figure 3-6: Test vs. calculated stresses using ACI 408 equation with $\phi = 0.82$ (data from ACI 408 database 10-2001)

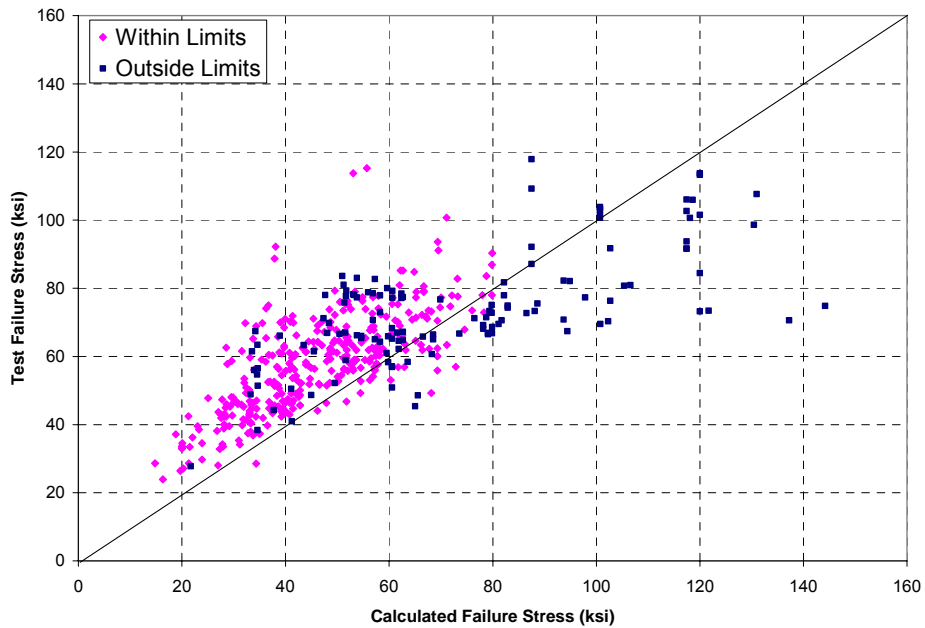


Figure 3-7: Test vs. calculated stresses using ACI 318 equation (data from ACI 408 database 10-2001, f_s and f_c' limits not applied)

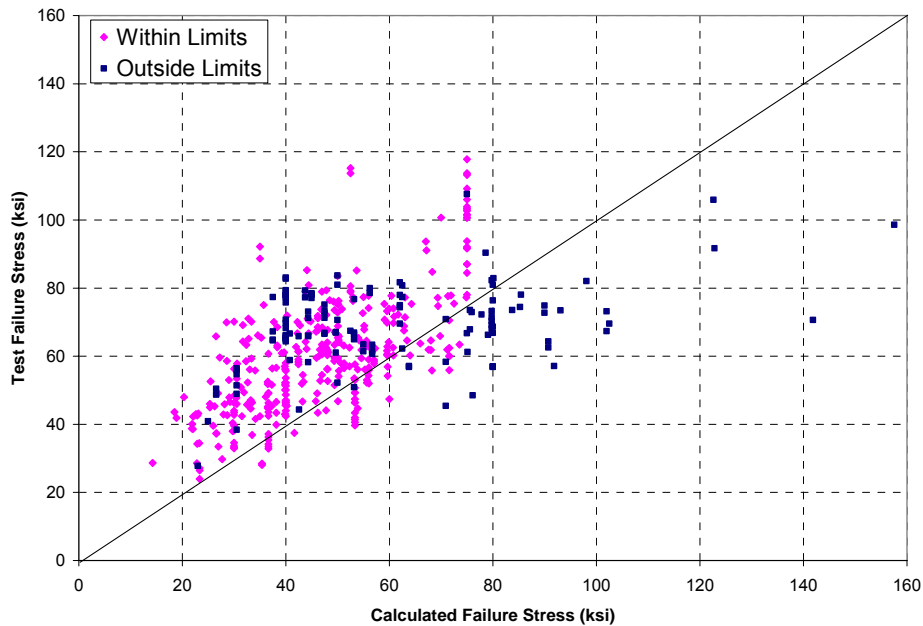


Figure 3-8: Test vs. calculated stresses using AASHTO LRFD equation (data from ACI 408 database 10-2001, f_s and f_c' limits not applied)

As noted, the previous data are based on the entire range of bar stresses and concrete strengths tested by researchers in bond. The ACI 318 building code limits stresses in tensile reinforcement to 80 ksi. The AASHTO LRFD bridge design specification limits bar stresses to 75 ksi. Both restrict concrete compressive strength to 10,000 psi. When these limits are applied to the results tabulated in the ACI 408 database of bond tests, the ACI 318 and AASHTO development length equations provide more acceptable results as shown in Table 3-2. The mean test/calculated failure stress ratios increase slightly, and the number of tests failing below their calculated failure stresses reduces drastically for both equations. However, 9% of tests still failed below their calculated failure stresses according to the ACI 318 equation and 13% of tests failed below their calculated failure stresses according to the AASHTO equation. These percentages are greater than the 6% produced by the design version of the ACI 408

equation for all bar stresses and concrete strengths and are on the upper limit of acceptable for design expressions. Nevertheless, the data indicate that the current ACI 318 and AASHTO equations provide sufficient conservatism when used within the limits of the variables mandated by the two codes.

<i>Distribution of Test/Calculated Failure Stress Ratios</i>									
<i>Equation</i>	<i>Calculated Stresses (ksi)</i>	<i>N</i>	<i>Mean</i>	<i>Std. Dev.</i>	<i>COV</i>	<i>Max</i>	<i>Min</i>	<i># < 1.0</i>	<i>% < 1.0</i>
ACI 318	≤ 80	348	1.31	0.28	0.21	2.42	0.72	32	9
AASHTO	≤ 75	351	1.34	0.34	0.26	2.63	0.74	47	13

Table 3-2: Performance of ACI 318 and AASHTO LRFD design code equations within the range of allowable design stresses and concrete strengths

Based on more limited data, when calculated failure stresses for the ACI 318 and AASHTO LRFD equations exceed the permissible maximum bar stresses, the conservatism of the design code equations diminishes drastically. This phenomenon is highlighted in Table 3-3.

<i>Distribution of Test/Calculated Failure Stress Ratios</i>									
<i>Equation</i>	<i>Calculated Stresses (ksi)</i>	<i>N</i>	<i>Mean</i>	<i>Std. Dev.</i>	<i>COV</i>	<i>Max</i>	<i>Min</i>	<i># < 1.0</i>	<i>% < 1.0</i>
ACI 318	> 80	24	0.93	0.15	0.16	1.35	0.70	17	71
AASHTO	> 75	17	0.81	0.14	0.18	1.15	0.62	15	88

Table 3-3: Performance of ACI 318 and AASHTO LRFD design code equations outside the range of acceptable design stresses ($f_c' \leq 10,000$ psi)

3.4 MMFX BOND RESEARCH

MMFX high strength reinforcement provides a guaranteed ultimate tensile stress of 150 ksi with a minimum yield stress of 100 ksi when measured using the 0.2% offset method (MMFX 2004). In order to mobilize this high strength, proper anchorage must be achieved; however, limited research has been conducted to extend current design code provisions to higher stress levels. The current database includes only 12 tests which

displayed bond failure at stresses in excess of 100 ksi. No tests have been reported with failure stresses in excess of 120 ksi which has been shown in previous research (El-Hacha and Rizkalla 2002) and will be shown in this research to be the yield strength of MMFX reinforcement when the 0.2% offset method is used.

Limited data exists on bond characteristics specifically for MMFX reinforcement. Ahlborn and DenHartigh (2002) indicated that MMFX reinforcement can be substituted as a one-to-one replacement for conventional A 615 Grade 60 reinforcement when considering bond. The expressions by Orangun, Jirsa, and Breen as well as the design provisions of ACI 318-99 and AASHTO Standard Specification provided conservative predictions of bond behavior for the 130 beam-end specimens used in their tests. However, the variables included in these tests were limited. Only No. 4 and No. 6 bars were studied. All tests included identical cover dimensions (1.5 in.) and were embedded in concrete of similar compressive strength (~5500 psi). Because the research was intended to be used only as a comparative study of MMFX and A 615 bond behavior, the bonded lengths chosen for the tests were not sufficient to develop the stresses in the upper stress range of MMFX reinforcement. Therefore, the conclusions of the research by Ahlborn and DenHartigh are limited to stresses at or below 60 ksi.

El-Hacha, El-Agroudy, and Rizkalla (2006) tested four beam-end specimens containing #4 or #8 MMFX bars and eight beam-splice specimens containing #6 or #8 MMFX bars. Data from the beam-end specimens indicated that the relationship between the splice length to bar diameter ratio and the stress in the MMFX bar transitions from nearly linear at low stresses to highly nonlinear at stresses in excess of 110 ksi. The results of the beam-splice specimens suggested that the nonlinear behavior of the MMFX bars above the reported proportional limit of 80 ksi significantly reduced the bond strength of the MMFX bars at high stresses. In agreement with the findings of Ahlborn

and DenHartigh; El-Hacha, El-Agroudy, and Rizkalla found that the ACI 318-05 design equation provides conservative estimates for splice failure stresses up to 80 ksi. Beyond 80 ksi, the design code equation becomes unconservative and must be modified.

CHAPTER 4

Experimental Program

4.1 BEAM-SPLICE TESTS

4.1.1 Test Matrix

The experimental program described herein is part of a joint investigation conducted by the University of Kansas, North Carolina State University, and the University of Texas at Austin. According to the original project proposal, each school would test 22 full scale beam splice specimens. Duplicate tests among pairs of schools were included in the test matrix to ensure consistency of results among researchers.

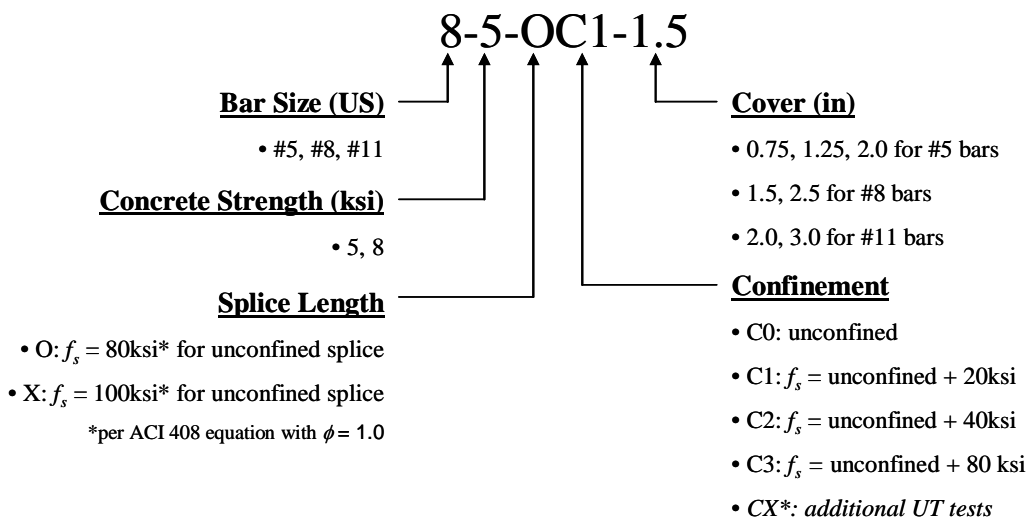
Test variables included bar size, concrete compressive strength, splice length, concrete cover, and amount of transverse reinforcement (confinement). The tests included three bar sizes – #5, #8, and #11 – and two concrete compressive strengths – 5000 psi and 8000 psi. The range of bottom cover values varied according to bar size. Cover values of 0.75 in., 1.25 in., and 2.0 in. were used for #5 specimens. Values of 1.5 in. and 2.5 in were used for #8 specimens; and values of 2.0 in. and 3.0 in. were used for #11 specimens. Splice lengths were chosen based on two target failure stress levels — 80 ksi and 100 ksi — when calculated according to the ACI 408 development length equation without consideration for transverse reinforcement or increased relative rib area and with the modification factor, ϕ , equal to 1.0.

The effect of transverse reinforcement was only investigated on the #8 and #11 specimens. For these bar sizes, three specimens were tested for each splice length. One specimen included an unconfined splice. The remaining two included varying levels of transverse reinforcement in the form of closed hoop shear ties. The spacing of the ties

was chosen to provide a 20 ksi or 40 ksi increase in predicted failure stress per the ACI 408 equation when compared to the unconfined splice of the same length. Due to a misinterpretation of confinement parameters during the design stage of the project, specimens from North Carolina State University contained double the transverse reinforcement necessary to provide the desired increases of 20 ksi and 40 ksi in failure stress. Therefore, the predicted increases in failure stresses for the confined splices tested at North Carolina State University were 40 ksi and 80 ksi over those of the unconfined splices. The effect of transverse reinforcement was not studied in the #5 specimens since they were intended to represent slabs where stirrups are rarely used.

At the University of Texas, an additional three beams not included in the original test matrix were tested to study the effect of concrete strength specifically. All test variables pertinent to bond except concrete strength were held constant between these beams containing 5000 psi concrete and a corresponding set of beams with a concrete strength of 8000 psi.

All of the test variables are represented in the standard specimen notation developed for this research program. A sample designation and the range of values for each parameter are shown below. The sample designation represents a specimen containing #8 bars embedded in 5000 psi concrete with 1.5 in. cover. The splice length is that which would result in a predicted failure stress of 80 ksi assuming the previous parameters, and the level of transverse reinforcement was calculated to provide a 20 ksi increase in failure stress over that of the unconfined splice, or 100 ksi.



The experimental test matrix for the three participating schools is given in Table 4-1. In this table, the standard specimen naming convention is used.

f'c	db	KU				NCSU				UT			
5 ksi	#5	Cover				Cover				Cover			
		3/4 in		1.25 in	2 in	3/4 in		1.25 in	2 in	3/4 in		1.25 in	2 in
		OC0		OC0						OC0		OC0	OC0
			XC0								XC0	XC0	
	#8	Cover				Cover				Cover			
			1.5 in	2.5 in			1.5 in	2.5 in			1.5 in	2.5 in	
			OC0,1,2				OC0,2,3				OC0,2		
			XC0,1,2				XC0,2,3				XC0,2		
											<i>OC0*,1*,2*</i>		
#11	Cover				Cover				Cover				
		2 in	3 in			2 in	3 in			2 in	3 in		
						OC0,2,3					OC0,1,2		
						XC0,2,3					XC0,1,2		
8 ksi	#8	Cover				Cover				Cover			
			1.5 in	2.5 in			1.5 in	2.5 in			1.5 in	2.5 in	
				OC0,1,2			OC0,2				OC0,1,2		
			XC0,1,2			XC0,2				XC0,1,2			
	#11	Cover				Cover				Cover			
			2 in	3 in			2 in	3 in			2 in	3 in	
		OC0,1,2					OC0,2,3						
		XC0,1,2					XC0,2,3						
Total		22				22				25			

Table 4-1: Experimental test matrix (duplicate tests bolded, tests not included in original matrix italicized)

Further discussion in this chapter will relate solely to the specimens and laboratory test setup for the research carried out by the University of Texas.

4.1.2 Specimen Design

Beams containing #8 and #11 bars included two splices of equal length located at mid-span of the beam. Side cover values were set equal to bottom cover values, and clear spacing between splices was set to twice the side cover values. These covers were chosen to create equal probability of failure by side splitting or face splitting.

To better represent the behavior of slabs, specimens containing #5 bars were wider, including four splices of equal length at mid-span of the beam. In these specimens, side covers were greater than bottom cover values as is typical in slab design. Clear spacing between splices remained equal to twice the side cover values.

Specimens were designed with sufficient strength to develop bar stresses in excess of the highest expected failure stress of the splices. #8 and #11 bar specimens were required to develop at least 150 ksi at the onset of concrete crushing. Since none of the #5 specimens contained transverse reinforcement, the requirements for design were relaxed. These specimens were designed to develop at least 120 ksi when the moment in the beams produced concrete crushing on the compression face.

Beam lengths were governed by available tie down points in the concrete strong floor at the University of Texas. The spacing of hydraulic rams ensured that the splices were completely within the constant moment region and that the required loads for failure were within the load carrying capabilities of the testing apparatus.

Beams were originally designed with the assumption that concrete at the extreme compression fiber reached the maximum usable strain value of 0.003 in/in simultaneous with the tension steel reaching the desired ultimate stress (150 ksi or 120 ksi). Distribution of concrete stress throughout the sections was estimated using the Whitney

stress block. Beam depths were chosen to satisfy strain compatibility. For design purposes, the stress-strain relationship for the MMFX reinforcement was taken as:

$$f_{MMFX} = 165 \cdot (1 - e^{-185 \cdot \epsilon_{MMFX}})$$

This stress-strain relationship was cited in a North Carolina State University research paper and was based on tension tests performed on MMFX reinforcing bars by several previous researchers (Dawood, *et al.* 2004).

After preliminary design, the depths of the #5 slab specimens were modified to a uniform depth of 12 in. to reduce the required amount of formwork. The depths of 8-8-XC0-1.5, 8-8-XC1-1.5, and 8-8-XC2-1.5 were also increased from 23 in. to 27 in. after specimen 8-8-OC2-1.5 nearly failed in flexure during its test.

Details of the specimen designs are given in Table 4-2. The general cross-sections for beam (#8 and #11) and slab (#5) specimens are shown in Figure 4-1 and Figure 4-2, respectively. An elevation view of the test specimens and the loading schematic is shown in Figure 4-3.

Specimen	Materials		Section		Splice	Cover			Comp. Reinf.		Transverse Reinforcement			Test Setup				
	Bar #	f'_c (ksi)	b (in)	h (in)	l_s (in)	cb (in)	cso (in)	$2 \cdot csi$ (in)	bar #	ct (in)	non-test area		test area	Span (ft)	ram spacing (ft)			
											Bar #	Spacing s_1 (in)	Spacing s_2 (in)					
5-5-OC0-3/4	5	5	13	12	33	0.75	1	2	5	1.5	3	5.0	N/A	12	5			
5-5-XC0-3/4					44													
5-5-OC0-1.25			35	12	18											1.25	3.75	7.5
5-5-XC0-1.25					25													
5-5-OC0-2			35	12	15											2	3.75	7.5
5-5-XC0-2					20													
8-5-OC0-1.5	8	5	10	27	47	1.5	1.5	3	8	1.5	4	8.0	N/A	16	6			
8-5-OC2-1.5					5.5													
8-5-XC0-1.5					N/A													
8-5-XC2-1.5					7.0													
8-5-OC0*-1.5					N/A													
8-5-OC1*-1.5					13.5													
8-5-OC2*-1.5			7.0															
8-8-OC0-1.5			8	10	23	40	1.5	1.5	3	8	1.5	4	8.5			N/A		
8-8-OC1-1.5						13.5												
8-8-OC2-1.5						7.0												
8-8-XC0-1.5						N/A												
8-8-XC1-1.5						18.5												
8-8-XC2-1.5	9.0																	
11-5-OC0-3	11	5	18	31	50	3	3	6	11	1.5	4	5.0	N/A	20	8			
11-5-OC1-3					8.0													
11-5-OC2-3					4.0													
11-5-XC0-3					N/A													
11-5-XC1-3					11.0													
11-5-XC2-3					5.5													

Table 4-2: Beam-splice specimen design details

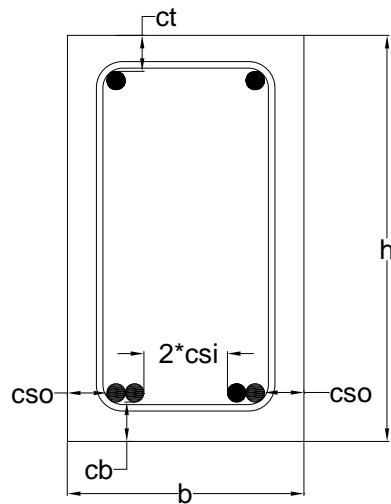


Figure 4-1: General cross-section for beam specimens (#8 and #11)

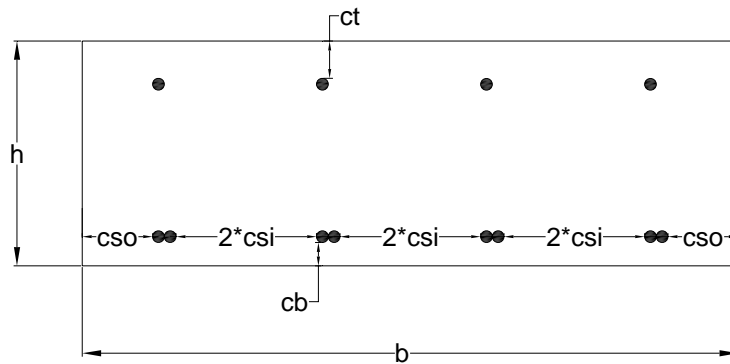


Figure 4-2: General cross-section for slab specimens (#5)

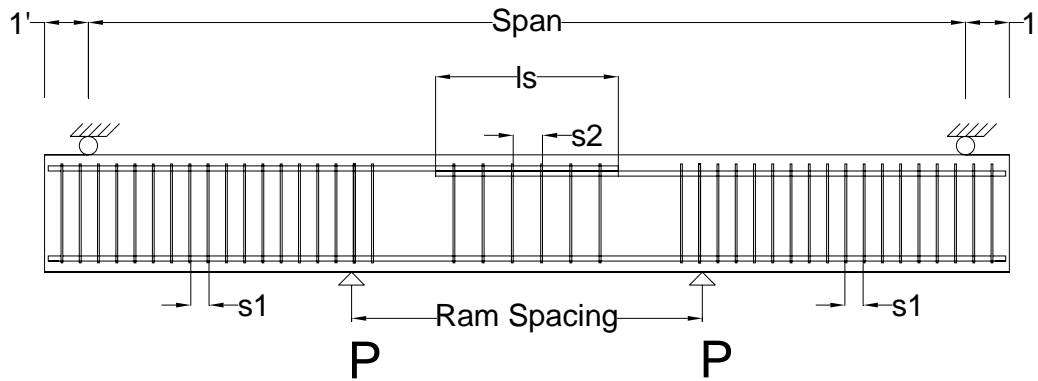


Figure 4-3: Elevation of test specimens and loading schematic

4.1.3 Specimen Fabrication and Instrumentation

All beam-splice specimens were fabricated and tested at the Ferguson Structural Engineering Laboratory at the University of Texas at Austin. Beams containing #8 and #11 bars were cast in groups according to splice length. In each group, only the amount of transverse reinforcement varied among the beams. A group of #8 specimens with the same splice length but varying amounts of transverse reinforcement is shown in Figure 4-4. Specimens containing #5 bars were cast in groups according to cover values. In

each group, only the splice length varied among the beams. A pair of specimens containing #5 bars with varying splice lengths is shown in Figure 4-5.



Figure 4-4: Varying levels of transverse reinforcement among a group of three specimens containing #8 bars



Figure 4-5: Varying splice length among a pair of specimens containing #5 bars

120 ohm electrical resistance foil strain gauges with a 5 mm gage length were applied to the spliced MMFX bars at the end of each splice. This location was chosen so that the maximum strains being developed in the spliced bars could be measured without interfering with the bond of the bars along the splice. The location of these strain gauges is shown on a confined #8 splice in Figure 4-6.

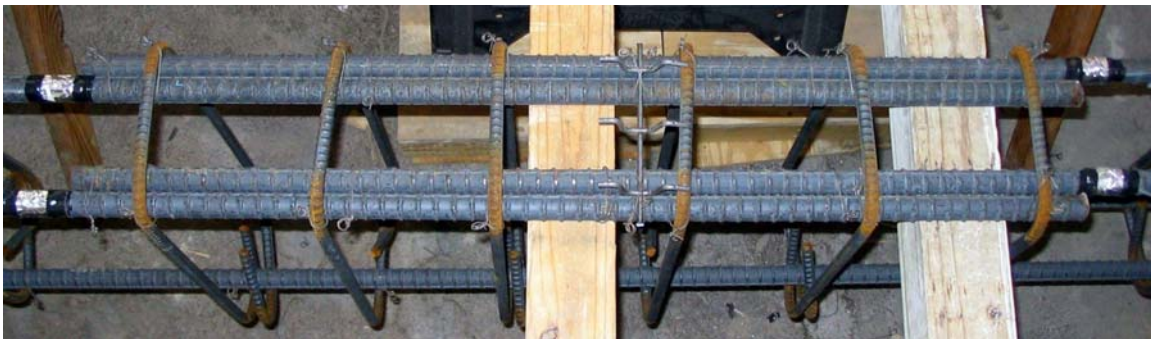


Figure 4-6: Confined #8 splices with strain gauges at the ends of the splices

Specimens were cast with the spliced bars at the bottom of the forms to prevent the adverse effects associated with top cast bars. Lifting inserts were cast into the top and bottom faces of the beams to allow the beams to be rotated and lifted in the inverted orientation for testing. Cover values were measured within the form prior to casting. When necessary, reinforcement cages were stiffened and/or supported laterally with additional reinforcement outside the testing area or with bar chairs in order to prevent movement of the cage during concrete placement.

Concrete was supplied by a local ready mix firm. Three standard mix designs were used throughout the course of testing. Mix design 1 was used for all specimens with 8000 psi concrete strength. Mix design 2 was used for specimens with 5000 psi concrete strength with the exception of 5-5-OC0-3/4 and 5-5-XC0-3/4 which used mix design 3. These two specimens required a special mix since the 1 in. course aggregate used in mix design 2 was too large for the 0.75 in. bottom and 1 in. side covers specified in these specimens. Details of the three concrete mixes are shown in Table 4-3.

Material	Designation	Mix		
		1	2	3
Cement	Type 1/11 ASTM C-150	510 lb	479 lb	388 lb
Fly Ash	Class C ASTM C 618	167 lb	85 lb	129 lb
Fine Aggregate	Concrete Sand ASTM C-33	1330 lb	1238 lb	1519 lb
Course Aggregate	1" ASTM #57, 3/8" ASTM #8	1" / 1801 lb	1" / 1962 lb	3/8" / 1602 lb
Water	TXDOT 421 Potable	27 gal.	30 gal.	30 gal.
Water Reducer	ASTM C494 Type A & F ASTM C494 Type B & D	2-6 oz./100cwt. 2-4 oz./100cwt.	2-6 oz./100cwt. 2-4 oz./100cwt.	2-6 oz./100cwt. 2-4 oz./100cwt.
Air Entrainment	ASTM C260	---	---	0.25-4 oz./100cwt.
Slump	---	7-8 in	3-6 in	6 in
Min. Compressive Strength	---	7000 psi	4000 psi	4000 psi

Table 4-3: Concrete mix proportions (per cubic yard)

4.1.4 Laboratory Test Setup and Testing Procedure

Standard 6 in. x 12 in. concrete cylinders were tested in accordance with ASTM C39 every seven days after casting until the concrete reached the desired compressive strength. At this time, the beam-splice specimens were tested.

The beams were loaded in four point bending in the inverted position to facilitate crack observation. For specimens containing #8 and #11 bars as well as for the two 13 in. wide specimens containing #5 bars, two hydraulic rams connected to the same pressure line created a near constant moment region in the center of the span by providing nearly identical load at two intermediate points along the beam. For the wider #5 specimens, this setup was modified to provide a more uniform load across the width of the slabs. Four hydraulic rams were used when testing these specimens, with two rams located at each line of loading.

As load was applied, the beams transferred end reactions through roller supports that reacted against built-up crossbeam sections comprised of back-to-back C10X30 channels. These crossbeams transferred load to the laboratory strong floor through high-strength threaded rods.

Load cells measured the applied load at each hydraulic ram, and a pressure transducer provided back-up data. A linear variable displacement transducer (LVDT) measured midspan deflection throughout the test. Strains in the spliced MMFX bars were monitored by strain gauges applied to the bars at the end of each splice as described previously.

The typical laboratory test setup for #8 and #11 specimens and for the 13 in. wide #5 specimens is pictured in Figure 4-7. The typical laboratory test setup for the wider #5 slab specimens is pictured in Figure 4-8.

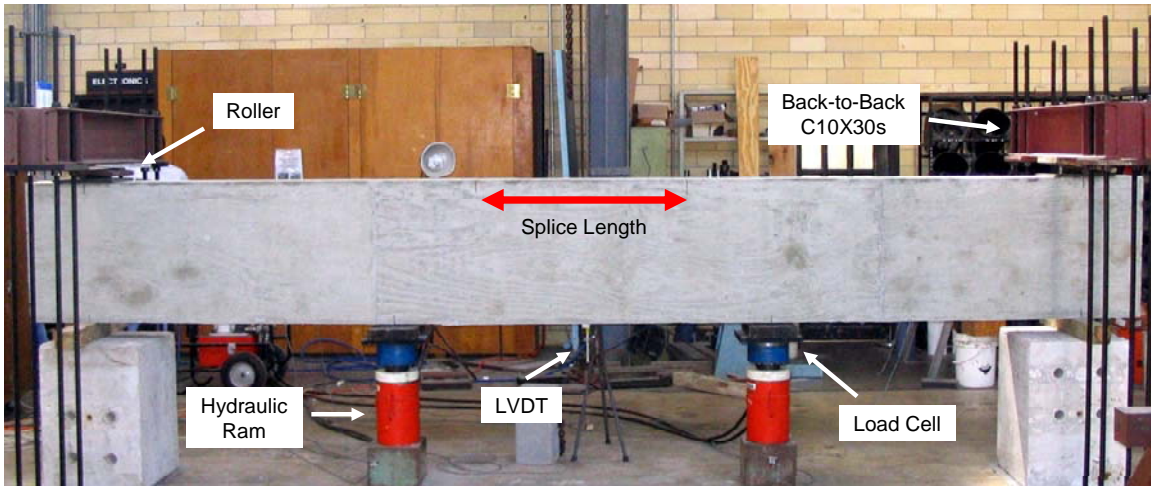


Figure 4-7: Typical laboratory test setup for narrow splice specimens

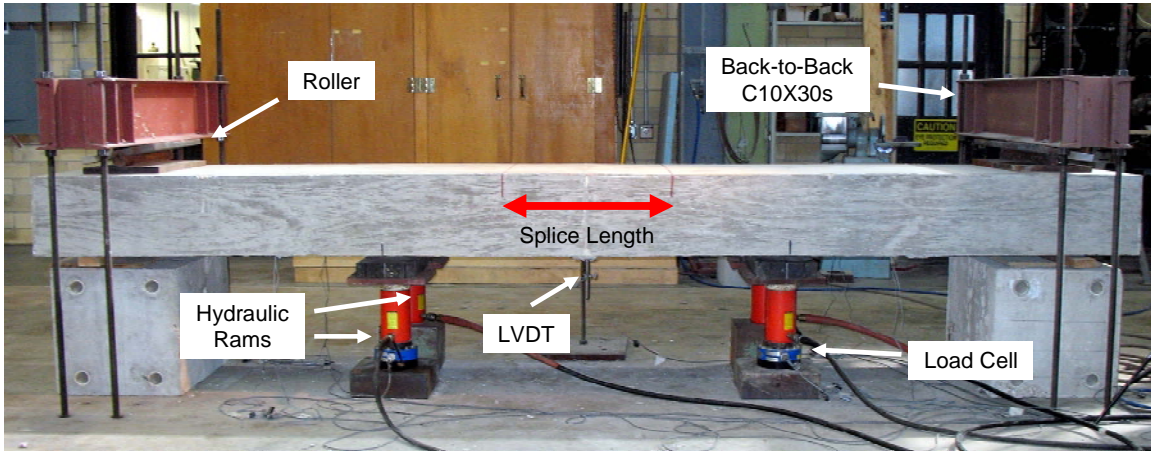


Figure 4-8: Typical laboratory test setup for wide splice specimens

Beams were loaded up to the cracking load. At this point, the load was held constant while cracks were traced and crack widths at the ends of the splice and in the center of the splice were measured with a crack comparator. Additional load was added in varying increments depending on the capacity of the beam being tested. These increments were typically 2.5 kip, 5 kip, and 10 kip for specimens containing #5, #8, and #11 bars, respectively. After each load increment, new cracks were traced and crack widths were again measured in the same locations as at the cracking load.

Due to the brittle and explosive nature of splice failures, it was deemed unsafe to approach the beams as they neared the anticipated failure load; therefore, cracks were no longer marked or measured near the expected failure load. The point at which these measurements were ceased varied from beam to beam. At this point, load was increased until failure of the splices was achieved and the beams lost all load carrying capacity. The peak load was recorded as the failure load.

After failure, the spalled concrete cover was examined to confirm that cover values matched those recorded prior to casting.

4.2 REINFORCEMENT TESTS

MMFX Steel Corporation of America provided all tension reinforcement for this project. All bars of a given size were rolled from the same heat to ensure consistent behavior among bars. They were then distributed to the three participating research universities as required.

In order to accurately relate steel strains observed in laboratory tests to corresponding stress values, a series of tension tests were performed on a sample of #5, #8, and #11 MMFX reinforcement. Although North Carolina State University reported a stress-strain relationship based on earlier research, additional tension tests were required for this project since the stress-strain relationship of steel reinforcement can vary from heat to heat.

4.2.1 Specimen Description

Reinforcement samples measuring approximately 3 ft. in length were used for tension testing. This length provided sufficient area for gripping at the ends of the specimens and enough length to attach an 8 in. gage extensometer. Samples of each bar size were obtained from a single bar due to the limited number of excess bars provided to

the University of Texas. This was not believed to affect the results since all bars of a given size were rolled from the same heat and should display almost identical behavior.

4.2.2 Laboratory Test Setup and Testing Procedure

Small notches spaced approximately 8 in. apart were made in the reinforcement samples in order to ensure that the knife edges of an 8 in. extensometer would not slip and to determine the total elongation upon completion of the test. The exact spacing of these notches was measured with calipers, and this length was used as the actual gage length in calculations. The typical test setup is shown in Figure 4-9.

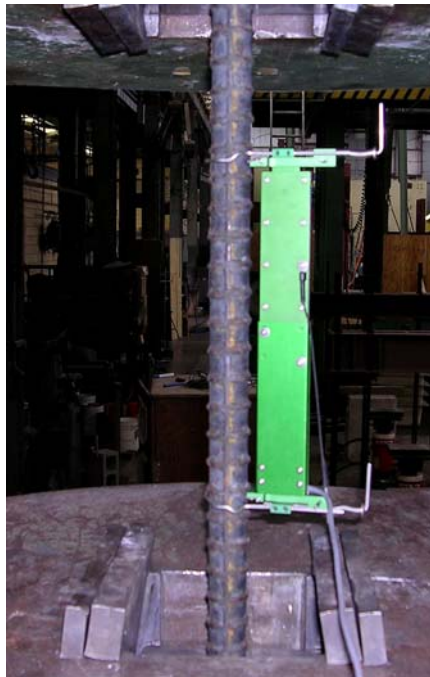


Figure 4-9: Typical test setup for reinforcement tension tests

A 600 kip capacity testing machine applied tension to each bar at a rate which produced a relatively constant increase in bar stress (approximately 15 ksi/min) in the initial linear stage of elongation. As each specimen entered its nonlinear range, the rate of stress increase decreased accordingly. The test was allowed to continue without

interference until the specimen had experienced 3.5-4.0% elongation. At this point, the application of load was temporarily stopped to remove the extensometer. The test then resumed until the bar ruptured.

After each test, the two pieces of the ruptured bar were fit together along the fracture surface; and the separation of the notches was again measured with calipers so that total elongation could be calculated.

CHAPTER 5

Experimental Results

5.1 REINFORCEMENT TESTS

5.1.1 #5 Bars

Four #5 bars were tested in tension according to the procedure described in Chapter 4. Four bars were chosen due to the amount of scatter in the data from test to test. In Figure 5-1, the stress-strain curves are plotted for the four tension tests as well as an exponential curve fit for the data obtained using the program Sigma Plot. Details of each tension test are shown in Table 5-1. In these tests, failure never occurred within the gage length notched into the bars prior to testing so measurements of total elongation do not accurately represent the ductility and necking observed during the tests.

The #5 MMFX bars maintained a linear stress-strain relationship with a modulus of approximately 28,400 ksi to their proportional limit of 80-90 ksi as indicated in Figure 5-1. At this point, the stress-strain curve became nonlinear. At a strain of about 0.02, the bars reached a stress of 155 ksi. Additional strain beyond this point resulted in very little additional bar stress.

The MMFX reinforcement did not display a well defined yield point like that observed in traditional Grade 60 reinforcement. A comparison of the two stress-strain relationships is shown in Figure 5-2. Using the 0.2% offset method, the approximate yield stress of #5 MMFX reinforcement used in this research program was 122 ksi. This is shown in Figure 5-3. Maximum stresses attained by the four bars were consistently between 160-161 ksi as indicated in Table 5-1.

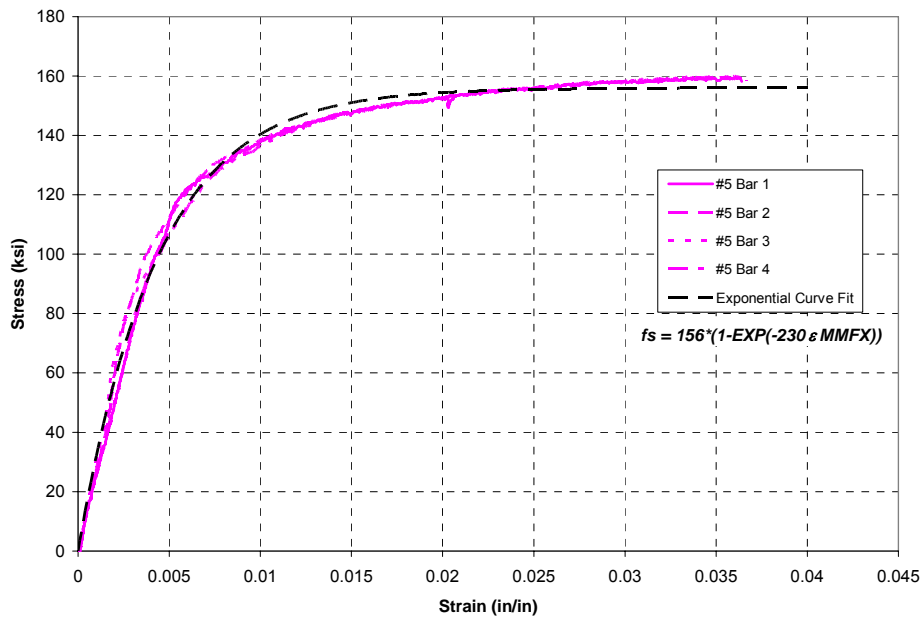


Figure 5-1: Stress-strain relationship for #5 MMFX bars (End of plot indicates removal of extensometer)

Results of Tension Tests on #5 MMFX Bars					
Test	l_o (in)	l_f (in)	ϵ_{tot} (in/in)	P_{max} (kip)	f_{max} (ksi)
Bar 1	8.292	8.679	0.0467*	49.6	160.0
Bar 2	8.310	8.685	0.0451*	49.7	160.3
Bar 3	8.278	8.650	0.0449*	49.9	161.0
Bar 4	8.310	8.650	0.0409*	49.9	161.0
Average	---	---	---	49.8	160.6

* Bar rupture occurred outside gage length

Table 5-1: Summary of results for #5 MMFX tension tests

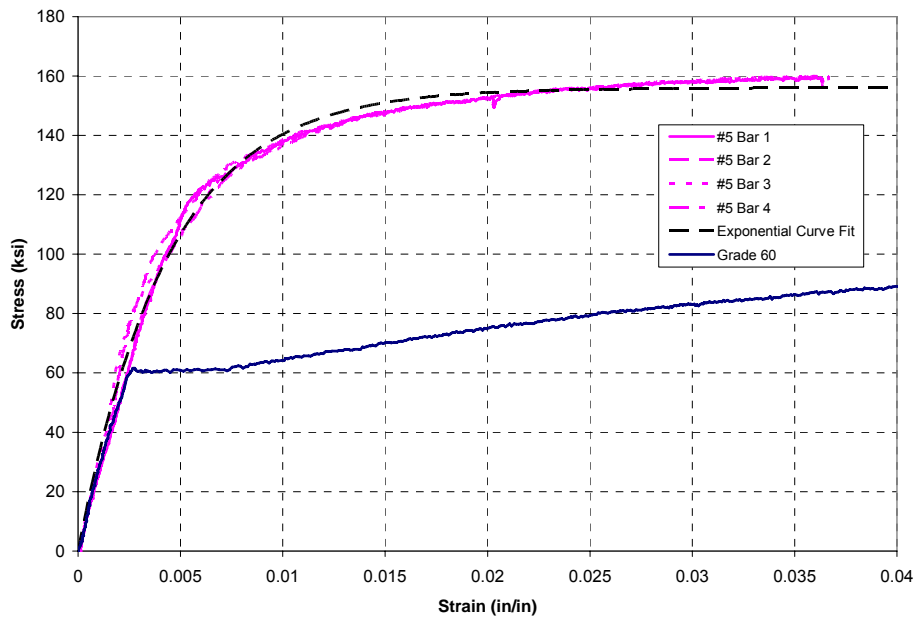


Figure 5-2: Comparison of MMFX and Grade 60 stress-strain behavior

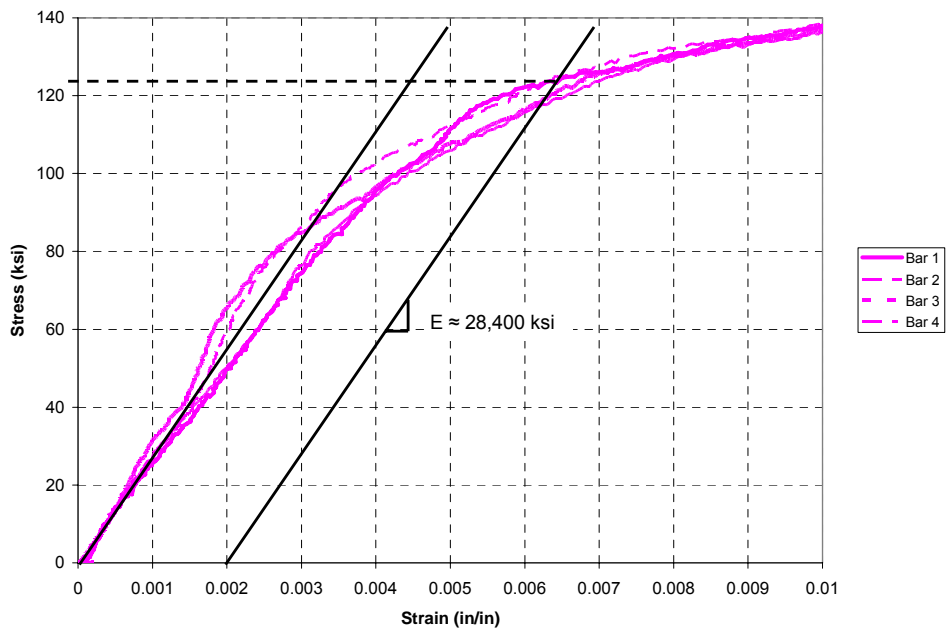


Figure 5-3: 0.2% offset yield - #5 MMFX bars

The #5 MMFX bars displayed some ductility prior to rupture. Necking coupled with a gradual reduction in load carrying capacity was observed before failure of all specimens. A post-failure picture of the #5 bars is provided in Figure 5-4.



Figure 5-4: #5 MMFX reinforcement specimens after testing

5.1.2 #8 Bars

Two #8 MMFX bars were tested in tension. Additional tests were unnecessary due to the consistency of the results between the first two tests. As shown in Figure 5-5, the stress-strain behavior of the #8 MMFX bars was nearly identical to that displayed by the #5 MMFX bars. A maximum stress between 161 ksi and 162 ksi for both #8 bars is reported in Table 5-2. Measurements of total elongation again underestimate the ductility exhibited by the bars during testing since both failures occurred outside the gage length marked prior to testing.

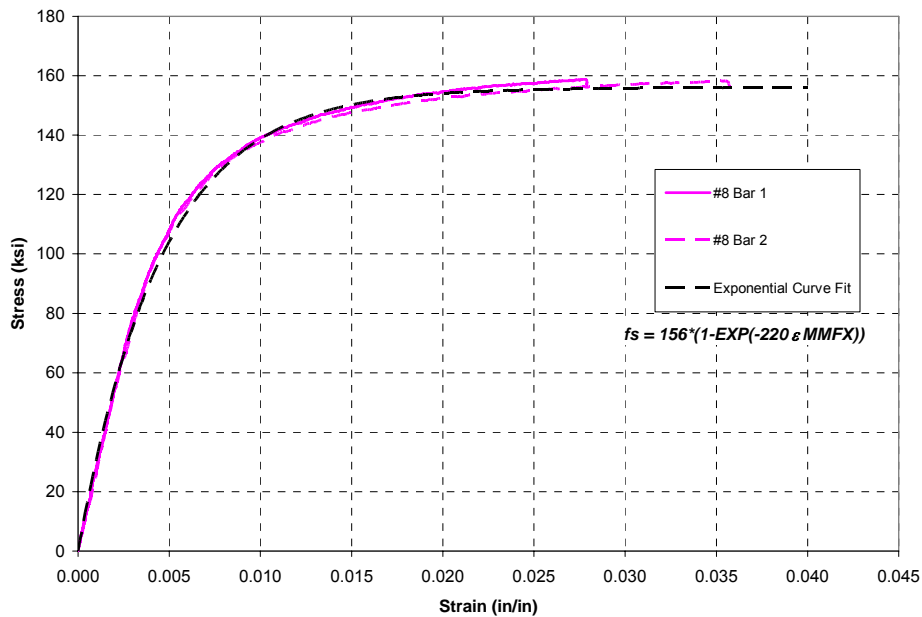


Figure 5-5: Stress-strain relationship for #8 MMFX bars (End of plot indicates removal of extensometer)

Results of Tension Tests on #8 MMFX Bars					
Test	l_o (in)	l_f (in)	ϵ_{tot} (in/in)	P_{max} (kip)	f_{max} (ksi)
Bar 1	8.110	8.440	0.0407*	127.7	161.6
Bar 2	8.150	8.570	0.0515*	127.8	161.8
Average	---	---	---	127.8	161.7

* Bar rupture occurred outside gage length

Table 5-2: Summary of results for #8 MMFX tension tests

The yield stress of the #8 MMFX bars was approximately 121 ksi when using the 0.2% offset method as shown in Figure 5-6. The initial modulus of approximately 28,000 ksi is also shown in this figure. Post-failure pictures of the #8 MMFX bars are provided in Figure 5-7. Again, necking and a gradual reduction in load capacity were witnessed prior to failure of both specimens.

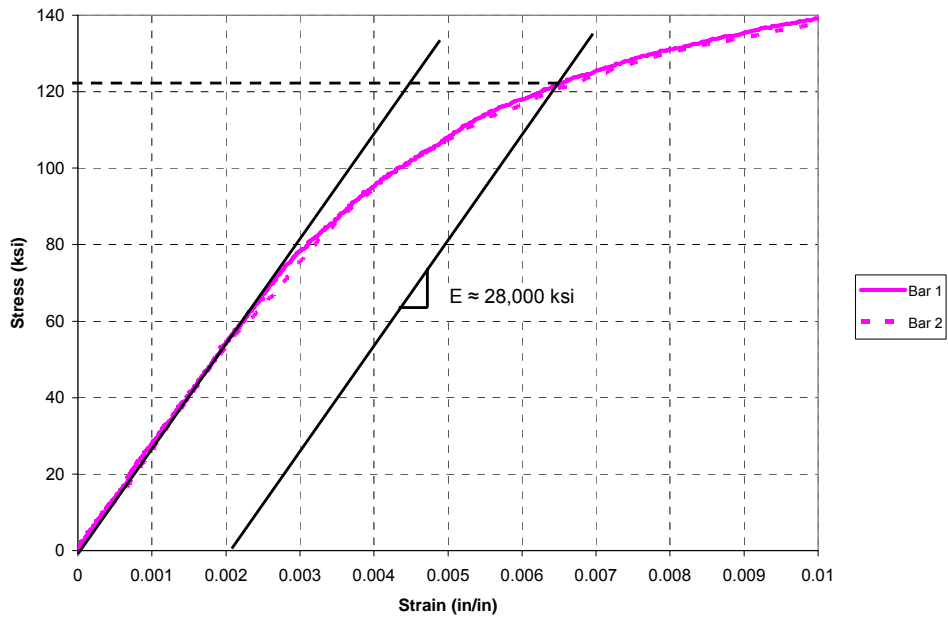


Figure 5-6: 0.2% offset yield - #8 MMFX bars



Figure 5-7: #8 MMFX reinforcement specimens after testing

5.1.3 #11 Bars

Three #11 bars were tested in tension. The stress-strain behavior for the three specimens is shown in Figure 5-6. While the general shape of the stress-strain curve for the #11 bars was the same as that for the #5 and #8 bars, the #11 bars displayed a higher initial modulus and strength than the bars of smaller size. The modulus of the #11 bars

was approximately 30,500 ksi as shown in Figure 5-9. Results shown in Table 5-3 indicate that the tensile capacity of the #11 bars was about 169 ksi which was 7-8 ksi higher than the ultimate stresses attained by the #5 and #8 bars.

All of the #11 specimens failed within the gage length that was marked prior to testing. As a result, the elongations listed in Table 5-3 are significantly higher than those reported for the #5 and #8 bars. The values shown for the #11 specimens are more representative of the actual ductility displayed by all sizes of MMFX bars since they include the substantial deformations experienced in and around the region of necking.

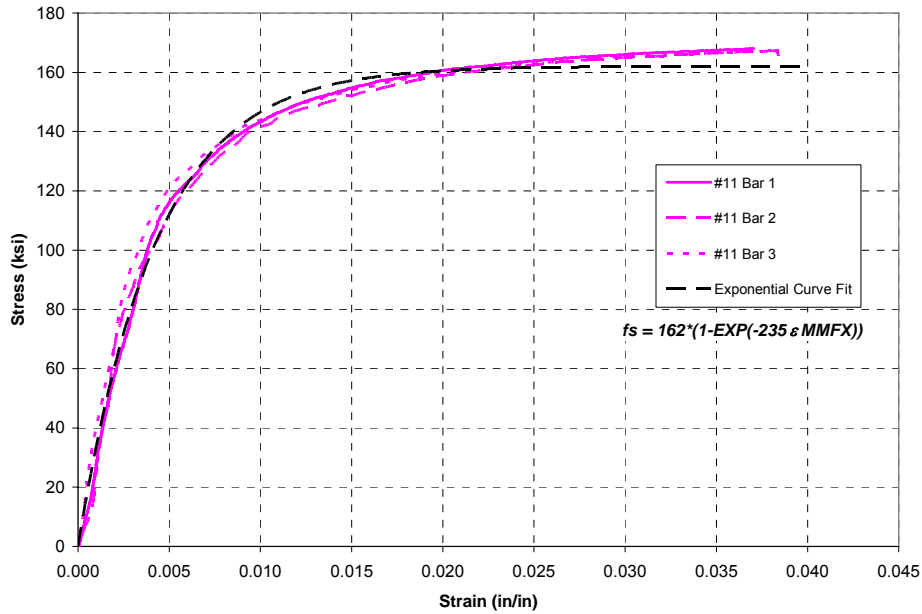


Figure 5-8: Stress-strain relationship for #11 MMFX bars (End of plot indicates removal of extensometer)

Results of Tension Tests on #11 MMFX Bars					
Test	l_o (in)	l_f (in)	ϵ_{tot} (in/in)	P_{max} (kip)	f_{max} (ksi)
Bar 1	8.345	9.243	0.1076	264.5	169.6
Bar 2	8.249	9.265	0.1232	263.4	168.8
Bar 4	8.255	9.294	0.1259	262.8	168.5
Average	---	---	0.1189	263.6	169.0

* Bar rupture occurred outside gauge length

Table 5-3: Summary of results for #11 MMFX tension tests

The data for the #11 bars during initial loading varied from bar to bar, but the yield stress of the #11 MMFX bars was about 122 ksi when using the 0.2% offset method as shown in Figure 5-9. Post-failure pictures of the #11 MMFX bars are shown in Figure 5-10.

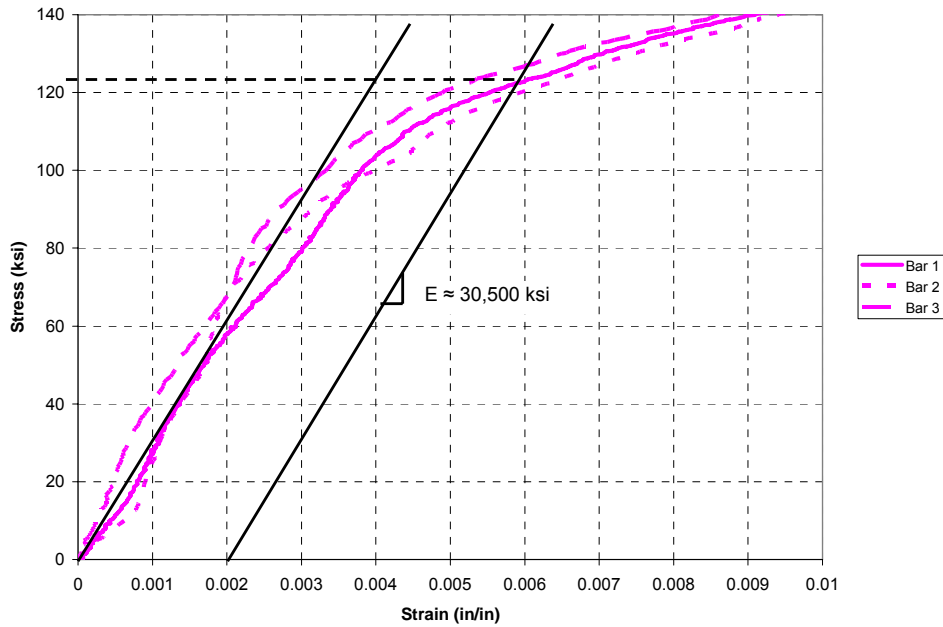


Figure 5-9: 0.2% offset yield - #11 MMFX bars

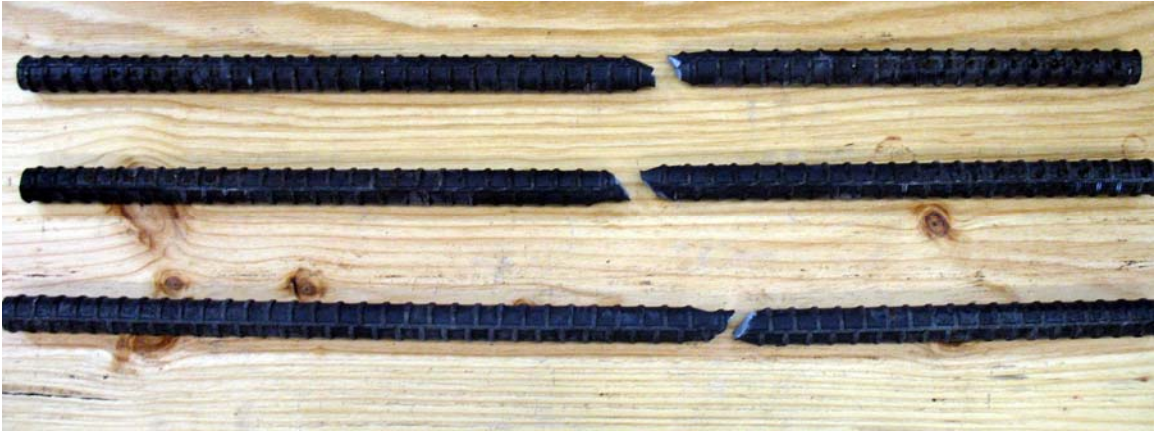


Figure 5-10: #11 MMFX reinforcement specimens after testing

5.2 BEAM-SPLICE TESTS

Forty-five beam-splice tests have been completed at the time of this writing. This number includes 25 tests conducted by the University of Texas, 17 tests conducted by North Carolina State University, and 3 tests conducted by the University of Kansas. The results of the tests conducted at the University of Texas are presented in Section 5.2.1. The results of tests conducted at the other two participating universities are presented in Section 5.2.2.

5.2.1 Tests Conducted at the University of Texas

The behavior and results of tests conducted on splices not confined by transverse reinforcement are outlined in Section 5.2.1.1. The behavior and results of splices confined by transverse reinforcement are covered in Section 5.2.1.2. The test results are separated because of the significant differences in behavior and ultimate capacity displayed by unconfined and confined splices.

5.2.1.1 *Splices not Confined by Transverse Reinforcement*

5.2.1.1.1 Behavior

Unconfined beam-splice specimens remained uncracked until stresses at the extreme tension fiber reached the maximum tensile capacity of the concrete. Estimating cracking load based on a maximum tensile capacity $f_{cr} = 7.5\sqrt{f_c}'$ provided reasonably accurate predictions. Within the pre-cracking stage of loading, all test specimens were less stiff than predicted through analysis. This discrepancy was likely due to microcracking present in the specimens prior to testing.

Flexural cracks directly above the loading points were the first cracks to form. In many tests, one or more additional flexural cracks formed between the load points and the ends of the splices. Flexural cracks rarely extended into the splice region at the initial cracking load.

At the cracking load, stresses in the MMFX steel reinforcement immediately increased to carry the tensile forces in the beam. The slope of the load-deflection plot also reduced due to the lower effective moment of inertia of the beam. Unlike during the pre-cracking stage of loading, the stiffness of the beams after cracking aligned well with the calculated stiffness. These phenomena can be seen in the typical bar stress-load and load-deflection plots shown in Figure 5-11 and Figure 5-12, respectively.

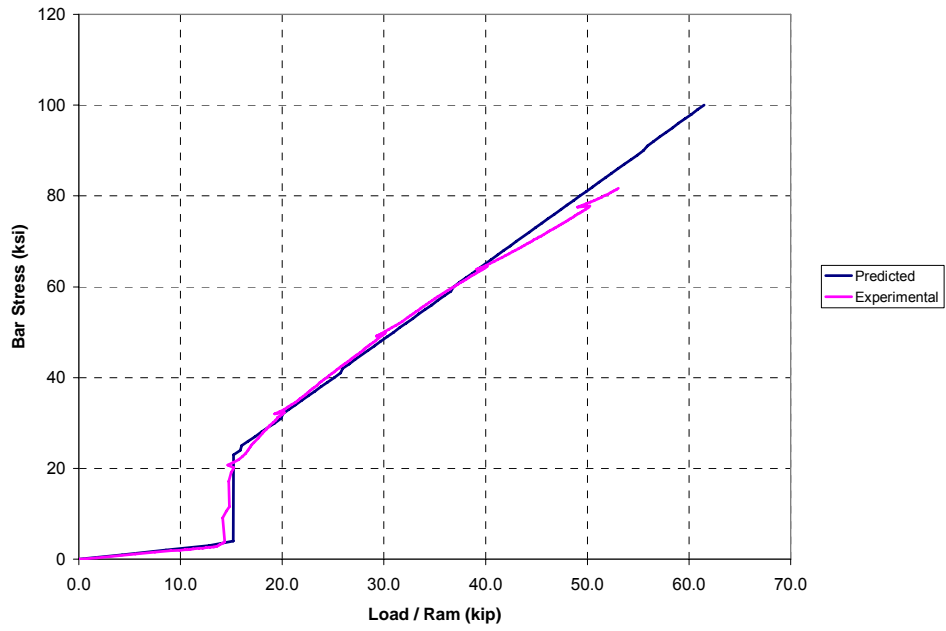


Figure 5-11: Typical bar stress-load plot for unconfined specimen (8-8-XC0-1.5)

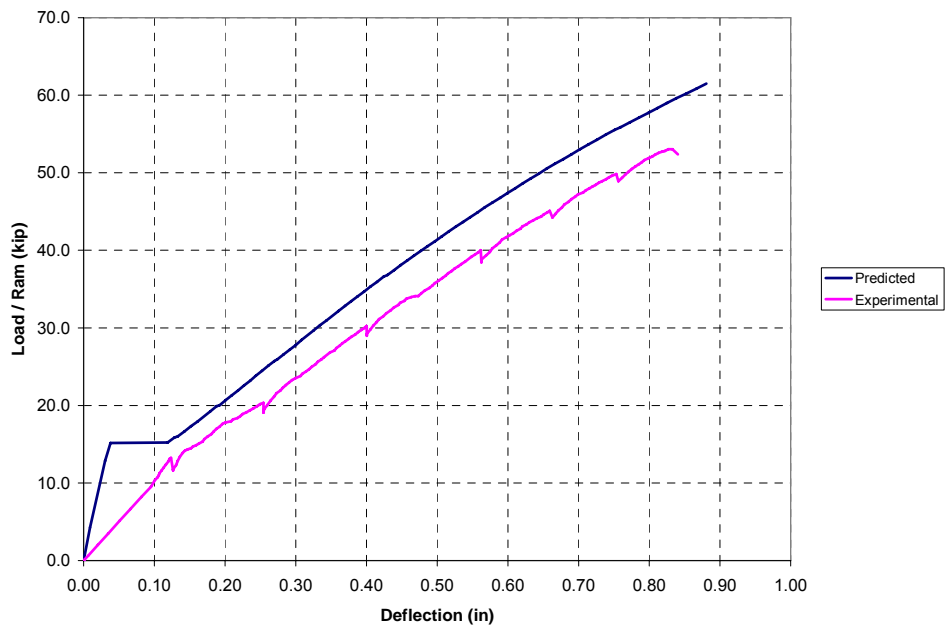


Figure 5-12: Typical load-deflection plot for unconfined specimen (8-8-XC0-1.5)

The application of additional load resulted in the formation of additional flexural cracks along the shear span of the beam and within the splice region. Flexural cracks also tended to form directly above the ends of each splice. Cracks in the shear span appeared at regular intervals and were usually located above stirrups. Shear cracks began to develop between the loading points and the supports as the applied shear exceeded the shear capacity of the concrete alone. A typical unconfined splice specimen in the early stages of loading is shown in Figure 5-13.



Figure 5-13: Cracking of typical unconfined specimen at early loading stages

As testing progressed, the cracks directly above the splice ends began to open at a rate greater than that of the flexural cracks along the remainder of the beam. Eventually, longitudinal face splitting cracks above the spliced bars began to form at the ends of the splices. This marked the first indication of impending failure at the splice. Specimens typically began to show longitudinal cracks in the splice region when the maximum stress in the spliced MMFX bars reached 40-50 ksi; however, these cracks were initiated at stresses as low as 35 ksi in specimen 11-5-OC0-3 and at stresses as high as 68 ksi in specimen 5-5-XC0-1.25. Longitudinal cracks were not observed in specimens 5-5-OC0-2 and 5-5-XC0-2, but this may be due to the fact that observations on these specimens

ceased well before failure. A typical cracking pattern along the splice in unconfined specimens at the onset of longitudinal splitting is shown in Figure 5-14.

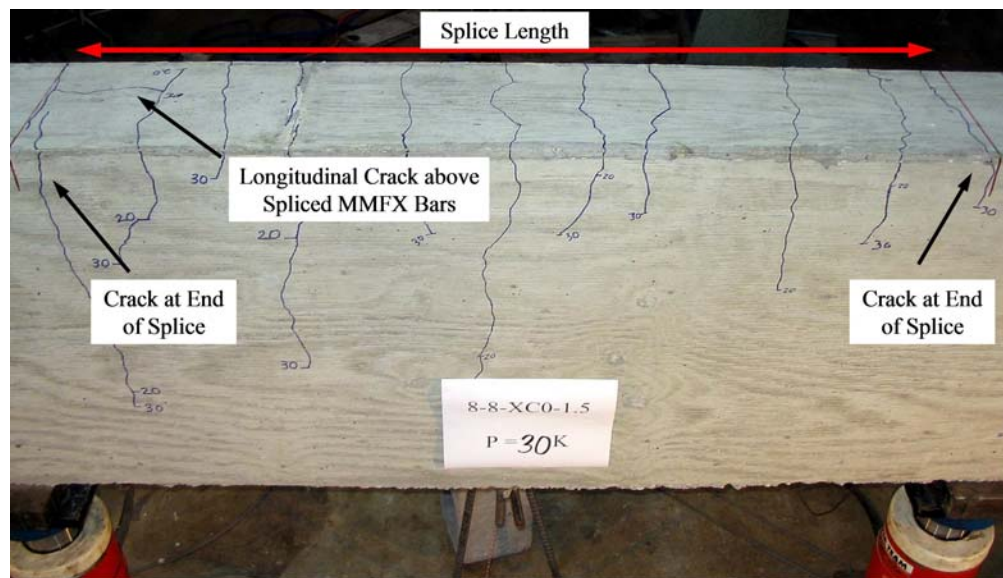


Figure 5-14: Cracking of typical unconfined splice at onset of longitudinal splitting

Near the failure load, the longitudinal face splitting cracks progressed from the ends of the splices toward the middle of the splices. The extent that these cracks propagated prior to failure varied from specimen to specimen. At this point, longitudinal side splitting cracks also began to form. These cracks initiated at the end of the splices at a depth equal to the depth of the spliced bars within the member. Similar to the face splitting cracks, the side splitting cracks progressed from the ends of the splices toward the center of the splices. The length of propagation varied from specimen to specimen. The cracking of an unconfined splice near failure is shown in Figure 5-15. Immediately prior to failure, the widths of the flexural cracks above the ends of the splices increased sharply as shown in Figure 5-16. Throughout the tests, the flexural cracks within the splice length remained small since this region contained double the amount of steel

present in other portions of the beam. The difference in crack widths at the ends of the splices and in the middle of the splices is highlighted in Figure 5-16.

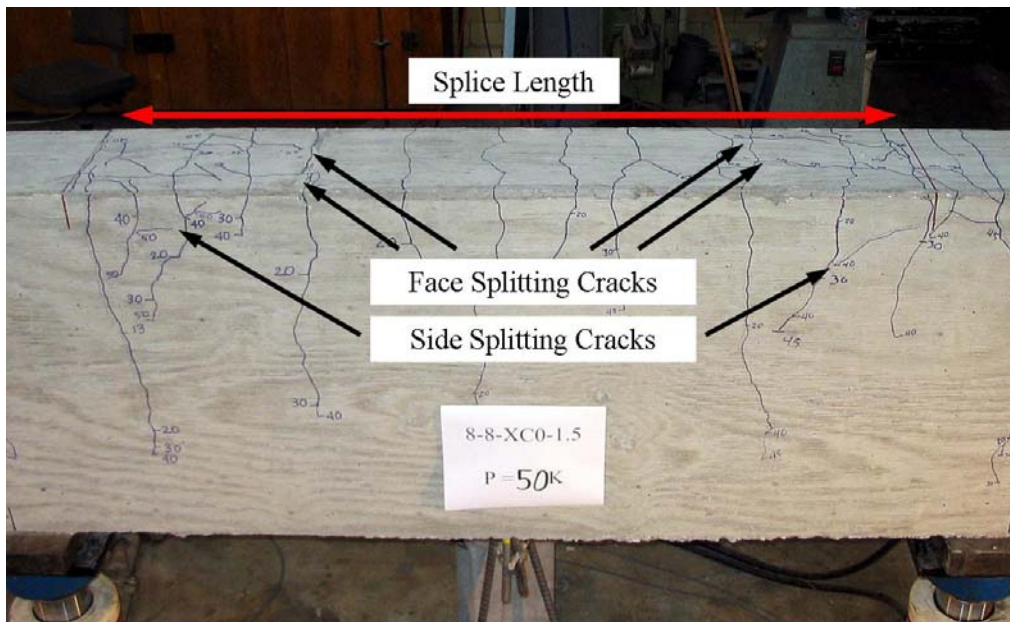


Figure 5-15: Cracking of typical unconfined splice near failure

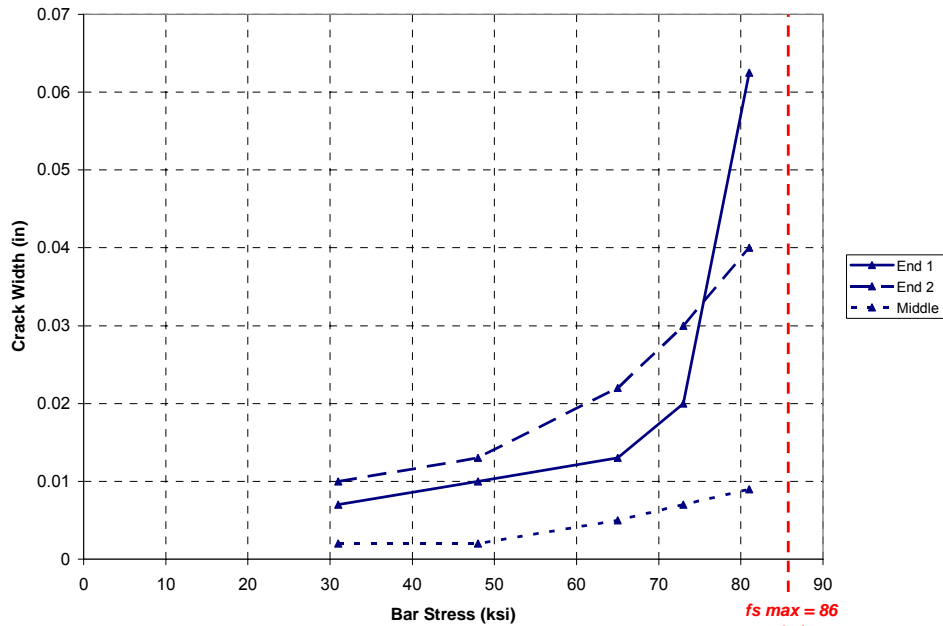


Figure 5-16: Measured crack widths for typical unconfined splice (8-8-XC0-1.5)

Failure of the splice was signaled by explosive spalling of the concrete cover along at least half of the splice length and complete and immediate loss of load carrying capacity of the beam. Since most unconfined splices failed with the MMFX bars developing stresses of 75-90 ksi, the reinforcement in the unconfined specimens did not reach strains high enough to provide visual warning of failure through the development of large deflections. Typical unconfined specimens maintained a linear load-deflection relationship from initial cracking to failure. A picture of an unconfined specimen at failure is shown in Figure 5-17. A picture of an unconfined splice after failure is provided in Figure 5-18.



Figure 5-17: Unconfined splice at failure

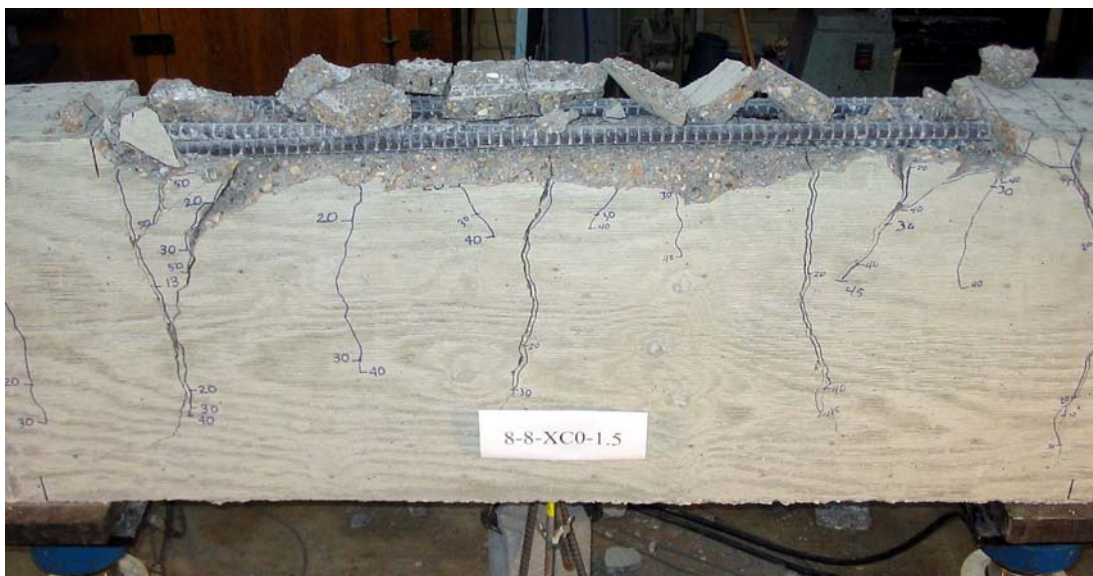


Figure 5-18: Unconfined splice after failure

The #5 beam-splice tests displayed noticeably different behavior than that of other unconfined tests due to their four splice design and due to the large ratio of maximum cover to minimum cover in the wider specimens. In all of the #5 specimens, the exterior splices failed before the interior splices. This phenomenon was clearly visible during

testing of the narrow #5 specimens (5-5-OC0-3/4, 5-5-XC0-3/4) and one wide #5 specimen (5-5-XC0-1.25). In the narrow specimens, the interior splices failed almost simultaneously with the exterior splices. In specimen 5-5-XC0-1.25, the splices failed progressively, with one exterior splice failing a few seconds after the first exterior splice and the two interior splices failing shortly after that. Although the incremental failure of splices was not obvious during testing for the remainder of the #5 specimens, strain gauge readings suggest that this type of failure was common. A bar strain vs. load plot for a four-splice test is shown in Figure 5-19.

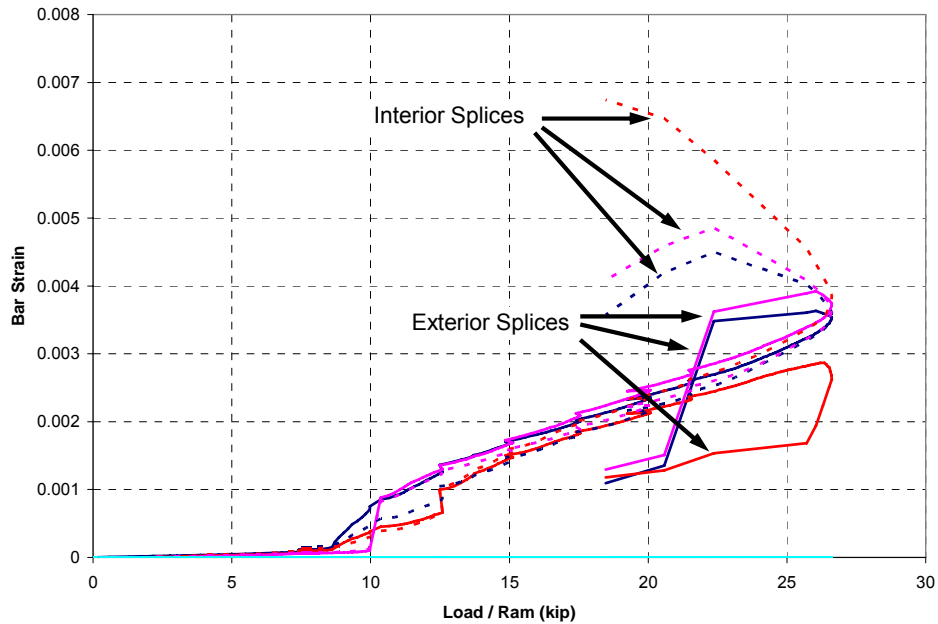


Figure 5-19: Bar strain vs. load for 5-5-OC0-1.25 highlighting initiation of failure by exterior splices (Gauges on bar 4 malfunctioned during this test)

The wide #5 specimens also did not display the typical face and side split failure observed in the remainder of the unconfined splices. The large side covers and bar spacings in relation to bottom covers promoted a “V-notch” failure mode. No evidence

of side splitting appeared before failure in any of the wide #5 specimens, and only one side split was observed after failure (5-5-XC0-2). Face splitting cracks were observed during testing in all of the wide specimens. After failure, face splitting cracks were present along the full length of all exterior splices; however, face splitting did not always propagate along the full length of the interior splices. This may be an indication of a rapid pullout of the interior spliced bars at the time that force was transferred from the failed exterior splices.

In all of the wide #5 specimens, failure was less violent than described for the typical unconfined splice. No loss of concrete cover occurred in these specimens; and due to the lack of horizontal splitting through the section, the cover could not be easily removed after failure. A wide #5 specimen after failure is pictured in Figure 5-20.

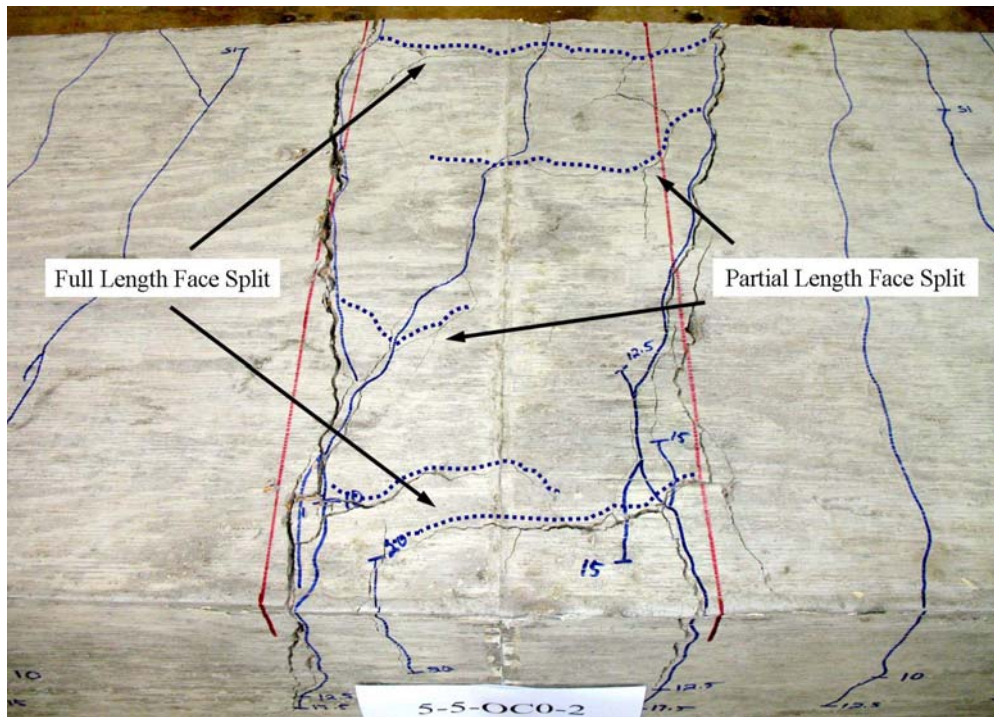


Figure 5-20: 5-5-OC0-2 after failure

5.2.1.1.2 Failure Stresses and Crack Widths

Failure stresses for all specimens were calculated based on the applied loads at the time of splice failure. Stresses in the spliced MMFX bars were determined using the ACI 408 standard moment-curvature method in which internal stresses are calculated through cracked section analysis. In the analyses, the distribution of concrete stresses was approximated using Hognestad's parabola which is defined by the relationship

$$f_c = -f_c' \left[2 \left(\frac{\varepsilon_{cf}}{\varepsilon_c'} \right) - \left(\frac{\varepsilon_{cf}}{\varepsilon_c'} \right)^2 \right]$$

where:

$$\varepsilon_c' = -\varepsilon_o$$

$$\varepsilon_o = \frac{2f_c'}{E_{ct}}$$

$$E_c = 57000\sqrt{f_c'}$$

f_c' = concrete compressive strength

ε_{cf} = concrete strain

f_c' , ε_{cf} , ε_c' are negative quantities

MMFX bar stresses were calculated using the stress-strain relationships derived from the tension tests described previously. For simplicity, the stress-strain behavior of the #5 bars was assumed to be identical to that of the #8 bars. The difference in stress-strain behavior between the #11 bars and the #5 and #8 bars warranted the use of a different stress-strain relationship. The following relationships were used in the determination of bar stresses.

$$\text{\#5 and \#8 Bars: } f_s = 156 \cdot (1 - e^{-220\varepsilon_s})$$

$$\#11 \text{ Bars: } f_s = 162 \cdot (1 - e^{-235\epsilon_s})$$

Calculated failure stresses based on the ACI 408, ACI 318, and AASHTO LRFD development length equations (Chapter 3) were computed for comparison with the test values. Each equation was solved for f_y and then f_y was replaced by the calculated failure stress f_s . The modification factor, ϕ , for the ACI 408 equation was taken as 1.0 since the equation was evaluated as a best fit expression in this research program. The respective bar stress limits of 80 ksi and 75 ksi for the ACI 318 and AASHTO equations were not applied so that the applicability of these design equations could be investigated at high bar stresses. As discussed in Chapter 3, the difference in purpose should be considered when comparing calculated stresses produced by the ACI 408, ACI 318, and AASHTO equations.

The results of the tests performed on unconfined splices at the University of Texas are tabulated in Table 5-4. As-built cover dimensions and concrete strengths are also shown.

Specimen	School	f'_c (psi)	l_s (in)	db (in)	c_{so} (in)	c_{si} (in)	cb (in)	s_2 (in)	Test f_s (ksi)	Calculated f_s (ksi)		
										ACI 408	ACI 318	AASHTO
8-8-OC0-1.5	UT	8300	40	1.00	1.60	1.40	1.50	N/A	80	82	92	100
8-5-OC0*-1.5	UT	5200	40	1.00	1.55	1.45	1.50	N/A	72	72	75	93
8-8-XC0-1.5	UT	7800	54	1.00	1.50	1.50	1.50	N/A	86	100	127	135
8-5-OC0-1.5	UT	5000	47	1.00	1.55	1.45	1.50	N/A	74	81	86	107
8-5-XC0-1.5	UT	4700	62	1.00	1.50	1.50	1.50	N/A	82	98	113	137
11-5-OC0-3	UT	5000	50	1.41	3.25	2.88	2.75	N/A	75	77	82	57
11-5-XC0-3	UT	5400	67	1.41	3.13	3.00	2.75	N/A	84	98	114	80
5-5-OC0-3/4	UT	5200	33	0.625	1.00	1.00	0.75	N/A	80	81	108	132
5-5-XC0-3/4	UT	5200	44	0.625	1.00	1.00	0.75	N/A	91	101	144	176
5-5-OC0-1.25	UT	5200	18	0.625	3.50	3.75	1.25	N/A	88	79	87	72
5-5-XC0-1.25	UT	5200	25	0.625	3.50	3.75	1.25	N/A	110	101	120	100
5-5-OC0-2	UT	5700	15	0.625	3.50	3.75	2.00	N/A	97	86	75	60
5-5-XC0-2	UT	5700	20	0.625	3.50	3.75	2.00	N/A	120	107	101	80

Table 5-4: Summary of results for UT unconfined tests

Measured end-of-splice crack widths for all unconfined specimens tested at the University of Texas are plotted in Figure 5-21. Mid-splice crack widths were not included in this plot since these cracks remained significantly smaller than the end-of-splice cracks for all tests.

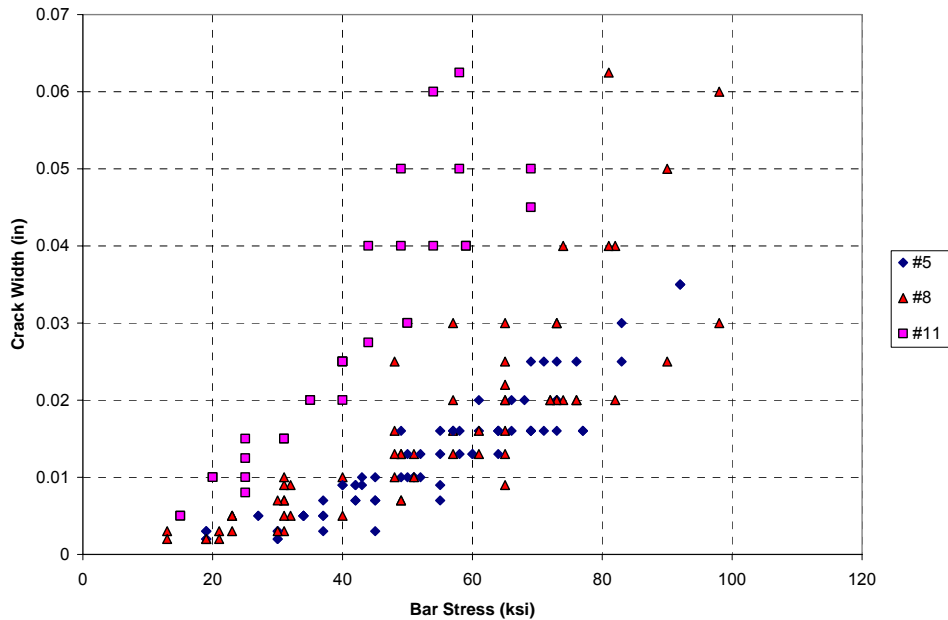


Figure 5-21: Measured end-of-splice crack widths for UT unconfined specimens

5.2.1.2 *Splices Confined by Transverse Reinforcement*

5.2.1.2.1 Behavior

The behavior of confined splice specimens was similar to the behavior of unconfined splice specimens until the stresses in the spliced MMFX bars exceeded the failure stresses of the identically designed unconfined splices. Splitting cracks developed in confined specimens within the same stress range reported for the unconfined splices regardless of the level of confinement provided. A comparison of a confined and an unconfined specimen near the failure load of the unconfined specimen is provided in

Figure 5-22. The similarity in cracking behavior between unconfined and confined splices is evident in this figure.

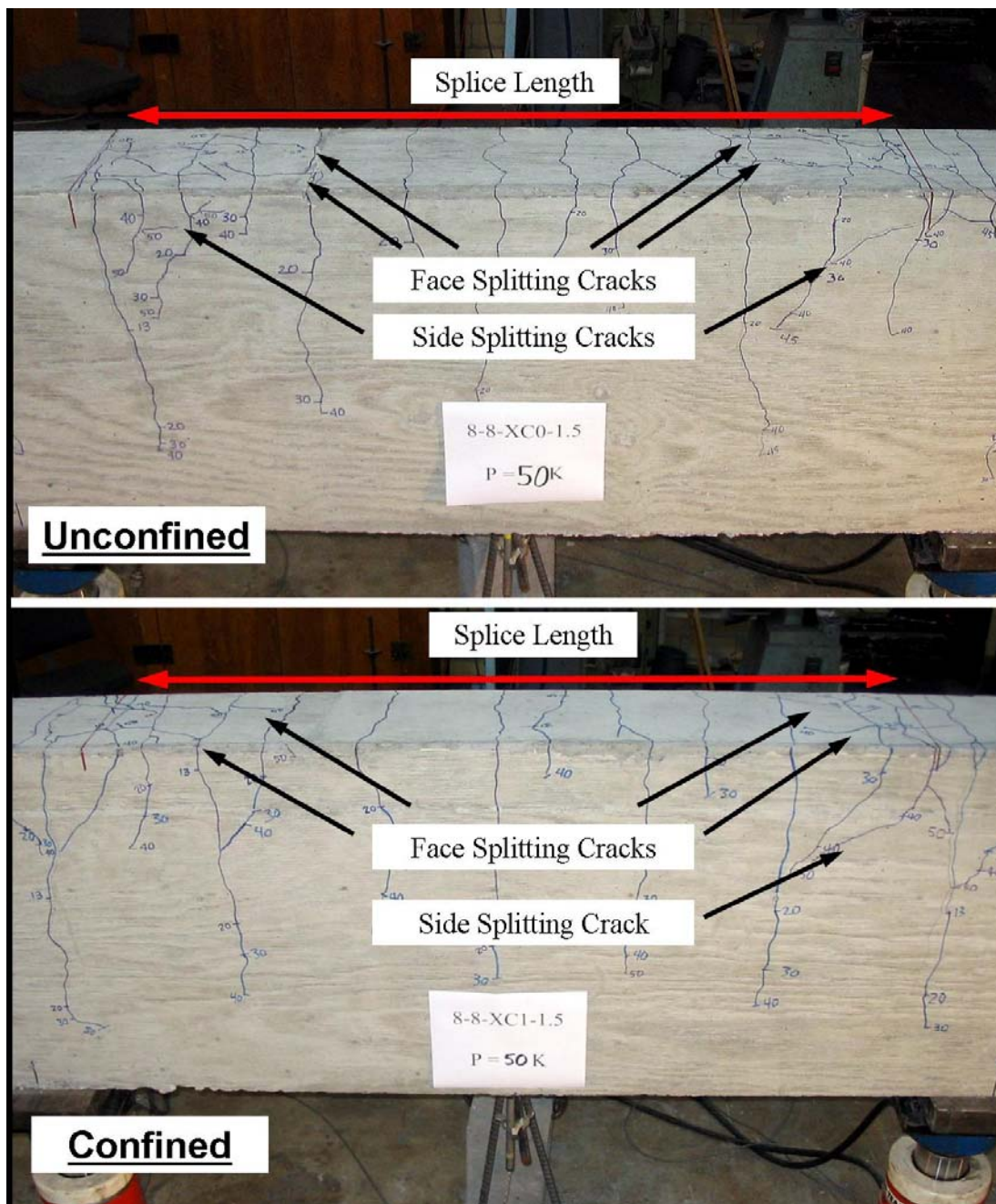


Figure 5-22: Comparison of cracking of unconfined and confined specimens near the failure load of the unconfined specimen

However, the load on confined specimens continued to increase beyond the failure load of the unconfined splice. Cracking near the splice ends became more severe, both in number of cracks and width of cracks, as the stresses in the MMFX bars increased. The number and severity of splitting cracks reduced significantly beyond the location of the first stirrup within the splice length. This served as a visual indication of the effectiveness of transverse reinforcement to arrest the propagation of splitting cracks. The effect of stirrups in preventing splitting crack growth is highlighted in Figure 5-23. Splitting cracks in the pictured specimen have progressed only slightly from the upper picture to the lower picture despite a 22% increase in the stress in the spliced MMFX bars. A few smaller cracks have developed between the end of the splice and the first stirrup line; but the end-of-splice crack has been most affected by the increased bar stress. It has begun to open significantly, growing from 0.02 in. to 0.03 in.

A closer view of the region near the end of the splice is shown in Figure 5-24. The large number of cracks in this region and the wide end-of-splice crack are evident. In this picture, the side splitting crack is inclined; but the angled crack is not due to shear since it is located within the constant moment region. Side-splitting cracks often are inclined because force transfer is primarily achieved by bearing of the bar lugs on the surrounding concrete at this phase of loading. The angled faces of the bar lugs cause the formation of angled compressive struts in the concrete. Principle tensile stresses are situated perpendicular to these angled compressive struts; hence, the cracks are inclined. This concept is well depicted in the failed specimen 11-5-XC1-3 pictured in Figure 5-25.

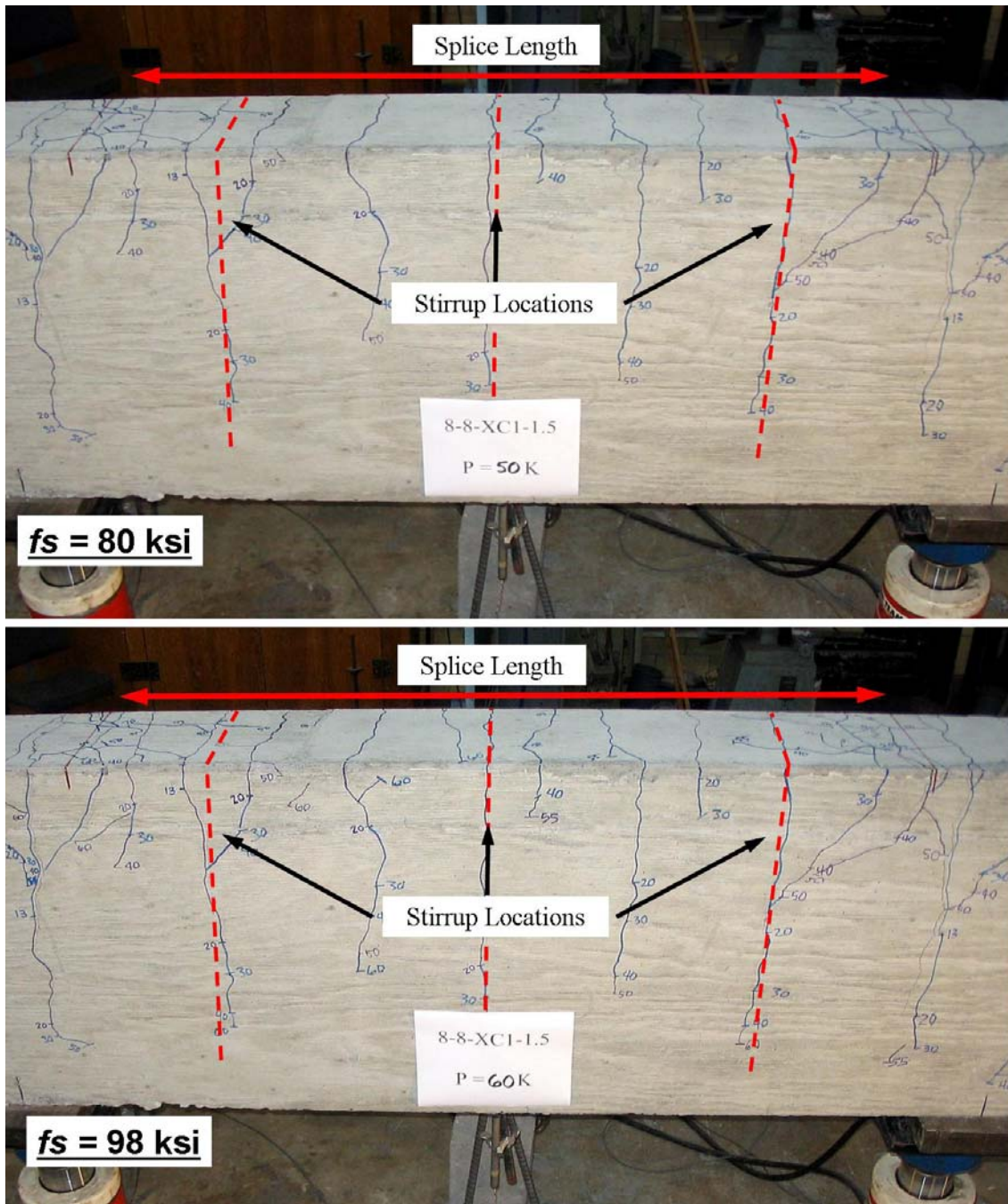


Figure 5-23: Effect of stirrups on arresting splitting cracks

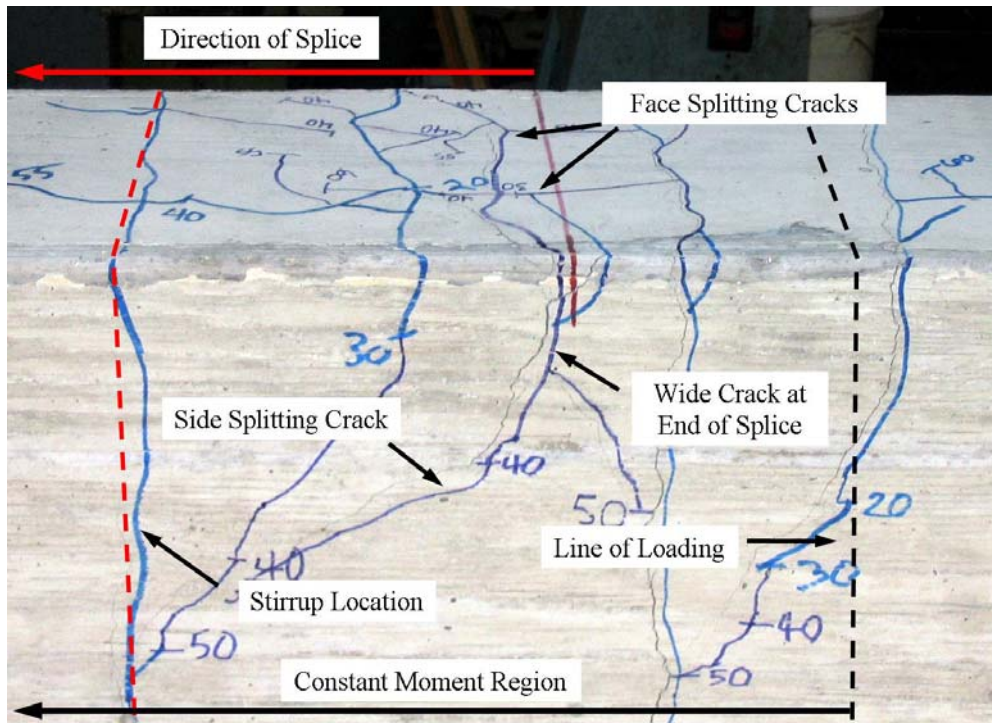


Figure 5-24: Cracking at the end of typical confined splice at 80% of failure load

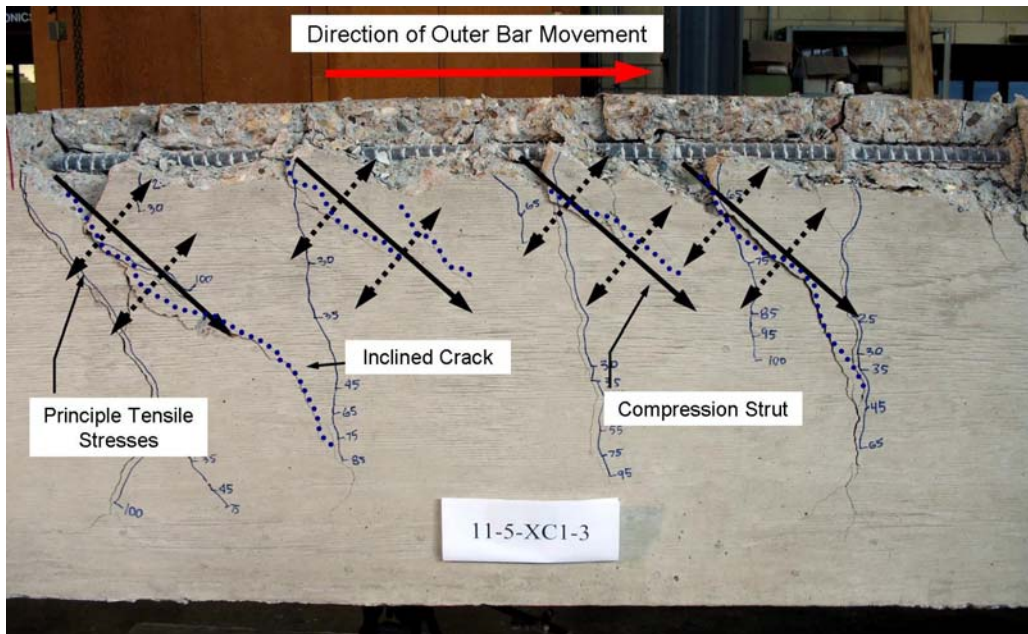


Figure 5-25: Formation of inclined side splitting cracks

As the confined specimens neared failure, cracks at the end of the splices continued to widen. In most cases, the widths of these end-of-splice cracks were substantially larger than those found in beams using Grade 60 reinforcement. This was especially true for the specimens containing #11 bars due to their wider bar spacings and larger cover values. In these specimens, crack widths were as large as 0.070 in. when the applied load was less than 60% of the failure load and as large as 0.125 in. near the failure load. Figure 5-26 shows the severity of these cracks.

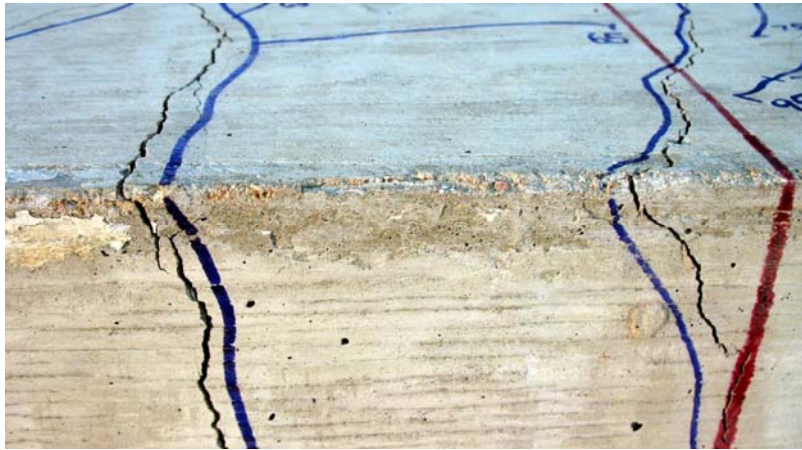


Figure 5-26: 0.08 in. crack at the end of a splice in specimen 11-5-XC2-3. Applied load is 68% of failure load.

The increased capacity of the confined splices allowed the MMFX bars to surpass the proportional limit of the MMFX stress-strain curve. As the bars entered the nonlinear range of response, beam deflections began to increase nonlinearly. Although failure of the confined splices displayed the same sudden brittle behavior described for the unconfined splices, the increased deflections exhibited by the confined splices as well as the increased number and width of cracks provided a visual indication of impending failure. This is demonstrated in Figure 5-27 with a set of three specimens containing #8

bars. The nonlinear load-deflection response for a highly confined (C2) specimen is shown in Figure 5-28.

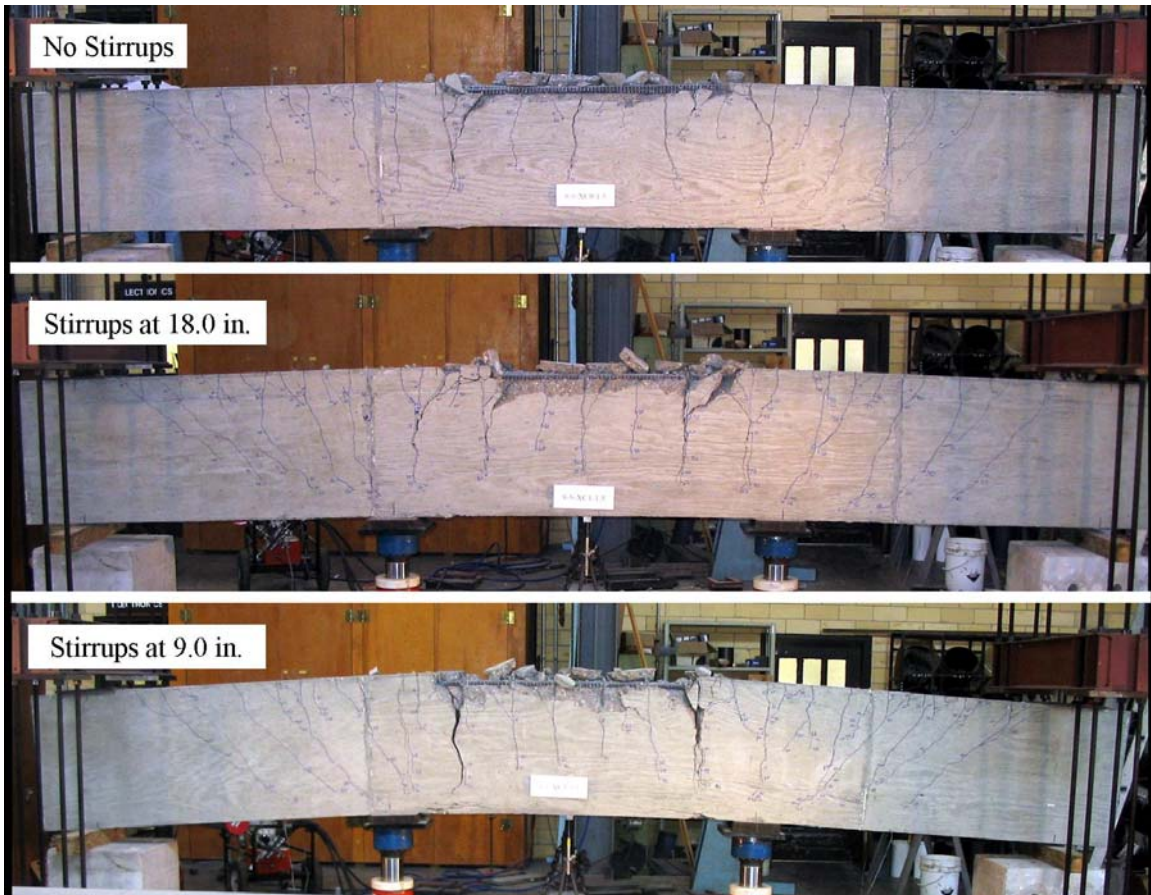


Figure 5-27: Increased cracking and deflections at failure for varying levels of confinement

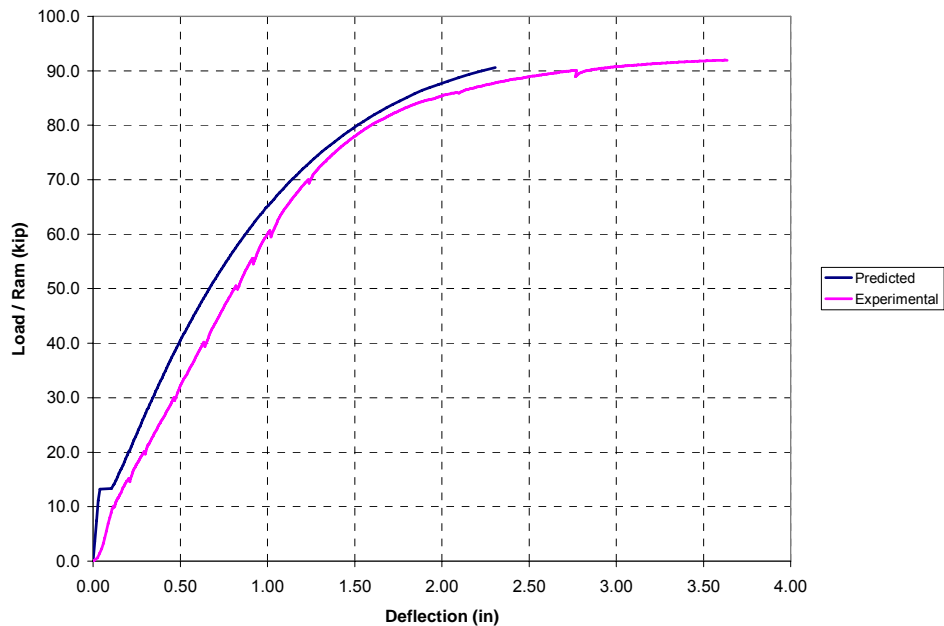


Figure 5-28: Nonlinear load-deflection plot for a highly confined specimen (8-5-XC2-1.5)

The measured crack widths for two identical #8 specimens with varying levels of transverse reinforcement are plotted in Figure 5-29. Mid-splice cracks were not included in this plot since they were previously shown to be significantly smaller than end-of-splice cracks. The plot shows that crack widths were relatively consistent among similarly designed specimens, regardless of the level of confinement. It also indicates the large size of the end-of-splice cracks, even at low ratios of bar stress to failure stress. A direct comparison of the cracks shown in Figure 5-29 and those of the identically designed unconfined splice shown in Figure 5-21 cannot be made because crack width measurements were ceased much earlier in relation to the splice failure stress for the confined specimens.

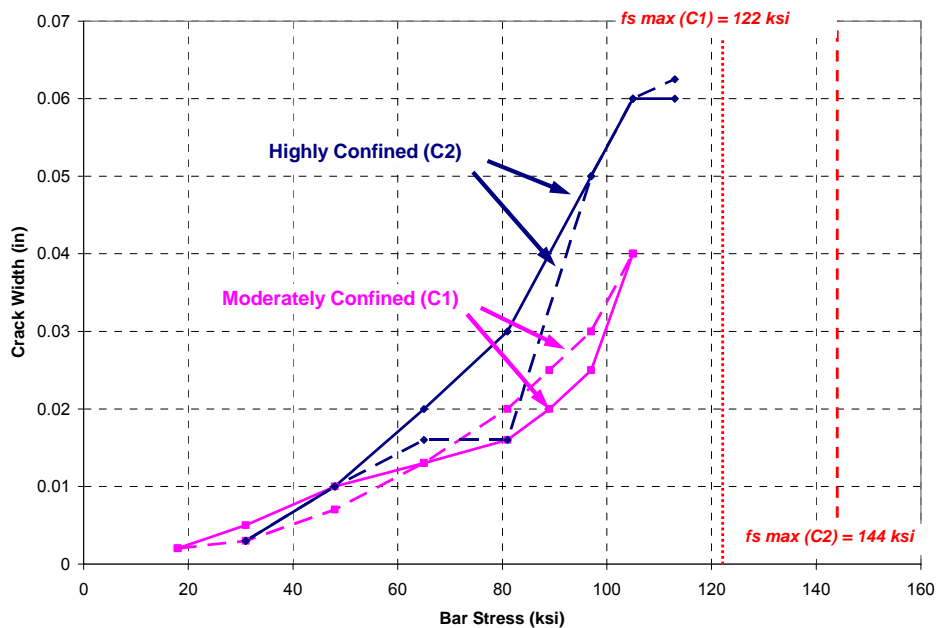


Figure 5-29: Comparison of measured crack widths for two confined specimens (8-8-XC1-1.5 and 8-8-XC2-1.5)

A few of the highly confined splices displayed slightly different behavior than that described for the typical confined specimen. In specimens 8-8-OC2-1.5, 8-5-XC2-1.5, and 11-5-XC2-3, concrete on the compression face of the beam began to crush near the failure load of the splice indicating an impending flexural failure. The amount of concrete crushing and spalling prior to splice failure varied among the three specimens, but the crushing was always confined to the region immediately adjacent to the load points in the constant moment region. As shown in Figure 5-30, specimen 8-8-OC2-1.5 was the only one of these three specimens that experienced a loss of load carrying capacity before splice failure. This suggests that the concrete crushing witnessed in the other two beams did not affect the results of the splice tests. Despite the slight reduction in load at the end of the 8-8-OC2-1.5 test, the results of this specimen were included in this study because the splice was clearly on the verge of failure at the maximum load.

The loss of member depth due to concrete spalling caused the reduction in load in the specimen. This also resulted in a small increase in the stress in the spliced bars and the ultimate failure of the splice. Therefore, the recorded maximum load carried by the beam serves as a conservative, yet reasonably accurate, estimation of the actual capacity of the splice.

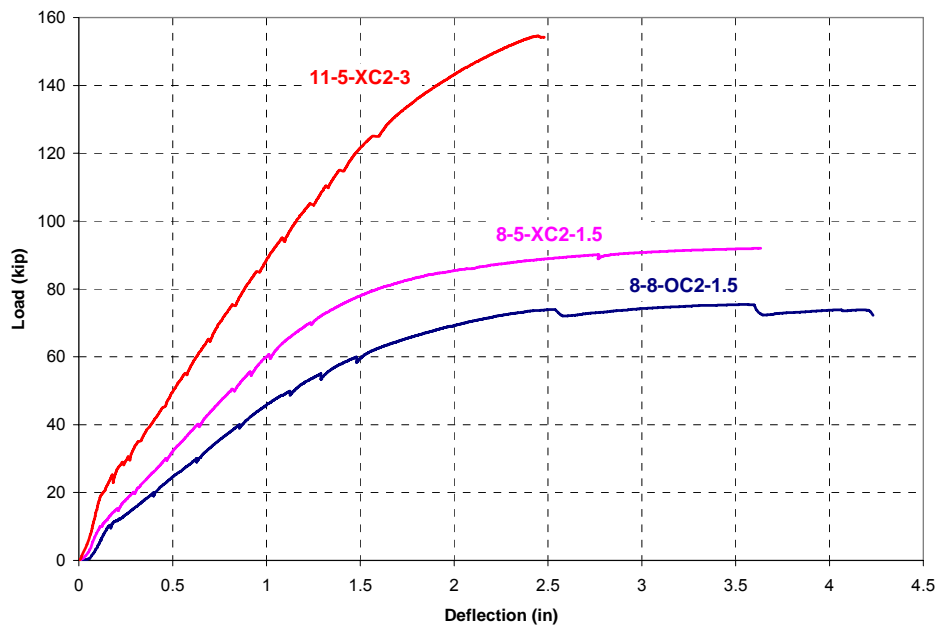


Figure 5-30: Load-deflection of confined specimens experiencing concrete crushing prior to splice failure

Another specimen, 8-5-OC2-1.5, experienced a rupture of one of the spliced bars during testing as shown in Figure 5-31. The failure sequence for this specimen is summarized in Figure 5-32. It is believed that bar 1 slipped a small amount at the peak load, and this caused a shift in tensile force from bar 1 to bar 2. Bar 2 maintained the additional tensile force through large strains and then ruptured. At this point, all tension needed to be carried by bar 1. Although it still possessed some tensile load capacity, the

bar 1 splice could not maintain the tension required; and a typical splitting failure soon occurred over bar 1. The events leading to the failure of specimen 8-5-OC2-1.5 are indicated on its load-deflection plot in Figure 5-33. Based on this failure sequence, the splice failure occurred when the first bar began to slip; and the peak load provides an accurate estimate of the splice strength for this specimen.



Figure 5-31: Ruptured #8 bar in specimen 8-5-OC2-1.5

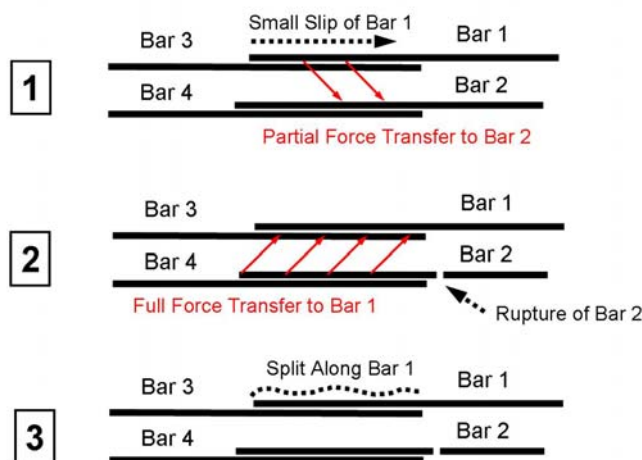


Figure 5-32: Failure sequence for specimen 8-5-OC2-1.5

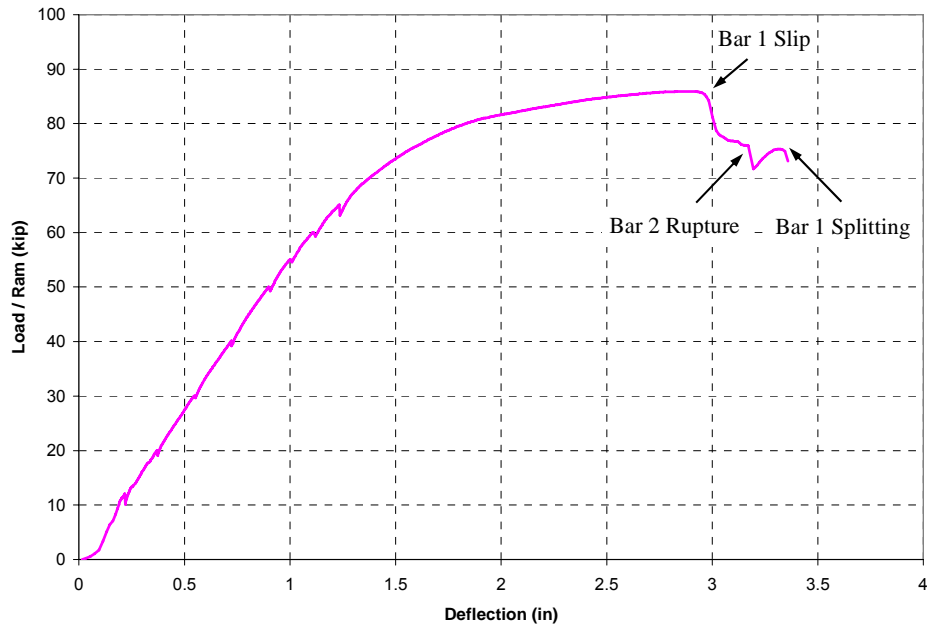


Figure 5-33: Failure sequence of specimen 8-5-OC2-1.5 demonstrated through load-deflection behavior

5.2.1.2.2 Failure Stresses and Crack Widths

Test failure stresses were determined for the confined splice specimens following the procedure used for the unconfined splice specimens. Calculated failure stresses per the ACI 408, ACI 318, and AASHTO LRFD equations were also determined for comparison. Relative rib areas of the #5, #8, and #11 bars were measured by the University of Kansas for use in the ACI 408 development length equation. The three bar sizes contained relative rib area values within the range of ordinary reinforcement. Their values were 0.0767 for the #5 bars, 0.0838 for the #8 bars, and 0.0797 for the #11 bars.

The results and as-built dimensions for the confined specimens tested at the University of Texas are listed in Table 5-5. The measured end-of-splice crack widths for UT confined splice tests are plotted in Figure 5-34.

Specimen	School	f'_c (psi)	l_s (in)	d_b (in)	c_{so} (in)	c_{si} (in)	c_b (in)	s_2 (in)	Test f_s (ksi)	Calculated f_s (ksi)		
										ACI 408	ACI 318	AASHTO
8-8-OC1-1.5	UT	8300	40	1.00	1.65	1.38	1.50	13.33	123	104	120	100
8-8-OC2-1.5	UT	8300	40	1.00	1.65	1.38	1.50	6.67	147	126	121	100
8-5-OC1*-1.5	UT	5200	40	1.00	1.65	1.38	1.50	13.33	99	88	95	93
8-5-OC2*-1.5	UT	5200	40	1.00	1.65	1.38	1.50	6.67	129	104	96	93
8-8-XC1-1.5	UT	7800	54	1.00	1.50	1.50	1.50	18.00	122	121	155	135
8-8-XC2-1.5	UT	7800	54	1.00	1.50	1.50	1.50	9.00	144	142	159	135
8-5-OC2-1.5	UT	5000	47	1.00	1.65	1.38	1.50	5.22	141	126	111	107
8-5-XC2-1.5	UT	4700	62	1.00	1.60	1.38	1.50	6.89	148	142	142	137
11-5-OC1-3	UT	5000	50	1.41	3.25	3.00	2.75	8.33	104	97	84	57
11-5-OC2-3	UT	5000	50	1.41	3.25	3.00	2.75	4.17	128	112	84	57
11-5-XC1-3	UT	5400	67	1.41	3.13	2.94	2.75	11.17	117	118	116	80
11-5-XC2-3	UT	5400	67	1.41	3.13	2.94	2.75	5.58	141	139	116	80

Table 5-5: Summary of results for UT confined tests

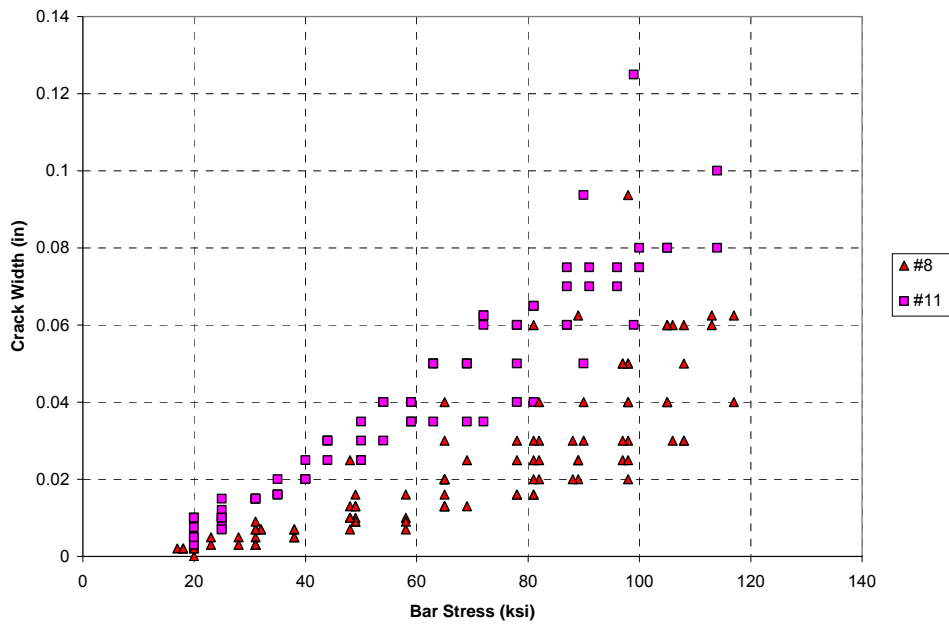


Figure 5-34: Measured end-of-splice crack widths for UT confined specimens

5.2.2 Tests Conducted at Other Participating Research Universities

5.2.2.1 Splices Not Confined by Transverse Reinforcement

Ten unconfined splice tests have been conducted at other universities as part of this MMFX bond research effort. Eight of these tests were carried out by researchers at North Carolina State University. The remaining two were tested by researchers at the

University of Kansas. The results and as-built dimensions of these specimens are summarized in Table 5-6. Detailed crack width data for these specimens were not provided in their reports.

Specimen	School	f'c (psi)	ls (in)	db (in)	cso (in)	csi (in)	cb (in)	s2 (in)	Test fs (ksi)	Calculated fs (ksi)		
										ACI 408	ACI 318	AASHTO
8-5-OC0-2.5	NCSU	6000	31	1.00	2.50	2.50	2.50	N/A	95	84	80	77
8-5-XC0-2.5	NCSU	5800	41	1.00	2.50	2.50	2.50	N/A	107	103	104	101
8-8-OC0-1.5	NCSU	8400	40	1.00	1.50	1.50	1.50	N/A	90	81	98	100
8-8-XC0-1.5	NCSU	10200	54	1.00	1.50	1.50	1.50	N/A	108	107	145	135
11-8-OC0-3	NCSU	6070	43	1.41	3.00	3.00	3.00	N/A	78	75	79	68
11-8-XC0-3	NCSU	8380	57	1.41	3.00	3.00	3.00	N/A	96	101	123	106
11-5-OC0-2	NCSU	5340	69	1.41	2.00	2.00	2.00	N/A	74	82	92	82
11-5-XC0-2	NCSU	4060	91	1.41	2.00	2.00	2.00	N/A	72	95	105	94
8-5-OC0-1.5	KU	5260	47	1.00	1.48	3.60	1.40	N/A	77	79	86	110
8-5-XC0-1.5	KU	5940	63	1.00	1.41	3.69	1.41	N/A	89	102	124	156

Table 5-6: Summary of results for non-UT unconfined tests

5.2.2.2 Splices Confined by Transverse Reinforcement

Ten confined splice tests have been conducted at other universities as part of this MMFX bond research program. Nine of the tests were performed at North Carolina State University, and one was performed at the University of Kansas. The results and as-built dimensions for these tests are listed in Table 5-7. Again, detailed crack width data for these tests were not provided.

Specimen	School	f'c (psi)	ls (in)	db (in)	cso (in)	csi (in)	cb (in)	s2 (in)	Test fs (ksi)	Calculated fs (ksi)		
										ACI 408	ACI 318	AASHTO
8-5-OC2-2.5	NCSU	6000	31	1.00	2.50	2.50	2.50	3.88	142	104	80	77
8-8-OC2-1.5	NCSU	8400	40	1.00	1.50	1.50	1.50	8.00	151	118	122	100
8-8-XC2-1.5	NCSU	10200	54	1.00	1.50	1.50	1.50	7.71	151	167	182	135
11-8-OC2-3	NCSU	6070	43	1.41	3.00	3.00	3.00	5.38	116	103	79	68
11-8-XC2-3	NCSU	8340	57	1.41	3.00	3.00	3.00	7.13	128	138	123	106
11-5-OC2-2	NCSU	5340	69	1.41	2.00	2.00	2.00	6.27	132	119	119	82
11-5-OC3-2	NCSU	5340	69	1.41	2.00	2.00	2.00	3.00	151	148	119	82
11-5-XC2-2	NCSU	4060	91	1.41	2.00	2.00	2.00	8.27	127	125	137	94
11-5-XC3-2	NCSU	4060	91	1.41	2.00	2.00	2.00	3.96	155	158	137	94
8-5-OC2-1.5	KU	6050	47	1.00	1.40	3.58	1.40	5.88	126	128	122	118

Table 5-7: Summary of results for non-UT confined tests

CHAPTER 6

Evaluation of Test Results

6.1 COMPARISON OF DUPLICATE TESTS

Several sets of duplicate tests were included in the original test matrix to ensure the consistency of results among the three participating universities. Seven pairs of duplicates are included in the dataset of 45 beams being analyzed in this thesis. Ideally, these beams would be perfect duplicates of each other with identical bar covers, spacings, confinement, and concrete strengths; but since the duplicate beams were built and tested in different laboratories, variations exist even between the duplicate beams. Therefore, a direct comparison of failure stresses cannot be used as a measure of consistency; and normalizing based on concrete strength alone will not capture the small differences in bar cover, spacing, or confinement levels. The most appropriate comparisons of duplicate beams appear to be the test/calculated failure stress ratios using the ACI 408 development length equation.

The comparison of the ACI 408, ACI 318, and AASHTO development length equations provided in Chapter 3 showed that the ACI 408 equation displayed the least variability in test/calculated failure stress ratios with a coefficient of variation of 0.13. Assuming that the data are normally distributed, this implies that approximately 68% of test/calculated ratios for bond tests reported in the ACI database 10-2001 are within $\pm 13\%$ of the mean. A predictive development length equation can at best provide consistency equal to that shown by two identical specimens; but due to the non-homogeneity of concrete and other factors, a moderate variation in bond strength should be expected even between two identical specimens. However, a reasonable expectation

would be that the average percentage difference between the test/calculated failure stress ratios for two duplicate tests should be less than 13%.

The ACI 408 test/calculated failure stress ratios for the seven pairs of duplicate specimens are compared in Table 6-1. Two pairs of duplicates show a difference in test/calculated ratios greater than 13%, but the average difference is 10.7%. Neither North Carolina State University nor the University of Kansas consistently report higher or lower test/calculated failure stress ratios than the University of Texas. Based on these findings, the experimental programs at the three participating universities appear to provide reasonably consistent data, and the data from all 45 beam-splice tests will be used in the following analyses.

<i>Specimen</i>	<i>School</i>	<i>fs (per ACI 408) ksi</i>	<i>fs (Test) ksi</i>	<i>Test/Calculated ACI 408</i>	<i>Difference in Test/Calculated Ratios %</i>
8-8-OC0-1.5	UT	82	80	0.98	---
	NCSU	81	90	1.11	13.9
8-8-OC2-1.5	UT	126	147	1.17	---
	NCSU	118	151	1.28	9.7
8-8-XC0-1.5	UT	100	86	0.86	---
	NCSU	107	108	1.01	17.4
8-8-XC2-1.5	UT	142	144	1.01	---
	NCSU	167	151	0.90	-10.8
8-5-OC0-1.5	UT	81	74	0.91	---
	KU	79	77	0.97	6.7
8-5-OC2-1.5	UT	126	141	1.12	---
	KU	128	126	0.98	-12.0
8-5-XC0-1.5	UT	98	82	0.84	---
	KU	102	89	0.87	4.3
Average	---	---	---	---	10.7

Table 6-1: Comparison of duplicate tests

6.2 PERFORMANCE OF DEVELOPMENT LENGTH EQUATIONS

To properly evaluate the ACI 408, ACI 318, and AASHTO LRFD development length equations for use with high strength reinforcement, the intended use of each equation must be considered. As described in Chapter 3, the ACI 408 equation (with modification factor, ϕ , equal to 1.0) was evaluated as a best fit equation for test data in this research program. The ACI 318 and AASHTO LRFD equations were considered as

design code equations. As such, the ACI 408 equation should ideally produce a mean test/calculated failure stress ratio near 1.0 with a low coefficient of variation and with approximately 50% of tests producing ratios greater than 1.0 and 50% of tests with ratios less than 1.0. The ACI 318 and AASHTO LRFD equations should ideally produce mean test/calculated failure stress ratios above 1.0 with low coefficients of variation and a very low percentage of tests (5-10%) producing ratios below 1.0.

6.2.1 All Specimens

The distribution of test/calculated failure stress ratios for all 45 beam-splice specimens tested in this MMFX bond research program is shown in Table 6-2 and Figure 6-1. Based on the previous evaluation criteria, the ACI 408 equation performs well with a mean of 1.03 and a relatively small coefficient of variation of 0.12. The two design code equations performed unsatisfactorily. Both equations displayed high variability in test/calculated failure stress ratios with coefficients of variation of 0.24 and 0.35 for the ACI 318 and AASHTO equations, respectively. The average value of 1.02 for the ACI 318 equation is significantly lower than desired for a design code equation where conservatism is required. The fact that 49% of tests failed at stresses lower than those calculated by the ACI 318 equation highlights the lack of conservatism. While the AASHTO equation shows a more appropriate design code mean value of 1.18, the large coefficient of variation still produces dangerously low test/calculated ratios in some cases and overly conservative test/calculated ratios in other cases. The AASHTO equation produced both the largest and smallest ratios of any of the three equations with a maximum value of 2.23 and a minimum value of 0.52

N = 45	Distribution of MMFX Results - All Specimens						
Equation	Mean	Std. Dev.	COV	Max	Min	# < 1.0	% < 1.0
ACI 408	1.03	0.12	0.12	1.36	0.76	19	42
ACI 318	1.02	0.25	0.24	1.77	0.63	22	49
AASHTO	1.18	0.41	0.35	2.23	0.52	12	27

Table 6-2: Distribution of test/calculated failure stress ratios for all specimens

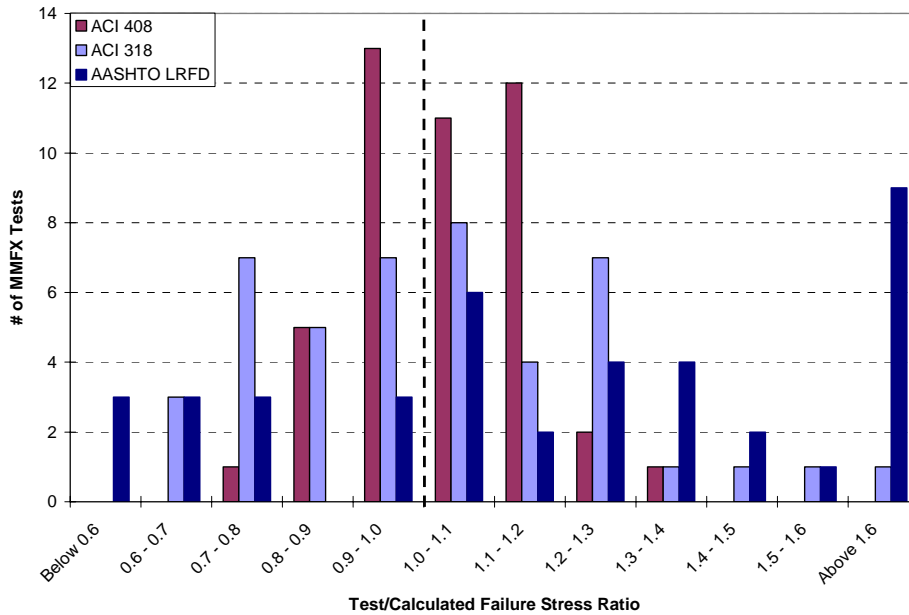


Figure 6-1: Distribution of test/calculated failure stress ratios for all specimens

6.2.2 Splices not Confined by Transverse Reinforcement

Separating the data into splices not confined by transverse reinforcement and splices confined by transverse reinforcement highlights the difference in performance of unconfined and confined splices. The distribution of test/calculated failure stress ratios for the unconfined splices is shown in Table 6-3 and Figure 6-2. The ACI 408 equation again performed satisfactorily with a mean test/calculated ratio near 1.0 (0.98) and with a low coefficient of variation of 0.11. The ACI 318 and AASHTO equations both provided extremely unconservative calculated failure stresses. The ACI 318 equation produced a

mean test/calculated failure stress ratio of only 0.88 with 78% of tests failing below the calculated failure stress, and the AASHTO equation produced a mean ratio of 0.93 with 48% of tests failing below the calculated failure stress. Again, despite having a higher mean value than the ACI 318 equation, the AASHTO equation showed the greatest variability with a coefficient of variation of 0.33. It produced both the largest and smallest ratios among the three equations with a maximum value of 1.62 and a minimum value of 0.52.

N = 23		Distribution of MMFX Results - Unconfined Specimens					
Equation	Mean	Std. Dev.	COV	Max	Min	# < 1.0	% < 1.0
ACI 408	0.98	0.11	0.11	1.14	0.76	14	61
ACI 318	0.88	0.18	0.20	1.28	0.63	18	78
AASHTO	0.93	0.30	0.33	1.62	0.52	11	48

Table 6-3: Distribution of test/calculated failure stress ratios for unconfined specimens

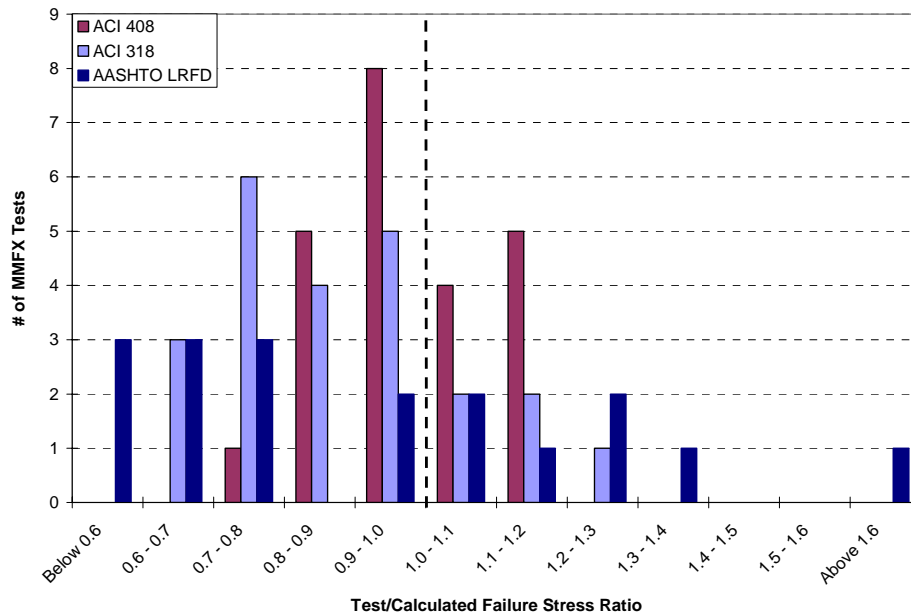


Figure 6-2: Distribution of test/calculated failure stress ratios for unconfined specimens

6.2.3 Splices Confined by Transverse Reinforcement

The distribution of test/calculated failure stress ratios for the confined splices is shown in Table 6-4 and Figure 6-3. In this table and figure, the increased conservatism of the development length equations in confined splices is highlighted. The ACI 408 equation produced a higher than ideal mean test/calculated failure stress ratio of 1.08, but it displayed low variability with a coefficient of variation of 0.11. Both the ACI 318 and AASHTO equations displayed larger variability, with coefficients of variation of 0.20 and 0.24, respectively. In contrast to its performance with the unconfined splices, the ACI 318 equation provided relatively conservative calculated failure stresses in the confined splices. Its mean value of 1.16 is more appropriate for a design code equation; but with a coefficient of variation of 0.20, the ACI 318 equation still provided unconservative calculated failure stresses for 18% of the confined tests. The AASHTO equation displayed the largest difference in performance between the unconfined and the confined specimens since the type of confinement used in this bond study did not qualify as confining reinforcement per the AASHTO equation. Ordinary closed hoop shear ties at moderate spacings were used in this experimental program. AASHTO only recognizes the beneficial effects of confinement if a splice is enclosed within spiral reinforcement with a diameter of at least 0.25 in. and spaced at a pitch not more than 4.0 in. Therefore, the calculated failure stress for a confined splice in this study was the same as the calculated failure stress for the identical unconfined splice. As expected, this produced overly conservative test/calculated failure stress ratios for the confined specimens with an average value of 1.44 and a maximum ratio of 2.23. Nevertheless, one confined splice did fail below its calculated failure stress.

<i>N = 22</i>	<i>Distribution of MMFX Results - Confined Specimens</i>						
<i>Equation</i>	<i>Mean</i>	<i>Std. Dev.</i>	<i>COV</i>	<i>Max</i>	<i>Min</i>	<i># < 1.0</i>	<i>% < 1.0</i>
ACI 408	1.08	0.11	0.11	1.36	0.90	5	23
ACI 318	1.16	0.23	0.20	1.77	0.79	4	18
AASHTO	1.44	0.34	0.24	2.23	0.90	1	5

Table 6-4: Distribution of test/calculated failure stress ratios for confined specimens

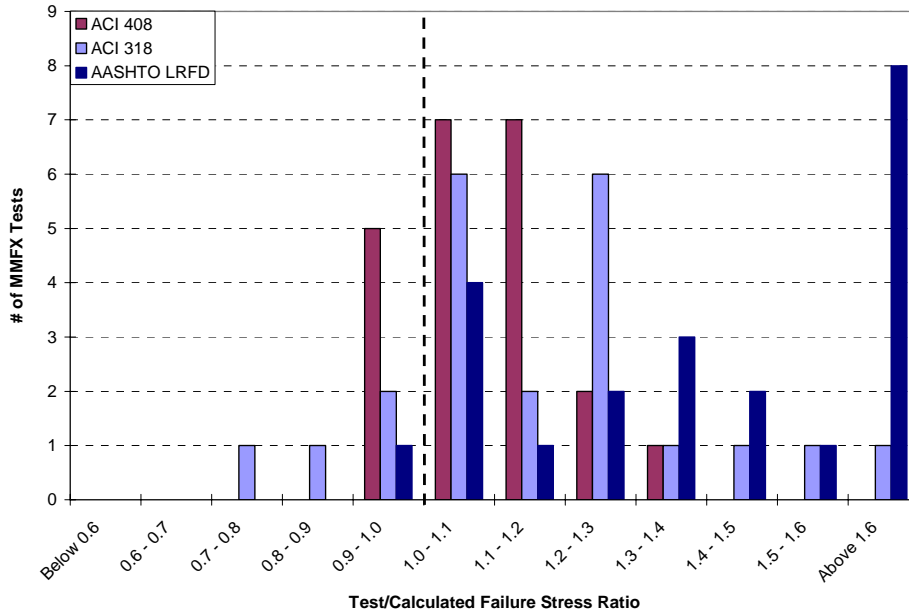


Figure 6-3: Distribution of test/calculated failure stress ratios for confined specimens

6.3 EFFECT OF SPLICE LENGTH

The effect of splice length will be investigated only on unconfined splices. Confined splices have not been considered because the addition of confining reinforcement creates difficulties in separating the effects of splice length and confinement terms when comparing the performance of development length equations.

In order to investigate the relative performance of splices of various lengths, the splice lengths must first be normalized to account for differences in bar diameter.

Required splice lengths increase with increasing bar diameter for a given bar stress. As discussed in Chapter 2, this is due to the larger rate of increase in bar area in relation to bar surface area with respect to bar diameter. The difference in the rate of change is proportional to the bar diameter; therefore, splice lengths have been normalized with respect to bar diameter for the following comparisons.

The reliability of the ACI 408, ACI 318, and AASHTO LRFD development length equations reduced with increasing values of l_s/d_b as evidenced by the negative sloping trends in Figure 6-4, Figure 6-5, and Figure 6-6. The negative effects of long splices were more pronounced in the ACI 318 and AASHTO equations. For all three equations, test/calculated failure stress ratios transitioned from predominately greater than 1.0 to predominately less than 1.0 at a value of l_s/d_b of approximately 40. For reference, this value corresponds to stresses of 115 ksi, 84 ksi, and 67 ksi for #5, #8, and #11 bars embedded in 5000 psi concrete and with a 2 in. clear cover on all sides according to the ACI 408 equation.

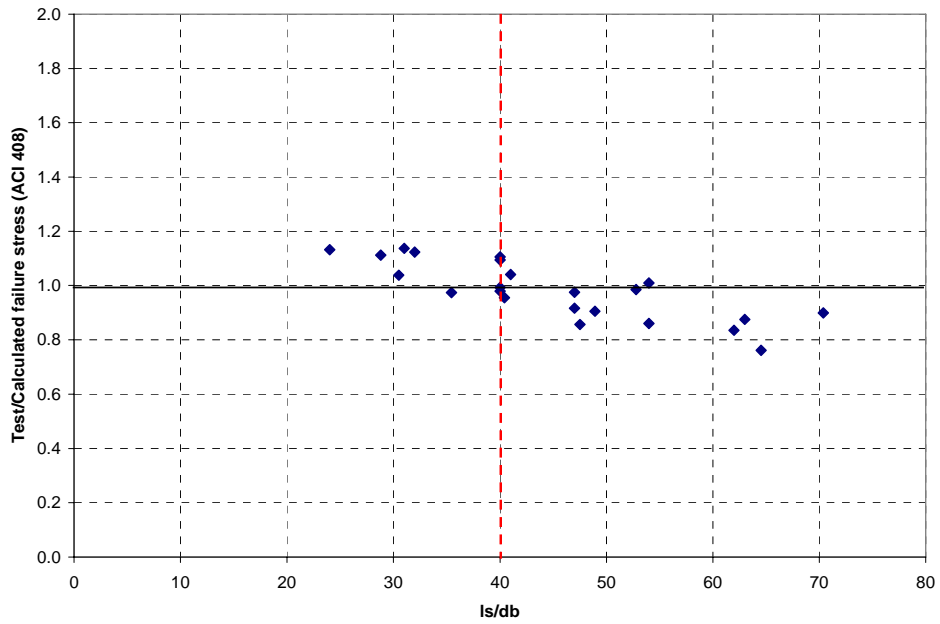


Figure 6-4: Effect of l_s/d_b on ACI 408 test/calculated failure stress ratios

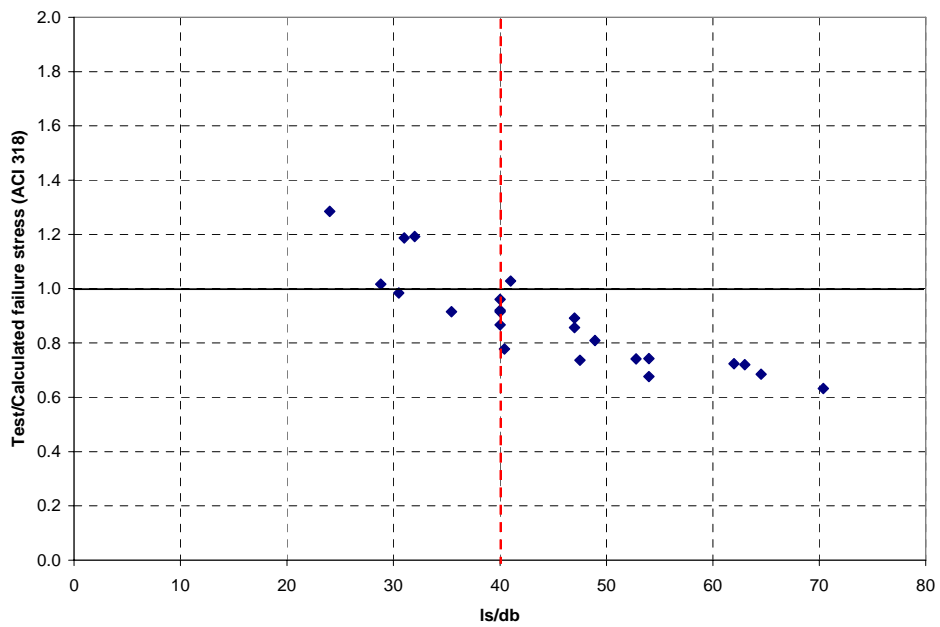


Figure 6-5: Effect of l_s/d_b on ACI 318 test/calculated failure stress ratios

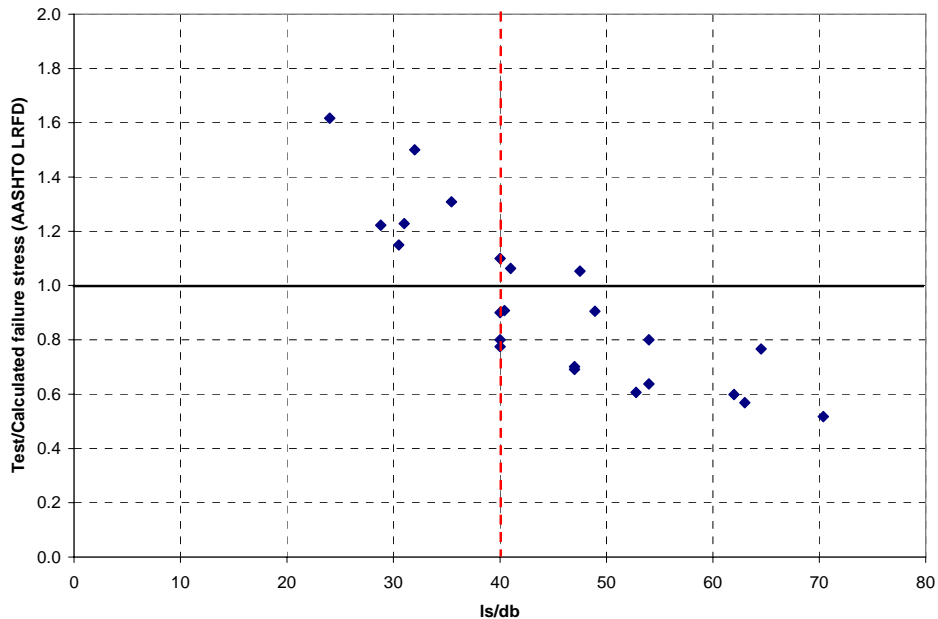


Figure 6-6: Effect of l_s/d_b on AASHTO LRFD test/calculated failure stress ratios

The negative effect of increasing l_s/d_b on the performance of the three development length equations can also be seen in the comparison of pairs of OC and XC splice specimens. According to the test matrix described in Chapter 4, unconfined OC specimens were designed to achieve 80 ksi in the MMFX bars at splice failure. The XC specimens were designed to achieve 100 ksi at splice failure. In a given pair of OC and XC specimens, the splice length was the only variable that was changed; therefore, the splice in an XC specimen was always longer than the splice in its corresponding OC specimen. As shown in Figure 6-7, Figure 6-8, and Figure 6-9, the test/calculated failure stress ratio for the XC specimen was also always lower than the ratio for the OC specimen, regardless of the equation used to calculate the failure stress. Again, the data indicate a reduction in conservatism of the development length equations with increasing l_s/d_b .

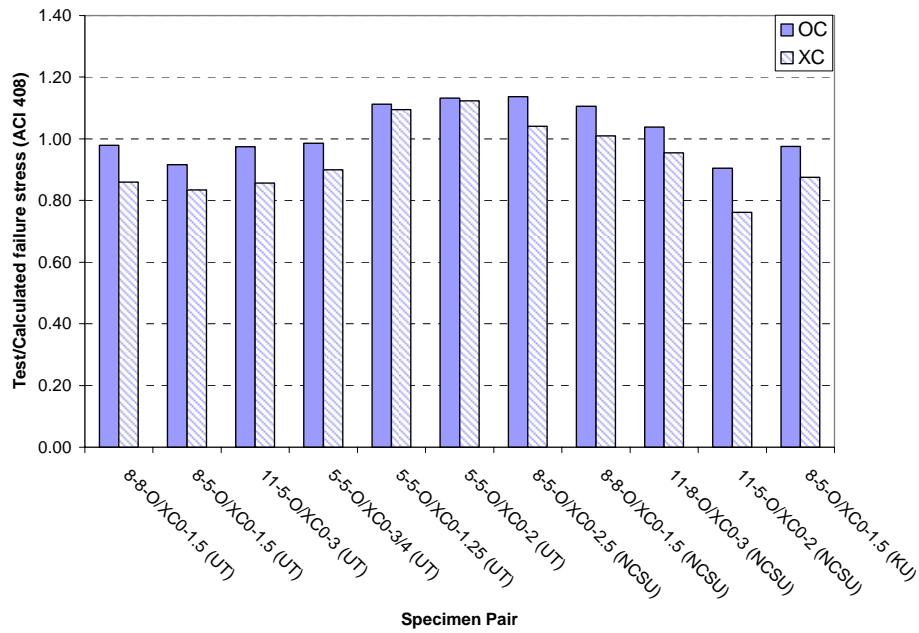


Figure 6-7: Comparison of ACI 408 test/calculated failure stress ratios for pairs of specimens containing shorter (OC) and longer (XC) splices

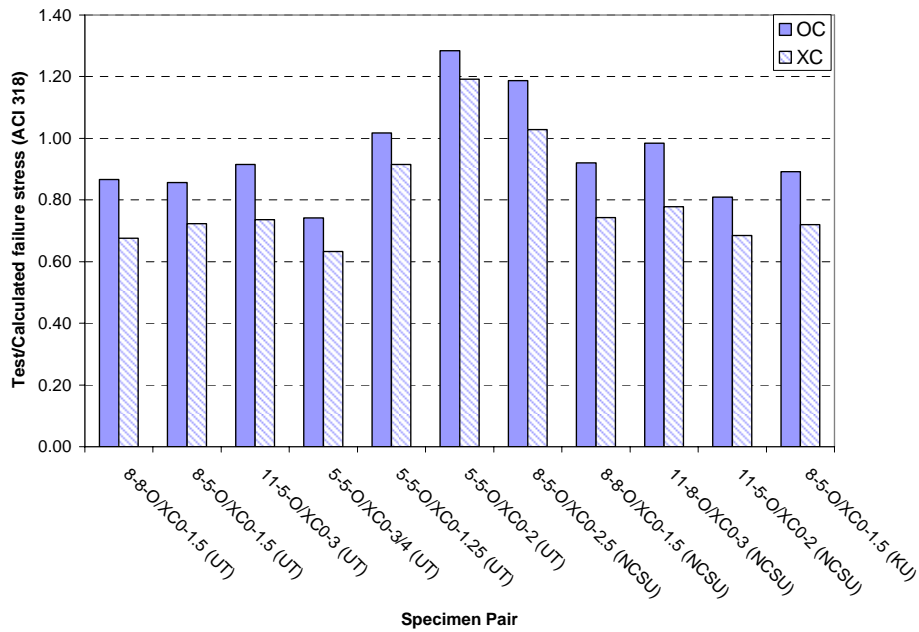


Figure 6-8: Comparison of ACI 318 test/calculated failure stress ratios for pairs of specimens containing shorter (OC) and longer (XC) splices

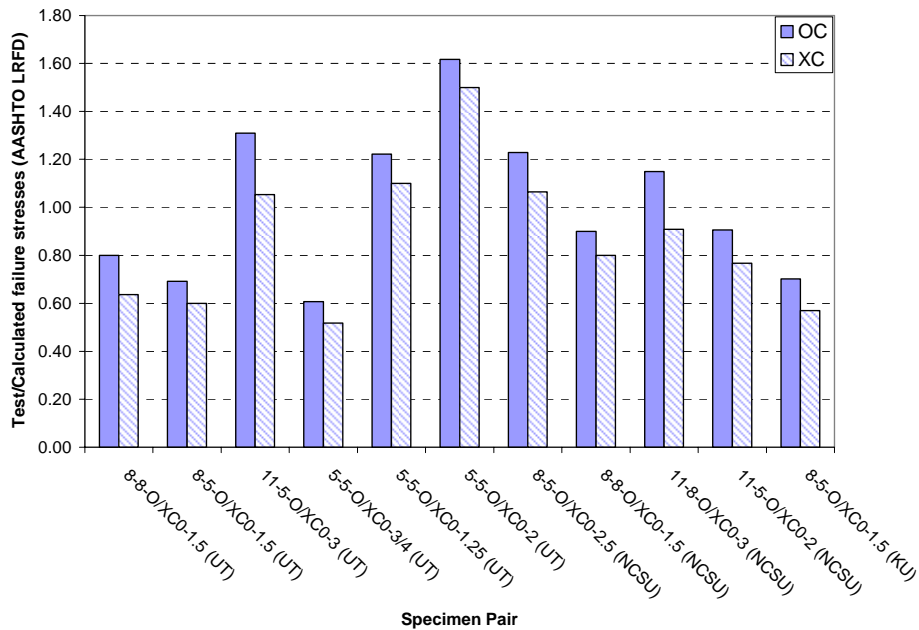


Figure 6-9: Comparison of AASHTO LRFD test/calculated failure stress ratios for pairs of specimens containing shorter (OC) and longer (XC) splices

To determine if the negative effect of l_v/d_b was unique to the MMFX tests, the data from this project were combined with the data of previous unconfined splice tests provided in ACI database 10-2001. A negative trend was not conclusive for the ACI 408 equation. As seen in Figure 6-10, the data show a slight negative slope; however, the low test/calculated failure stress ratios at high values of l_v/d_b are no smaller than the low ratios at low values of l_v/d_b . Therefore, the negative trend could be a result of a lack of tests at high l_v/d_b values rather than a reduction in conservatism as l_v/d_b increases.

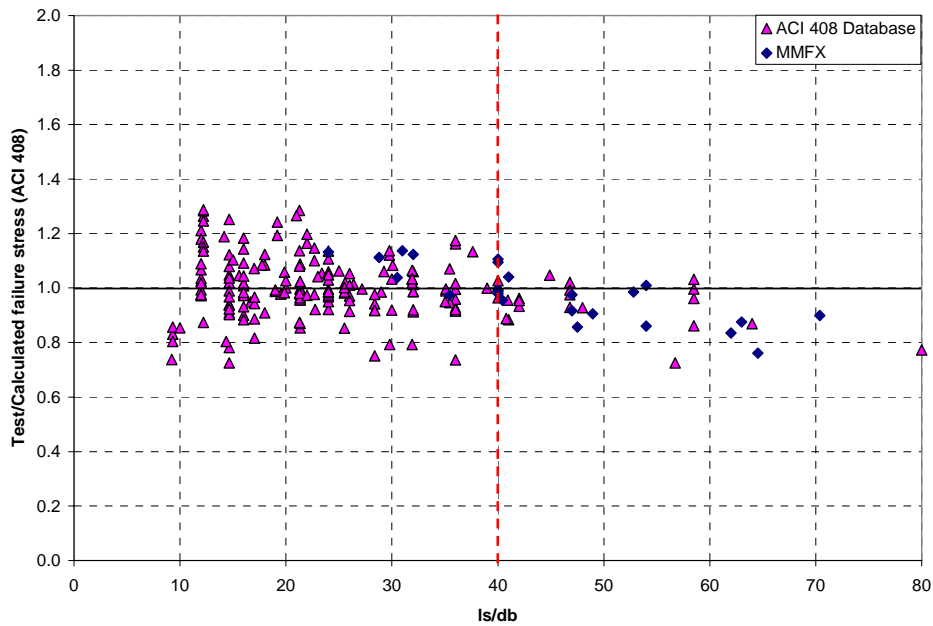


Figure 6-10: Effect of l_s/d_b on ACI 408 test/calculated failure stress ratios (data from ACI 408 database 10-2001)

The negative effect on the conservatism of the ACI 318 and AASHTO development length equations is highlighted in Figure 6-11 and Figure 6-12, respectively. Both plots show clear negative trends. From these plots, the average test/calculated failure stress ratio for both equations again falls below 1.0 near an l_s/d_b value of 35 to 40.

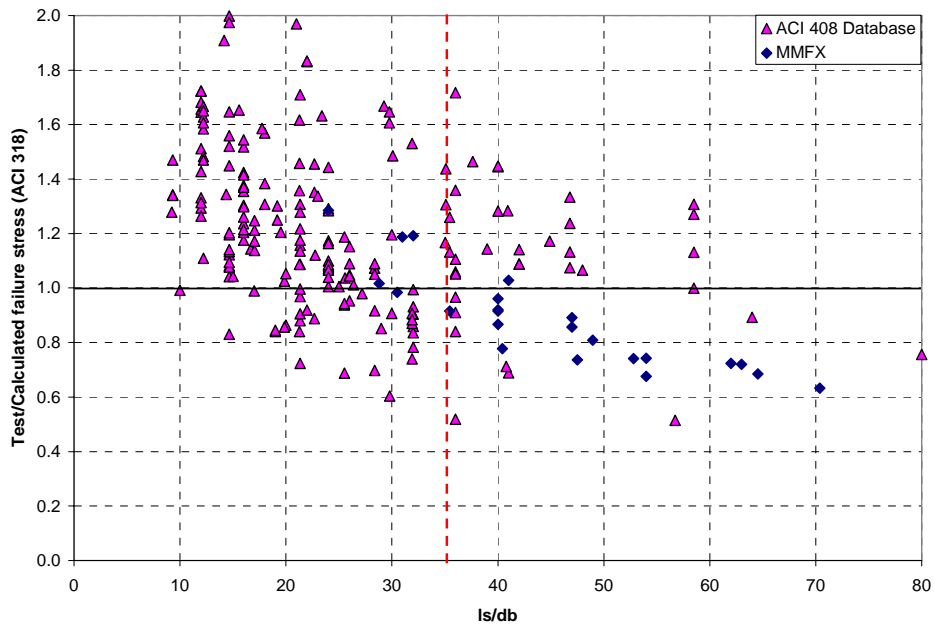


Figure 6-11: Effect of l_s/d_b on ACI 318 test/calculated failure stress ratios (data from ACI 408 database 10-2001, bar stress and concrete strength limits not applied)

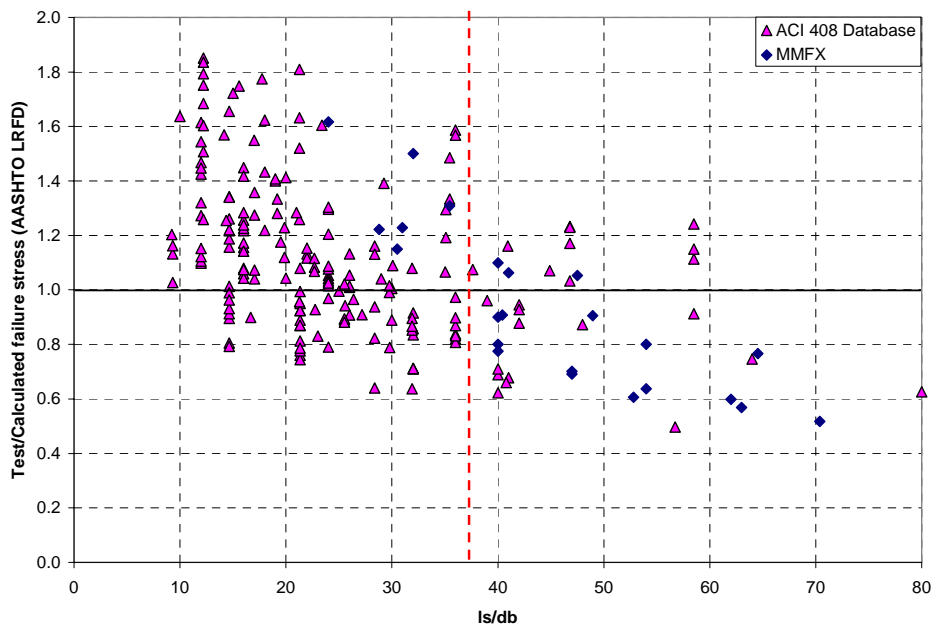


Figure 6-12: Effect of l_s/d_b on AASHTO test/calculated failure stress ratios (data from ACI 408 database 10-2001, bar stress and concrete strength limits not applied)

6.4 EFFECT OF CONFINEMENT

Adding confining reinforcement around splices increased both the stress in the spliced bars and the deflections of the specimens at failure. The load versus deflection behavior for a group of three splices with varying levels of confinement (8-8-XC0-1.5, 8-8-XC1-1.5, 8-8-XC2-1.5) is plotted in Figure 6-13. In this group of specimens, the addition of stirrups spaced at 18.0 in. resulted in a 42% increase in the failure stress and a 64% increase in the deflection over the values of the unconfined specimen. Stirrups spaced at 9.0 in. resulted in a 67% increase in the failure stress and a 207% increase in the deflection over the values of the unconfined specimen.

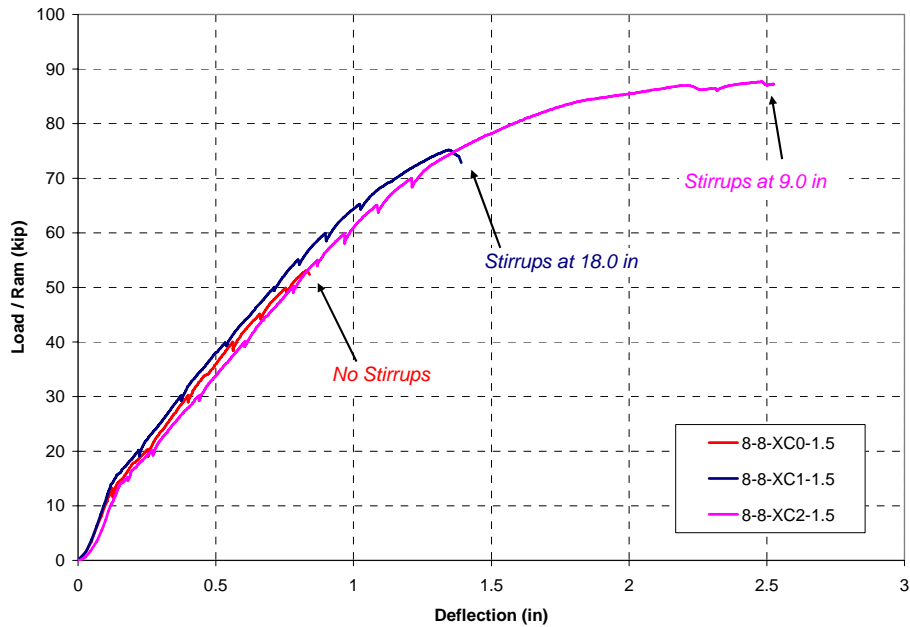


Figure 6-13: Load-deflection for a group of three splices with varying levels of transverse reinforcement

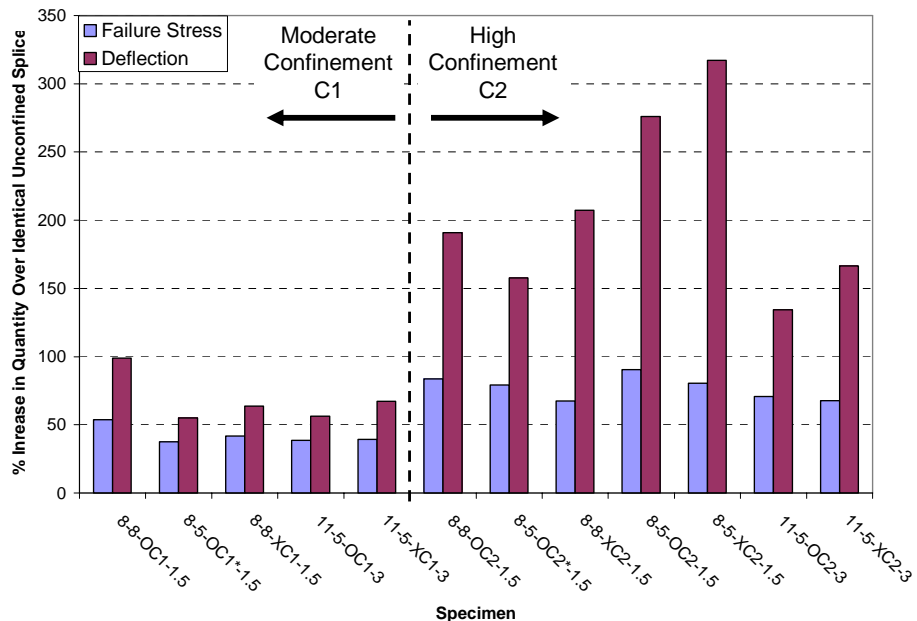


Figure 6-14: Increases in failure stresses and deflections relative to unconfined splice – UT tests

The behavior shown in Figure 6-13 was typical of the confined specimens in this study. As shown in Figure 6-14, C1 specimens provided a 42% increase in failure stress and a 68% increase in deflection, on average, over the values attained by the corresponding unconfined (C0) splice. C2 specimens provided a 74% increase in failure stress and a 171% increase in deflection, on average.

The respective increases of 42% and 74% in failure stresses in C1 and C2 specimens represent greater increases than predicted by the ACI 408 and the ACI 318 development length equations. Calculations using the ACI 408 equation predict an average increase of 23% in failure stress for C1 specimens and an increase of 47% for C2 specimens. Using the ACI 318 equation, the average expected increase in failure stress for C1 and C2 specimens was 16% and 20%, respectively.

The lower expected increases in failure stress provided by the ACI 318 equation when compared to the ACI 408 equation result from the limit of 2.5 enforced on its cover and confinement term, $\left(\frac{c_b + K_{tr}}{d_b}\right)$. The limit is placed on this term to prevent the possibility of a pullout failure; however, results from the MMFX tests indicate that this limit could be relaxed. Values of $\left(\frac{c_b + K_{tr}}{d_b}\right)$ for confined specimens in this research program ranged from 2.44 to 5.0, and splitting failure was observed in all specimens. The ACI 408 equation recognizes the conservatism of the ACI 318 limit and limits its cover and confinement term $\left(\frac{c\omega + K_{tr}}{d_b}\right)$ to a value of 4.0. This increase resulted in the ACI 408 equation reflecting increased confinement benefits between the C1 and C2 specimens while the benefits of confinement appear to level off between the C1 and C2 specimens when using the ACI 318 equation.

The effect of the different limits on the cover and confinement terms in the ACI 318 and ACI 408 equations is demonstrated in Figure 6-15 and Figure 6-16, respectively. ACI 318 test/calculated failure stress ratios resulting from an increase in the cover and confinement limit from 2.5 to 4.0 are shown in Figure 6-17. Although MMFX data indicated that confinement remained effective at $\left(\frac{c_b + K_{tr}}{d_b}\right)$ well in excess of 2.5, the values plotted in Figure 6-17 indicate that modifying the limit on this term in the ACI 318 equation would result in unconservative predictions of failure stresses in many cases. The 2.5 limit does not accurately predict the point at which the pullout mode begins to govern failure, but the low limit provides the conservatism necessary for a design code equation. Therefore, a modification to the cover/confinement limit in the ACI 318 equation is not recommended.

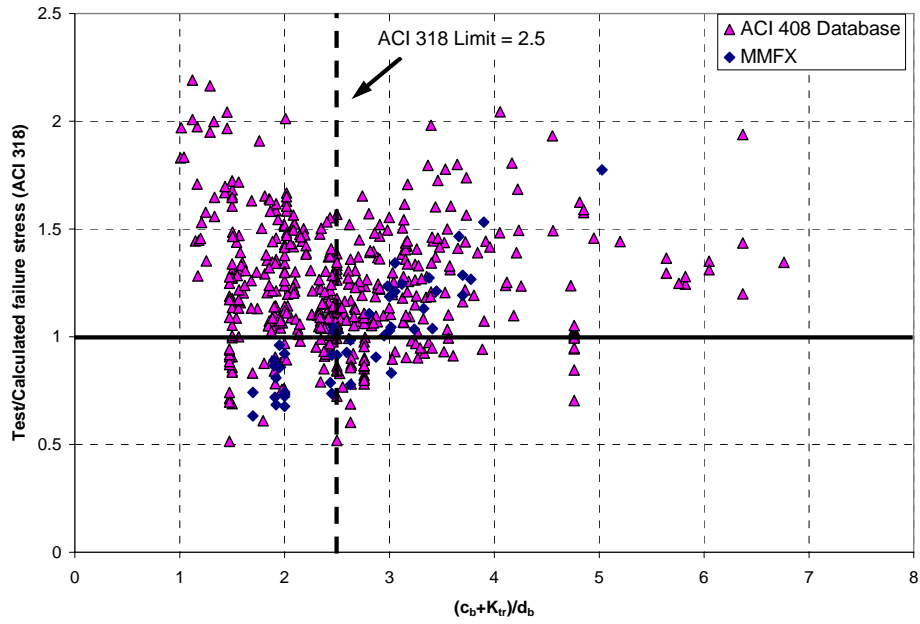


Figure 6-15: Test/calculated failure stress ratios versus cover/confinement term in ACI 318 equation (bar stress and concrete strength limits not applied)

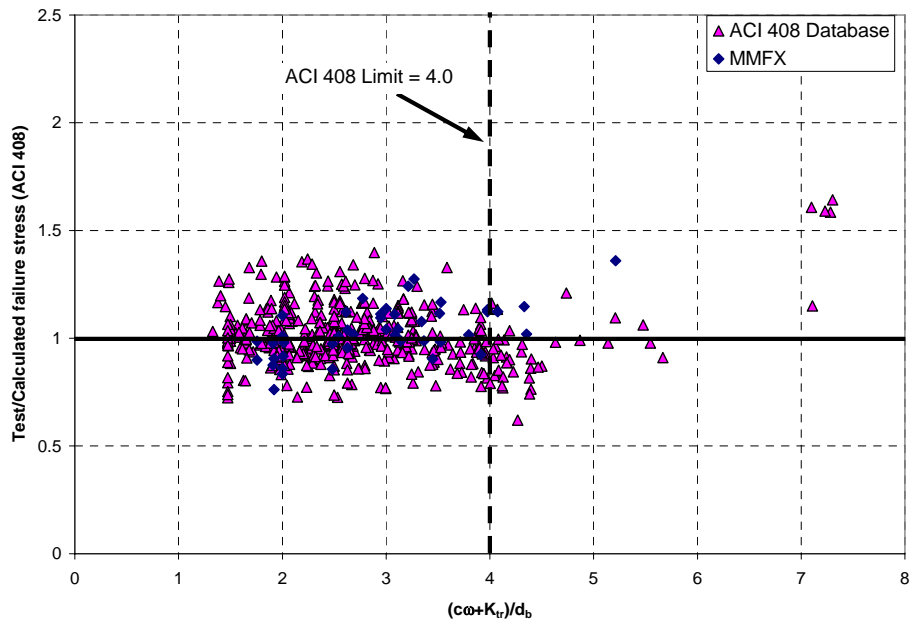


Figure 6-16: Test/calculated failure stress ratios versus cover/confinement term in ACI 408 equation

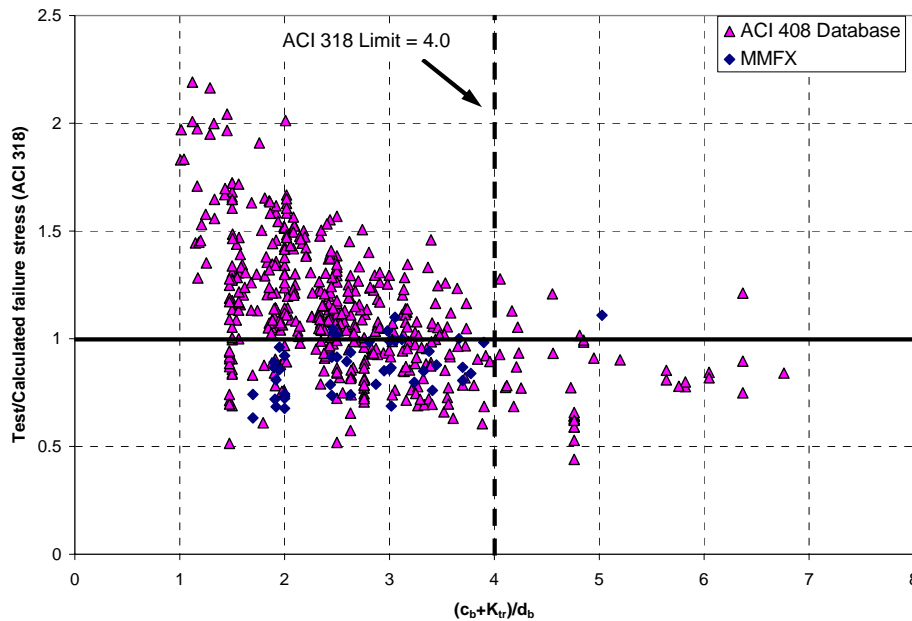


Figure 6-17: Test/calculated failure stress ratios versus cover/confinement term in ACI 318 equation (limit changed to 4.0, bar stress and concrete strength limits not applied)

While the ACI 408 equation predicted increased beneficial effects of confinement between the C1 and C2, the assumption of a failure stress increase proportional to the increase in the area of confining reinforcement was not substantiated by the test results. As indicated in Table 6-5, doubling the amount of transverse reinforcement between C1 and C2 specimens should result in a proportional increase in the failure stress over the unconfined C0 specimen according to the ACI 408 equation. However, the test results indicate that the C2 specimens only provided an average increase of 1.77 times that of the C1 specimens, and only one C2 specimen (8-5-OC2*-1.5) provided a failure stress increase greater than two times that of its corresponding C1 specimen, as shown in Table 6-6.

Specimen Group	Calculated f_s (ACI 408)			# of stirrups			% increase in f_s over C0		
	C0	C1	C2	C1	C2	C2/C1	C1	C2	C2/C1
8-8-OCx-1.5	82	104	126	3	6	2	27	54	2.00
8-5-OCx*-1.5	72	88	104	3	6	2	22	44	2.00
8-8-XCx-1.5	100	121	142	3	6	2	21	42	2.00
11-5-OCx-3 [†]	77	97	112	6	12	2	26	45	1.75
11-5-XCx-3	98	118	139	6	12	2	20	42	2.05
Average	---	---	---	---	---	2	23	45	1.96

†: Confinement term in C2 specimen exceeds ACI 408 limit of 4.0

Table 6-5: Expected increases in failure stresses over unconfined C0 specimens for C1 and C2 specimens based on ACI 408 calculated failure stress predictions – UT specimens

Specimen Group	Test f_s			# of stirrups			% increase in f_s over C0		
	C0	C1	C2	C1	C2	C2/C1	C1	C2	C2/C1
8-8-OCx-1.5	80	123	147	3	6	2	54	84	1.56
8-5-OCx*-1.5	72	99	129	3	6	2	38	79	2.11
8-8-XCx-1.5	86	122	144	3	6	2	42	67	1.61
11-5-OCx-3	75	104	128	6	12	2	39	71	1.83
11-5-XCx-3	84	117	141	6	12	2	39	68	1.73
Average	---	---	---	---	---	2	42	74	1.77

Table 6-6: Actual increases in failure stresses over unconfined C0 specimens for C1 and C2 splices – UT specimens

The disproportionate increase in failure stress with respect to the area of confining reinforcement may be a result of the increasing nonlinearity of the MMFX steel stress-strain relationship between the typical C1 and C2 failure stresses. Failure stresses for C1 specimens tested at the University of Texas ranged between 99 and 123 ksi. Failure stresses for the UT C2 specimens ranged from 129 to 147 ksi. As shown in Figure 6-18, the stress-strain relationship of the MMFX steel becomes increasingly nonlinear between these two stress ranges. Therefore, the effective stiffness of the bars reduces sharply between the C1 and C2 failure stress ranges. Research by Pay (2005) indicated that bond strength reduces with reduced bar stiffness so a reduction in the effect of confinement could be a result of the reduced effective stiffness of the bars at high stresses.

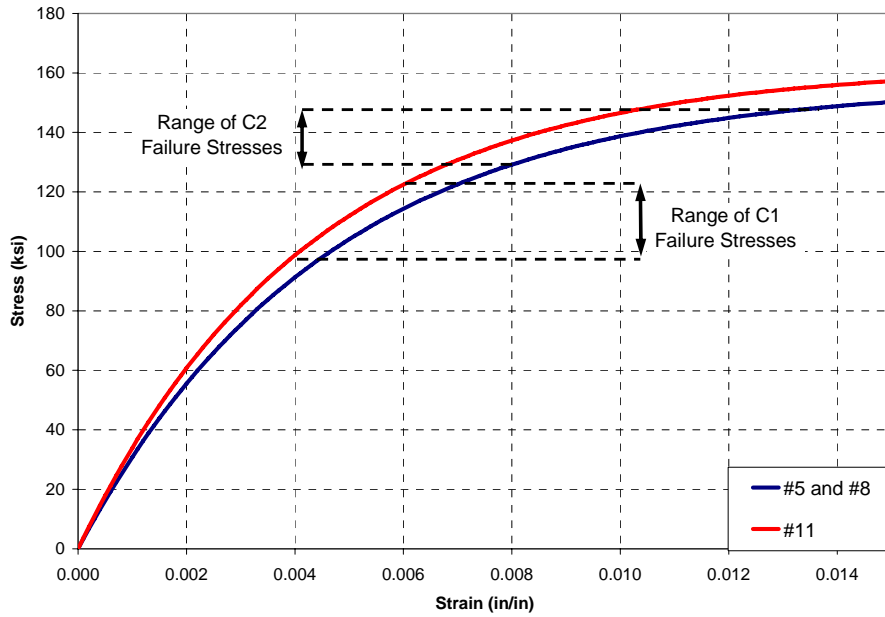


Figure 6-18: Increasing nonlinearity of MMFX stress-stress behavior between C1 and C2 failure stresses

This hypothesis is further defended by the values given in Table 6-6. The C2 splices in two specimen groups (8-5-OCx*-1.5 and 11-5-OCx-3) failed at relatively low stresses of 128-129 ksi. These two specimens produced the largest ratios for the comparison of percentage increase in failure stresses over the unconfined splices provided by C2 and C1 specimens. They also produced the ratios closest to the value of 2.0 suggested by the ACI 408 equation. Ratios for the remaining three specimen groups (11-5-XCx-3, 8-8-XCx-1.5, and 8-8-OCx-1.5) decreased with increasing failure stresses for the C2 splice. The ratios are plotted in Figure 6-19 to highlight this concept.

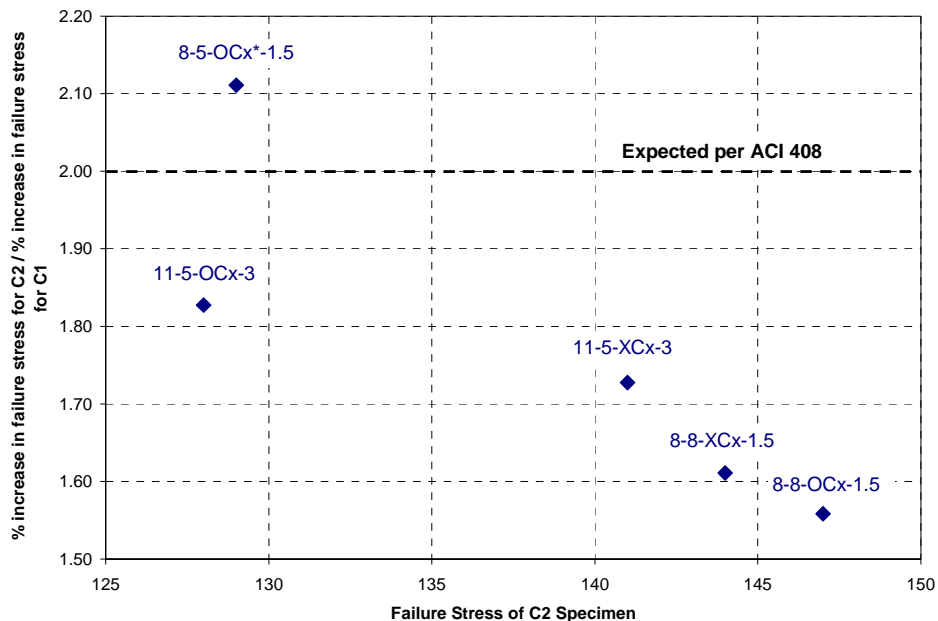


Figure 6-19: Reduction in the efficiency of confinement with increasing failure stress

Although the material nonlinearity resulted in a less than proportional increase in failure stress with respect to area of confining reinforcement, it produced substantially greater than proportional increases in deflections with respect to area of confining reinforcement. This is demonstrated in Table 6-7 with pairs of C1 and C2 specimens tested at the University of Texas. On average, the increase in deflections of C2 specimens was 2.6 times the deflection increase of the C1 specimens when compared to the deflection of unconfined specimens at failure.

Specimen Group	Deflection (in)			# of stirrups			% increase in deflection over C0		
	C0	C1	C2	C1	C2	C2/C1	C1	C2	C2/C1
8-8-OCx-1.5	0.87	1.73	2.53	3	6	2	99	191	1.93
8-5-OCx*-1.5	0.71	1.10	1.83	3	6	2	55	158	2.87
8-8-XCx-1.5	0.83	1.36	2.55	3	6	2	64	207	3.25
11-5-OCx-3	1.05	1.64	2.46	6	12	2	56	134	2.39
11-5-XCx-3	1.04	1.74	2.77	6	12	2	67	166	2.47
Average	---	---	---	---	---	2	68	171	2.58

Table 6-7: Comparison of deflection increases over unconfined C0 specimens for pairs of C1 and C2 beams – UT specimens

6.5 CRACK WIDTHS

The crack width plots shown in Chapter 5 showed all crack widths measured at the ends of the splices in specimens tested at the University of Texas. The plots indicate the crack width trends for the #5, #8, and #11 specimens through the full range of stresses experienced by the spliced bars. In design, crack widths are controlled for serviceability concerns; therefore, crack width measurements during service level loadings are most relevant for evaluating the impact of crack widths on design. Service loads are typically defined as loads at or below approximately 60% of the ultimate design load. In order to filter crack width measurements that are representative of service level cracks, all measurements taken above 60% of the failure load for a given specimen have been removed from the crack width database for the following analyses.

The service level end-of-splice crack widths for the #5 specimens tested at the University of Texas are plotted in Figure 6-20. For reference, the crack width limitations used to develop serviceability guidelines in pre-1999 versions of the ACI 318 code are also shown on the plot. As expected, the data indicated a linear increase in crack widths with an increase in service stress. Crack width theory would suggest that the wide #5 specimens with large covers and bar spacings (5-5-O/XC0-1.25, 5-5-O/XC0-2) would produce larger cracks than the narrow #5 specimens with small covers and bar spacings (5-5-O/XC0-3/4). However, the crack widths for the three different #5 specimen designs were relatively consistent for a given bar stress.

Crack widths remained small in all specimens when the bar stresses were below 55 ksi. At bar stresses above 55 ksi, the crack widths of the #5 specimens exceeded 0.013 in. — a value that has been considered acceptable for concrete members with exterior exposure. The limit of 0.016 in. for concrete members with interior exposure was surpassed by the #5 specimens at bar stresses of approximately 60 ksi. Assuming

service loads represent 60% of the ultimate load, the 0.013 in. and 0.016 in. service crack width limits allow for bar stresses of 92 ksi and 100 ksi at ultimate load, respectively.

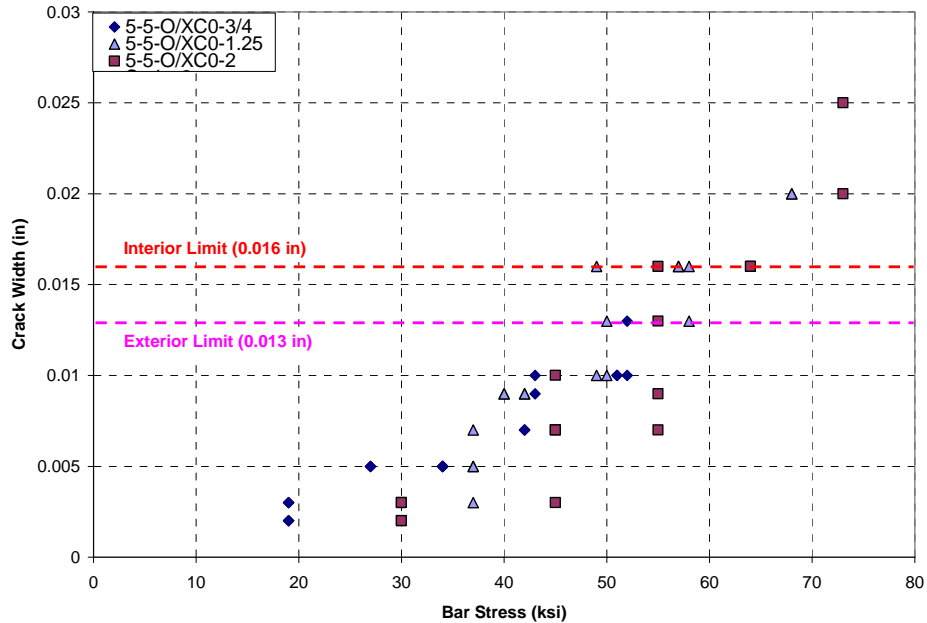


Figure 6-20: End-of-splice crack widths for UT #5 specimens (load at or below 60% of failure load)

The service level end-of-splice crack widths for the #8 specimens tested at the University of Texas are plotted in Figure 6-21. The ACI limits for interior and exterior exposure are again included for reference. Since the theoretical crack widths for all of the #8 specimens were the same, the predicted crack widths computed according to the equation developed by Gergely and Lutz (1968) are also included.

The Gergely-Lutz equation predicts the maximum crack width in a flexural member as

$$w = 0.076 \beta f_s \sqrt[3]{d_c A}$$

where:

w = *expected maximum crack width in 0.001 in. units*

β = *ratio of distances to the neutral axis from the extreme tension fiber and from the centroid of A_s . (1.1 for #8 specimens, 1.2 for #11 specimens)*

f_s = *steel stress in ksi*

d_c = *cover of outermost bar of A_s , measured to the center of the bar*

A = *tension area per bar measured as the area centered around the c.g. of the tension bars divided by the number of tension bars.*

Since crack width data are highly variable, Figure 6-21 indicates the range of Gergely-Lutz $\pm 50\%$ rather than a single line for predicted crack widths.

The #8 crack width data showed a slight nonlinear increase with increasing bar stress. The majority of the data were within the range of predicted crack widths, but a few data points are well outside of the Gergely-Lutz $\pm 50\%$ limits. These points were more common at high bar stresses.

Similar to the #5 specimens, crack widths remained relatively small at stresses below 50-55 ksi. At this point, the average crack width exceeded the 0.013 in. exterior exposure limit. The average crack width exceeded the 0.016 in. interior exposure limit around 60 ksi. Again, these values suggest that the stresses at ultimate load in the #8 bars would need to be limited in beams of similar design to 92 ksi and 100 ksi for exterior and interior elements, respectively.

Above 60 ksi, the crack width data began to display more scatter. Most data remained within the expected range of widths; however, a few very large values were recorded at higher stresses. The most severe service level crack measured 0.0625 in. at a

bar stress of 89 ksi. This value was 2.5 times that predicted by the Gergely-Lutz equation.

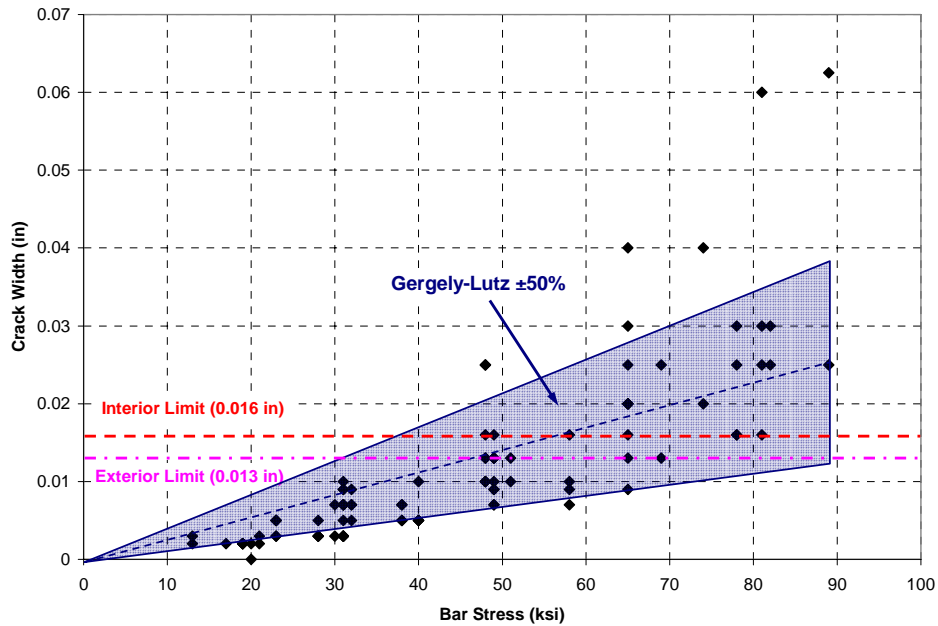


Figure 6-21: End-of-splice crack widths for UT #8 specimens (load at or below 60% of failure load)

The service level end-of-splice crack widths for the #11 specimens tested at the University of Texas are plotted in Figure 6-22. Similar to the #5 specimens, the data indicated an approximately linear relationship between bar stress and crack width. The rate of increase of crack widths with increasing bar stress was greater than predicted by the Gergely-Lutz equation. As a result, crack widths in the #11 specimens were smaller than predicted by the Gergely-Lutz equation at low stresses and larger than predicted by the Gergely-Lutz equation at high stresses. Nevertheless, the majority of the crack widths were within the predicted range of widths bounded by the Gergely-Lutz equation $\pm 50\%$.

Due to large spacing and cover values in the #11 specimens, crack widths in these beams exceeded the 0.013 in. and 0.016 in. limits at substantially lower stresses than the crack widths in the #5 and #8 specimens. The average crack width exceeded the exterior limit of 0.013 in. at a bar stress of approximately 28 ksi. The interior limit of 0.016 in. was surpassed at an approximate bar stress of 32 ksi. These values imply that ultimate bar stresses in beams of similar design should be restricted to 47 ksi and 53 ksi for exterior and interior exposures, respectively.

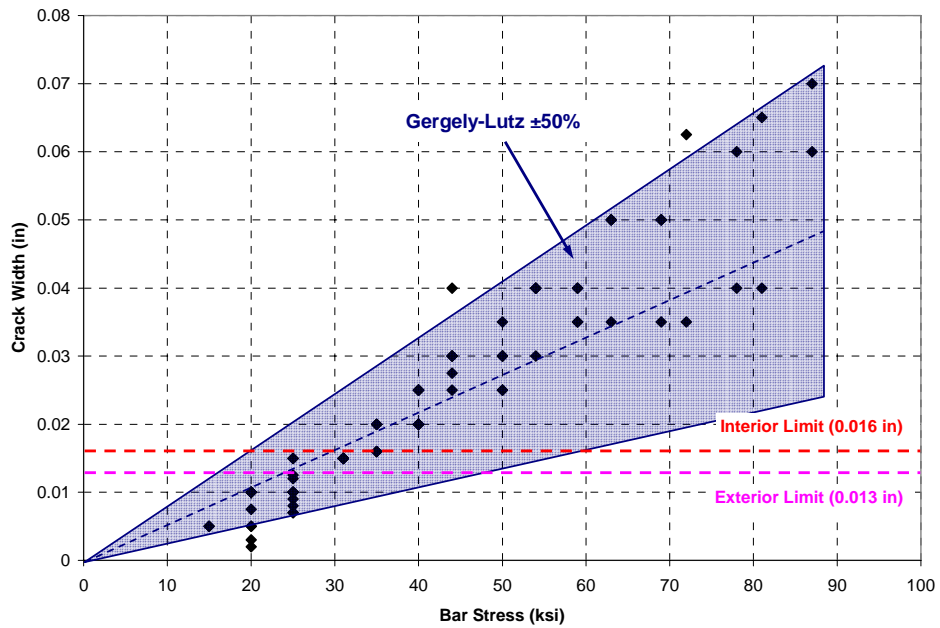


Figure 6-22: End-of-splice crack widths for UT #11 specimens (load at or below 60% of failure load)

CHAPTER 7

Implementation of Results

7.1 INTRODUCTION TO DESIGN CONSIDERATIONS

The results of this research program have provided insight for the design of flexural concrete members reinforced with MMFX high strength reinforcement. Although this study was focused primarily on the splice behavior of reinforcing bars at high stresses, the general behavior of the test specimens offered an understanding of the primary differences between design for ordinary Grade 60 reinforcement and high strength MMFX reinforcement. Splice specific design recommendations are presented in Section 7.2. General design considerations are discussed in Section 7.4.

7.2 SPLICE DESIGN RECOMMENDATIONS

The data analyses provided in Chapter 6 indicated that the current development length equations included in the ACI 318 building design code and the AASHTO LRFD bridge design code are inadequate for use at high bar stresses. This is largely due to the lack of data for high strength reinforcing bars at the time of development of these equations. The ACI 318 equation was developed based on a best fit expression for data from splice tests failing primarily at or below the ACI limit of 80 ksi. The AASHTO equation was not developed empirically, but its theoretical basis does not appear to apply at high stress levels.

Since the best fit development length equation recommended by ACI Committee 408 was based on the results of splice tests in a wider range of bar stresses and concrete strengths, it aligns more favorably with the test data obtained in this research program. When using the ACI 408 equation, variability in the ratios of test to calculated failure

stresses were consistently and significantly less than when using the ACI 318 or AASHTO equations. The mean value of 1.03 for test/calculated ratios for specimens in the MMFX research program, provides further indication of suitability of the ACI 408 equation for determining splice strength over a wide range of bar stresses. For reference, the ACI 408 development length equation is

$$l_d = \left(\frac{\left(\frac{f_y}{\phi f_c^{1/4}} - 2400\omega \right) \psi_t \psi_e \lambda}{76.3 \left(\frac{c\omega + K_{tr}}{d_b} \right)} \right) d_b$$

where:

f_y = yield stress of reinforcing bar (psi)

f_c' = concrete compressive strength (psi) < 16,000 psi

d_b = bar diameter (in)

c_{si} = one-half clear spacing between bars (in)

c_{so} = side cover of reinforcing bars (in)

c_b = bottom cover of reinforcing bars (in)

c_s = minimum of $c_{si} + 0.25$ in. or c_{so} (in)

c_{min} = minimum of c_s or c_b (in)

c_{max} = maximum of c_s or c_b (in)

c = $c_{min} + d_b/2$ (in)

$\omega = \left(0.1 \frac{c_{max}}{c_{min}} + 0.9 \right) \leq 1.25$

$K_{tr} = \frac{0.52 t_r t_d A_{tr}}{sn} \sqrt{f_c'}$

$t_d = 0.78 d_b + 0.22$

$t_r = 9.6R_r + 0.28$ or 1.0 in the absence of specific values of bar relative rib area during design

A_{tr} = area of transverse reinforcement crossing the plane of splitting (in^2)

n = number of bars being developed or spliced in the plane of splitting

s = spacing of transverse reinforcement (in)

ϕ = modification factor = 0.82 when using load factors given in ACI 318-05

$\psi_t = 1.3$ where horizontal reinforcement is placed such that more than 12 in. of fresh concrete is cast below the developed length or splice
= 1.0 for all other cases.

$\psi_e = 1.5$ for epoxy-coated bars

= 1.0 for all uncoated bars

$\psi_t\psi_e$ need not exceed 1.7

$\lambda = 1.3$ or $6.7\sqrt{f'_c}/f_{ct} \geq 1.0$ for lightweight concrete

= 1.0 for normalweight concrete

and the term $\frac{c\omega + K_{tr}}{d_b}$ is limited to 4.0 to prevent pullout failure.

In order to safely apply the ACI 408 equation in design, an appropriate modification factor must be included in the calculation. As stated in Chapter 3, ACI Committee 408 recommends this factor, ϕ , be taken as 0.82 when the load factors included in the ACI 318-05 building code are used. The distributions of test/calculated ratios for the MMFX splice tests when this value of ϕ is used are shown in Table 7-1 and Figure 7-1.

Splice Type	N	Distribution of MMFX Results Using ACI 408 Equation ($\phi = 0.82$)						
		Mean	Std. Dev.	COV	Max	Min	# < 1.0	% < 1.0
All	45	1.26	0.15	0.12	1.66	0.93	1	2
Unconfined	23	1.20	0.13	0.11	1.39	0.93	1	4
Confined	22	1.32	0.14	0.11	1.66	1.10	0	0

Table 7-1: Distribution of MMFX test/calculated failure stress ratios when using the ACI 408 development length equation with $\phi = 0.82$

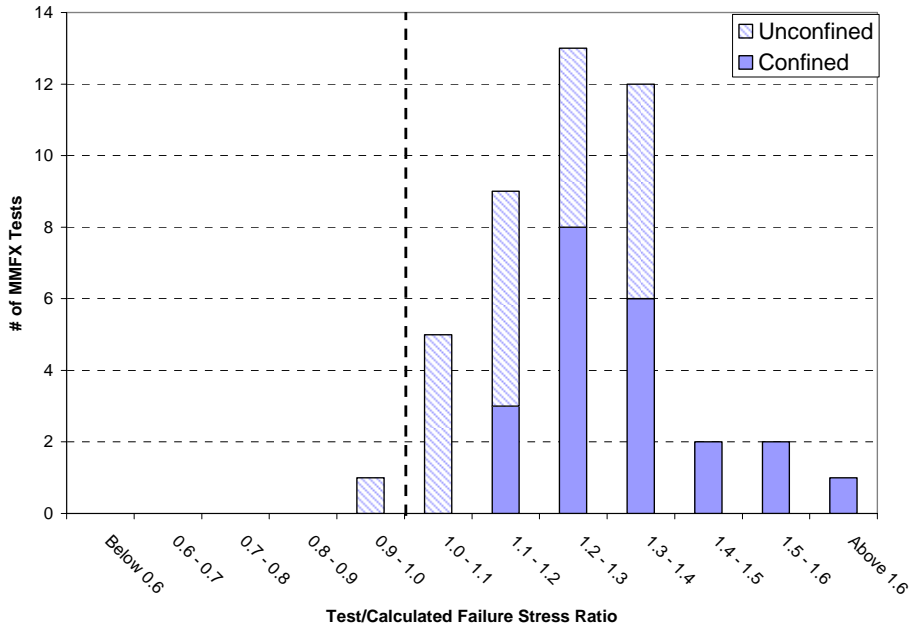


Figure 7-1: Distribution of MMFX test/calculated failure stress ratios when using the ACI 408 development length equation with $\phi = 0.82$

The mean test/calculated failure stress ratios for unconfined and confined splices are both well above 1.0 as expected for a design equation. Because of the increased mean values and the low coefficients of variation for both the unconfined and confined splices, only one splice failed at a bar stress less than calculated by the equation. Based on these data, the ACI 408 equation with a modification factor of 0.82 provides a conservative estimate of failure stresses for splices of bars over a range of high stresses up to 150 ksi.

When the data from ACI 408 database 10-2001 are included in the analyses, the combined distributions of test/calculated failure stress ratios for previous bond tests and MMFX bond tests failing at bar stresses greater than 75 ksi exhibited the same consistent conservatism as shown in Table 7-2 and Figure 7-2. Therefore, the use of the ACI 408 development length equation with a modification factor of 0.82 is recommended for calculating required splice lengths of bars expected to develop stresses in excess of 75 ksi. Equivalently, the following equation with the modification factor of 0.82 pre-multiplied to the ACI 408 equation may be used.

$$l_d = \left(\frac{\left(\frac{f_y}{f_c^{1/4}} - 1970\omega \right) \psi_s \psi_e \lambda}{63 \left(\frac{c\omega + K_{tr}}{d_b} \right)} \right) d_b$$

Splice Type	N	Distribution of All Results Using ACI 408 Equation ($\phi = 0.82$, $f_s > 75$ ksi)						
		Mean	Std. Dev.	COV	Max	Min	# < 1.0	% < 1.0
All	134	1.31	0.19	0.15	2.00	0.94	2	1.5
Unconfined	27	1.20	0.13	0.11	1.42	0.94	1	4
Confined	107	1.34	0.20	0.15	2.00	0.99	1	1

Table 7-2: Distribution of test/calculated failure stress ratios when using the ACI 408 development length equation with $\phi = 0.82$ (Data includes all bond tests in the ACI 408 database 10-2001 and the MMFX research program failing at bar stresses > 75 ksi)

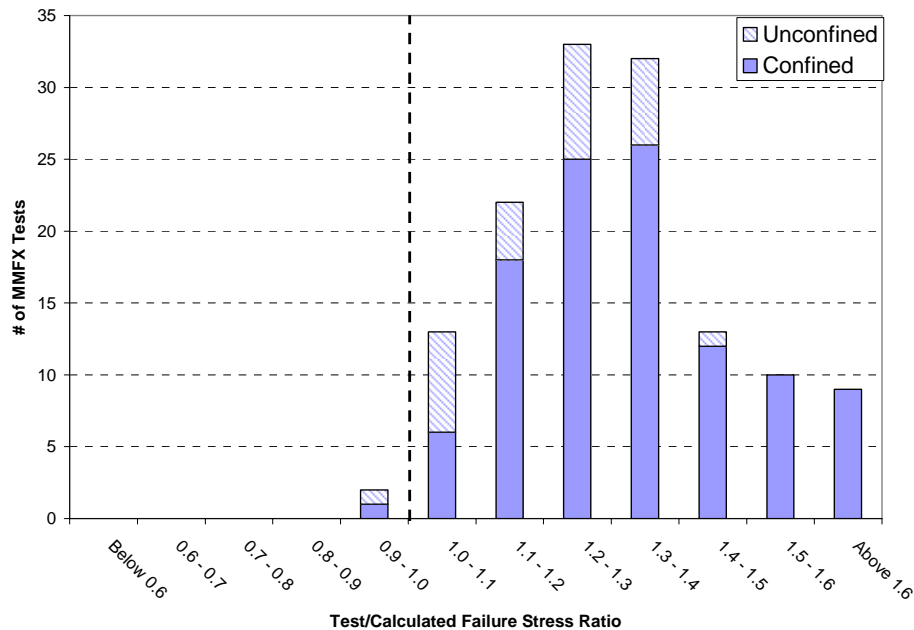


Figure 7-2: Distribution of test/calculated failure stress ratios when using the ACI 408 development length equation with $\phi = 0.82$ (Data includes all bond tests in the ACI 408 database 10-2001 and the MMFX research program failing at bar stresses > 75 ksi)

7.3 REQUIREMENTS FOR TRANSVERSE REINFORCEMENT

Splices of reinforcing bars at high stress should include at least a minimal amount of confining transverse reinforcement. The results of this research program cannot provide a definitive value for minimal transverse reinforcement, but the minimum transverse reinforcement required for shear (§11.5.6.3 of ACI 318-05) may be used as a guideline for bar splices until this issue is studied in more detail. As indicated by the distribution of test/calculated ratios, the ACI 408 development length equation displays more conservatism in confined splices than in unconfined splices. The addition of confinement also provides a considerable increase in ductility. Given the brittle and sudden nature of bond failure, allowing flexural members to extend into the nonlinear

range of their load-deflection behavior is crucial in providing adequate warning of impending failure.

The requirement for minimal confining reinforcement does not apply to splices of widely spaced #5 or smaller bars with large covers. Test results in this research program indicate that stresses as high as 120 ksi can safely be developed in unconfined splices of #5 bars. These splices performed better than other splices at high stresses since the values of l/d_b required to develop high stresses in spliced bars of this configuration are usually less than 40 — the threshold at which the ratios of test to calculated failure stresses are approximately 1.0 as described in Chapter 6. The requirement for minimal confining reinforcement is also not extended to these splice configurations because the effectiveness of confinement reduces as bar size reduces. This is demonstrated by the limit of 4.0 imposed on the cover and confinement term $\frac{c\omega + K_{tr}}{d_b}$. For example, a #5 splice with 4.0 in. clear spacing between splices and 2.0 in. clear cover produces a value of $\frac{c\omega + K_{tr}}{d_b}$ equal to 3.7. Adding confinement will provide minimal, if any, additional strength or ductility since the splice failure mode will likely convert to a pullout failure. Research on short splices of #5 MMFX bars conducted by Donnelly (2007) confirms this conclusion.

7.4 GENERAL DESIGN CONSIDERATIONS

The results of this study show that MMFX high strength reinforcement can be lap spliced to develop bar stresses up to 150 ksi. However, designing a member for both strength and serviceability while taking advantage of the high strength of MMFX reinforcement presents many challenges.

A simple example beam is presented to demonstrate the important design issues related to MMFX and other high strength reinforcing bars. The example beam is a 14 in.

wide by 28 in. deep simply supported beam with a 20 ft. span. The design includes 1.5 in. of clear cover to the #4 stirrups and a concrete compressive strength of 5000 psi. A variable number of #8 bars reinforce the beam in tension. The number of bars is dependent on the assumed yield strength, f_y , used in design. Details of the span, loading, and dimensions of the example beam are given in Figure 7-3 and Figure 7-4.

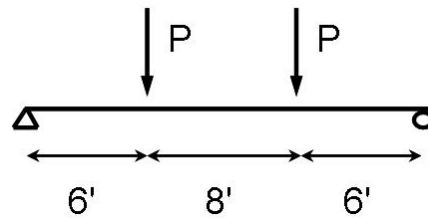


Figure 7-3: Span and loading of example beam

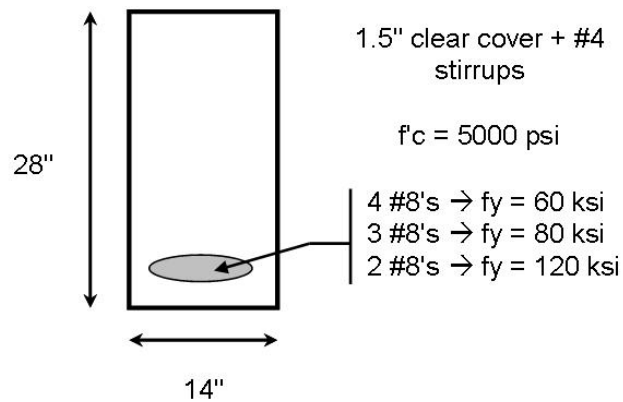


Figure 7-4: Details of example beam

Four cases of the example beam are examined. One case is reinforced with ordinary Grade 60 reinforcement. The remaining three cases are reinforced with MMFX reinforcement. The Grade 60 beam was designed for a tension controlled failure using customary reinforced concrete design principles. Design of the three MMFX beams was

carried out by assuming different yield strengths of the MMFX reinforcement — 60 ksi, 80 ksi, and 120 ksi. After design of each MMFX beam, the strains in the steel were checked to ensure that the beams could attain at least the strain necessary to develop the assumed yield stress.

The following three sections describe issues related to the ultimate behavior, deflections, and crack widths for the different beam designs. Although the example beams were not constructed and tested in the laboratory, the good correlation between calculated and actual flexural behavior, deflections, and crack widths displayed by specimens in this research project substantiate the claims made in the following sections.

7.4.2 Ultimate Behavior

All four example beams possess equal strength assuming that failure of each example beam occurs when the stress in the reinforcing steel reaches the design stress. This assumption is valid for the example beam reinforced with Grade 60 reinforcement. However, it does not hold for the example beams reinforced with MMFX steel since MMFX does not display a yield plateau. As shown in Figure 7-5, the MMFX beams continue to carry load above the design load of 60 kip.

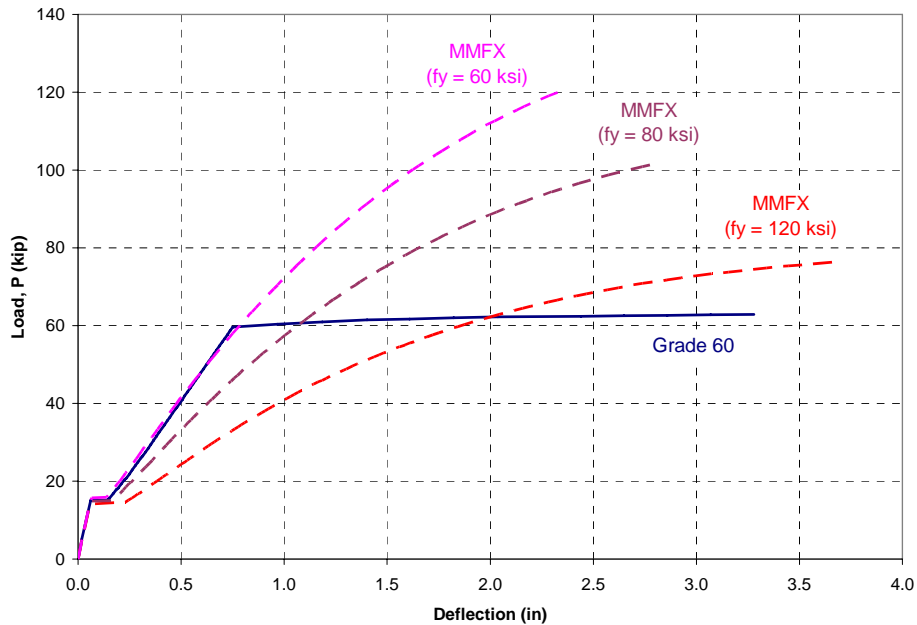


Figure 7-5: Calculated load-deflection for example beam assuming varying design yield strengths for the MMFX reinforcement

This may appear to provide conservatism to the MMFX designs; but if ductile failure is the primary goal of the designer, the ability of the MMFX designs to carry more than the design load may lead to undesirable brittle failure modes. Reinforced concrete members are typically designed to avoid brittle failures such as those caused by shear or bond. Strength reduction factors vary for different modes of failure to promote certain failure modes over others. This explains why the strength reduction factor for flexure in tension controlled members is 0.90 and the strength reduction factor for shear is 0.75. The ductile flexural failure of a tension controlled member is more desirable than brittle failure by shear.

Since the example beams reinforced with MMFX reinforcement can exceed their design strengths, the difference in strength reduction factors between flexure and shear may not be sufficient to prevent the occurrence of a brittle failure. For example, the

design load effects for shear and flexure are proportional to the ratio of the strength reduction factor for flexure to the strength reduction factor for shear. Therefore, the design load for shear would be $0.90/0.75 = 1.20$ times that of the design load for flexure. This results in a design shear of $60 \times 1.20 = 72$ kip for the example beams. As seen in Figure 7-5, the three example beams reinforced with MMFX steel are all capable of reaching 72 kip so an overload to 72 kip could cause a shear failure in these beams instead of a flexural failure. This may be of little concern in the beam designed for a yield strength of 120 ksi since the beam would have experienced significant deflections from the overload; but the deflections experienced by the beams designed based on a 60 ksi and 80 ksi assumed yield would provide little warning of failure.

The issue may be more severe for bond failure. A strength reduction factor is not applied to development lengths. It is usually assumed that the required safety is provided by the strength reduction factor used in flexural design calculations and by the inclusion of more steel than necessary in design. Where ductility and/or structural integrity would be severely compromised by a bond failure, development lengths are increased by 30-70% (ACI 318 Class B, AASHTO Class B, C). However, since bar stresses in members reinforced with MMFX reinforcement can continue to increase above the yield strength assumed in design, these traditional methods of avoiding bond failure may not be sufficient to prevent this brittle mode of failure from occurring.

The additional load carrying capacity above that calculated based on the assumed yield strength also raises concerns for applications in seismic areas. In seismic design, members are expected to yield for several reasons. Yielding allows for the dissipation of large amounts of energy without an increase in applied load on the structure. This reduces design loads and makes them more predictable. Yielding also allows for the redistribution of moments in statically indeterminate structures. Without the ability to

yield, designs with MMFX steel will be subject to larger and less predictable seismic loads. Desirable levels of ductility may not be achievable, and failure may occur by brittle failure rather than through the desired ductile mode. For these reasons, the use of MMFX steel in seismic design is not recommended at this time, especially in fuse members expected to yield.

7.4.3 Deflections

Designers may wish to utilize the high strength of MMFX reinforcement for several reasons. The reduction in necessary steel may offset the increased cost of MMFX over conventional Grade 60 reinforcement. Fewer bars may increase constructability in crowded beams and connections. As shown above, utilizing the high strength in design also produces larger deflections at the design load, thereby providing a better indication of distress and impending failure.

However, this final reason for utilizing the high strength of MMFX reinforcement leads to an argument why the use of the high strength may be undesirable. Not only do ultimate deflections increase with higher assumed MMFX yield strengths, but service load deflections also increase. Large service deflections can lead to issues with vibrations, aesthetics, and damage to non-structural elements. To avoid these problems, service deflections are usually limited to certain acceptable values.

The effects of assumed yield strength on service load deflections are shown in Figure 7-6. Service deflections are approximately proportional to the assumed yield stress. Therefore, the service deflection for the example beam designed assuming a 120 ksi yield strength would be roughly twice the service deflection of the beam designed assuming a 60 ksi yield strength. In this case, the increase in deflection due to the higher assumed yield strength caused the computed deflections for the 120 ksi yield example beam to exceed the ACI 318 limit of $L/360 = 0.67$ in. As the service deflection of a

baseline Grade 60 beam becomes closer to the ACI limit (i.e. – due to a longer span or lower stiffness), service deflections will become a greater issue for alternate designs reinforced with MMFX reinforcement, especially those designed with high assumed yield strengths.

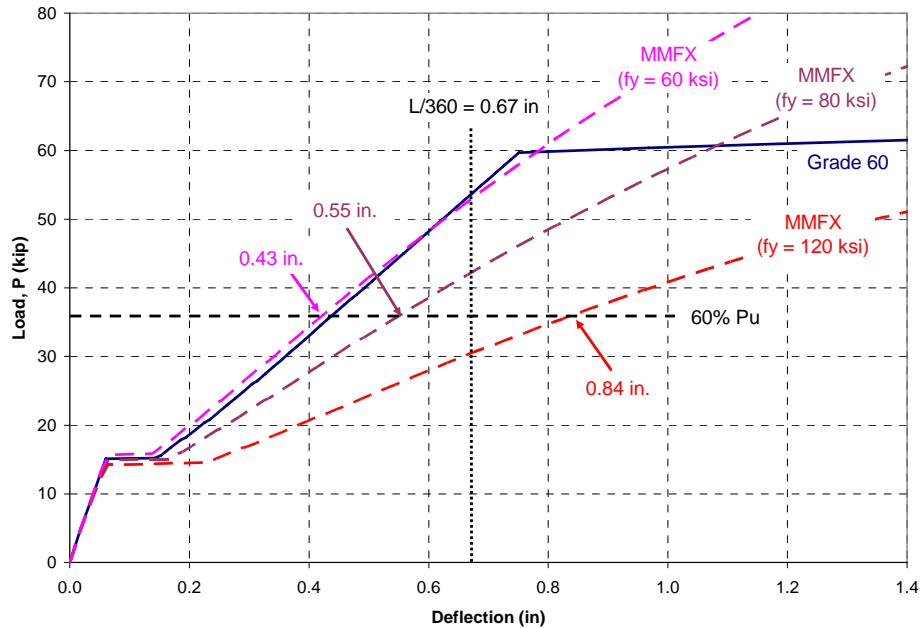


Figure 7-6: Calculated service load deflections for the example beam assuming varying design yield strengths for the MMFX reinforcement

7.4.4 Crack Widths

Given the inherent corrosion resistance of MMFX steel, large cracks in beams reinforced with MMFX bars may not be as much of a concern as with beams reinforced with ordinary Grade 60 bars from a corrosion perspective; but crack widths must also be limited for other reasons such as aesthetics and freeze/thaw effects. Therefore, crack widths should still be limited in designs incorporating MMFX reinforcement.

Crack widths increase as stresses in the reinforcing bars increase. Since the use of a higher assumed yield strength for MMFX reinforcement will result in a higher bar stress for a given load, crack widths will also increase for a given load. The effects of the different assumed yield strengths in the example beams on the computed crack widths are highlighted in Figure 7-7. In this figure, the expected crack widths were computed using the Gergely-Lutz equation. The limits of 0.013 in. and 0.016 in. for service crack widths of exterior and interior members are included in the figure for reference.

As expected, the example beams designed with higher assumed yield strengths produce larger computed crack widths. The increase in crack widths between the designs is proportional to the increase in assumed yield strength. Again, the example beam designed with an assumed yield strength of 120 ksi does not satisfy the serviceability limits; and as the crack widths of a baseline Grade 60 beam design approach the acceptable service crack limits, crack widths will become an even more serious issue in alternate designs using the high strength of MMFX reinforcement.

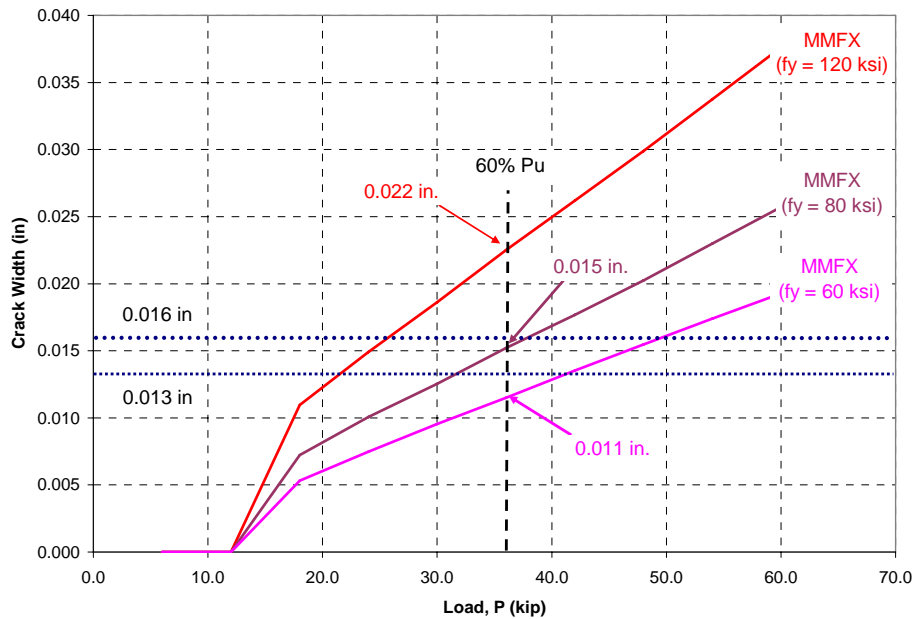


Figure 7-7: Calculated crack widths for the example beam assuming varying design yield strengths for the MMFX reinforcement

7.4.5 General Design Overview and Future Research

As shown in Sections 7.4.2, 7.4.3, and 7.4.4, the use of MMFX steel for concrete reinforcement complicates the design process for flexural members because certain assumptions about behavior are no longer valid and certain limitations for serviceability are difficult to satisfy. However, this does not imply that MMFX reinforcement cannot be successfully utilized in reinforced concrete design. Further research is necessary before general design recommendations can be developed; but in the absence of more experimental data, designers should be careful to balance the ultimate behavior and serviceability concerns outlined in the previous sections.

Future research on members reinforced with MMFX steel should focus on the impact of large cracks and deflections at service loads, the fatigue performance of MMFX bars used at high service stresses, the probability of and issues with experiencing

non-flexural failures, moment redistribution in statically indeterminate members, and the seismic performance and design implications associated with a reinforcing steel that does not yield.

CHAPTER 8

Conclusions

8.1 RESEARCH SUMMARY

MMFX microcomposite steel reinforcement is manufactured through a patented proprietary process that results in a high strength, corrosion resistant material. The high chromium content (9-10%) and the unique microstructure of MMFX steel are believed to contribute to the inherent corrosion resistance of the material. An appraisal report compiled by the Concrete Innovation Appraisal Service (Zia 2003) evaluated the findings of several independent research studies related to the corrosion resistance of MMFX reinforcement. The authors of the report concluded that there is sufficient evidence that MMFX steel exhibits improved corrosion resistance over conventional ASTM A 615 reinforcing steel and that this corrosion resistance can lead to longer service lives and lower life-cycle costs.

The low carbon content (0.08%) of MMFX steel leads to its high strength. MMFX steel guarantees a minimum ultimate tensile strength of 150 ksi and a minimum yield strength of 100 ksi when measured using the 0.2% offset method (MMFX 2004). Tension tests conducted on MMFX reinforcing bars as part of this project and in previous research programs indicate that the tensile strength can be significantly higher (160-177 ksi), and the 0.2% offset yield strength is more commonly near 120 ksi (El-Hacha and Rizkalla 2002).

To utilize MMFX steel reinforcement most efficiently, designers may wish to take advantage of the material's high strength in addition to its corrosion resistance; however the current ACI 318-05 building code limits the allowable yield stress in tensile

reinforcement to 80 ksi. The AASHTO LRFD bridge code limits tensile yield strengths to 75 ksi. Structural tests on laboratory specimens reinforced with steel that experiences stresses well in excess of these limits must be conducted to substantiate a change in the maximum design stresses. These tests are necessary because many of the design equations included in the ACI 318 and AASHTO LRFD codes have been developed from empirical data, and they were not intended to be used beyond the limits of the variables included in the supporting research.

Development length equations are an example of such empirical equations. The development length equation included in the ACI 318-05 building design code was based on the results of splice tests failing primarily at or below 80 ksi. The AASHTO LRFD development length equation is based on theoretical assumptions of bond behavior and empirically developed limits of bond stresses. A recently proposed development length equation provided by ACI Committee 408 is based on a larger database of tests than those used for the development of the ACI 318 and AASHTO LRFD design equations, but the bar stresses at failure were still limited to less than 120 ksi. Only 12 tests were available between 100 and 120 ksi.

The goal of this research program was to increase the current database of splice tests at high stresses. The data were used to evaluate the adequacy of the ACI 318, AASHTO LRFD, and ACI 408 development length equations at high bar stresses and to develop design recommendations for the splicing and development of MMFX steel at stresses above the current code limits of 75-80 ksi.

According to the original test matrix, 22 beam-splice specimens are being tested at each of the three participating research universities — the University of Texas, the University of Kansas, and North Carolina State University. Test variables included bar size, concrete compressive strength, splice length, concrete cover, and amount of

transverse reinforcement (confinement). All splices were designed to fail in the stress range of 80-140 ksi. In addition to the bar stresses at splice failure, crack widths and deflections were monitored to examine serviceability concerns related to high stresses in tensile reinforcement. Tension tests were also performed on each size of MMFX reinforcement in order to accurately relate bar strains with bar stresses.

8.2 CONCLUSIONS

Based on the results of 25 beam-splice tests conducted at the University of Texas, 22 beam-splice tests conducted at North Carolina State University, and 3 beam-splice tests conducted at the University of Kansas, the following conclusions were developed for the splice behavior of MMFX high strength reinforcement.

- Lap splices using MMFX high strength reinforcement developed bar stresses up to 155 ksi.
- The ACI 408 development length equation provided relatively accurate estimates of failure stresses for splices with and without confining transverse reinforcement.
- Both the ACI 318 and AASHTO LRFD development length equations provided unconservative calculated failure stresses for unconfined splices. The two equations provided reasonably conservative calculated failure stresses for confined splices.
- The use of the ACI 408 development length equation resulted in less scatter of test/calculated failure stress ratios for splices with and without confining reinforcement than the use of either the ACI 318 or the AASHTO LRFD development length equations.
- The conservatism of the ACI 408, ACI 318, and AASHTO LRFD development length equations reduced in unconfined splices as the ratio of splice length to bar diameter (l_s/d_b) increased. Test/calculated failure stress ratios for all three

equations transitioned from predominately greater than 1.0 to predominately less than 1.0 at values of l_s/d_b between 35 and 40.

- The addition of confining transverse reinforcement provided an increase in failure stress. This increase was greater than predicted by either the ACI 408 or ACI 318 equation. The increase in failure stress between two identical splices with varying levels of confinement was less than proportional to the increase in confining reinforcement between the two specimens.
- The addition of confining transverse reinforcement provided an increase in beam deflections at failure. The increase in deflections between two identical splices with varying levels of confinement was significantly greater than proportional to the increase in confining reinforcement between the two specimens.
- Service level crack widths were consistently greater than the limits of 0.013 in. and 0.016 in. used as a basis for serviceability provisions included in pre-1999 editions of the ACI 318 building code. Crack widths were very large in specimens containing #11 bars that had wide bar spacings and large covers.
- Splices of bars expected to experience stresses greater than 75 ksi should be designed using the ACI 408 development length equation with the modification factor, ϕ , equal to 0.82.
- A minimum level of transverse reinforcement should be included for all splices above 75 ksi except for those with #5 or smaller bars with large bar spacings and covers.
- Designers should be aware of the ultimate and service level concerns related to the use of MMFX bars.

APPENDIX

Beam-Splice Specimen Details

Splice details for specimens tested at the University of Texas are given in Table A-1. Splice details for specimens tested at North Carolina State University and the University of Kansas are given in Table A-2. The details are reported using the terminology and layout consistent with the data reported in the ACI 408 database 10-2001. The notation is as follows.

A_b	Bar area
A_t	Area of one leg of a stirrup
b	Beam width
c_{si}	One-half clear spacing between bars
c_{so}	Side clear cover
c_b	Bottom clear cover
d	Beam effective depth
d_b	Bar diameter
d_{tr}	Nominal stirrup diameter
f'_c	Concrete compressive strength
f_{sc}	Ultimate bar stress determined using moment-curvature method
f_{su}	Ultimate bar stress determined using working stress method or ultimate strength method
f_y	Bar yield strength
f_{yt}	Stirrup yield strength

h	Beam height
l_s	Splice length
N_b	Number of spliced or developed bars
N_l	Number of legs per stirrup
N_s	Number of stirrups along splice or development length; multiple legged stirrups at one location are treated as a single stirrup
R_r	Relative rib area of bar (ratio of projected rib area normal to bar axis to the product of the nominal bar perimeter and the center-to-center rib spacing)
*	Not Provided
†	Nominal Dimension

TEST#	School	l_s in.	d_b in.	R_r	b in.	h in.	d in.	c_{so} in.	c_{sl} in.	c_b in.	N_b	d_{tr} in.	N_s	N_l	A_b in. ²	A_t in. ²	f_c psi	f_y ksi	f_{yt} ksi	f_{sc} ksi	f_{su} ksi
8-8-OC0-1.5	UT	40	1.00	0.0838	10.25	22.38	20.38	1.60	1.40	1.50	2	0	0	0	0.79	0.00	8300	*	*	80	*
8-8-OC1-1.5	UT	40	1.00	0.0838	10.13	23.25	21.25	1.65	1.38	1.50	2	0.5	3	2	0.79	0.20	8300	*	*	123	*
8-8-OC2-1.5	UT	40	1.00	0.0838	10.13	23.25	21.25	1.65	1.38	1.50	2	0.5	6	2	0.79	0.20	8300	*	*	147	*
8-5-OC0-1.5	UT	40	1.00	0.0838	10.25	27.50	25.50	1.65	1.45	1.50	2	0	0	0	0.79	0.00	5200	*	*	72	*
8-5-OC1-1.5	UT	40	1.00	0.0838	10.25	27.50	25.50	1.65	1.38	1.50	2	0.5	3	2	0.79	0.20	5200	*	*	99	*
8-5-OC2-1.5	UT	40	1.00	0.0838	10.25	27.50	25.50	1.65	1.38	1.50	2	0.5	6	2	0.79	0.20	5200	*	*	139	*
8-8-XC0-1.5	UT	54	1.00	0.0838	10.25	27.50	25.50	1.50	1.50	1.50	2	0	0	0	0.79	0.00	7600	*	*	86	*
8-8-XC2-1.5	UT	54	1.00	0.0838	10.25	27.50	25.50	1.50	1.50	1.50	2	0.5	3	2	0.79	0.20	7600	*	*	122	*
8-5-OC0-1.5	UT	47	1.00	0.0838	10.25	27.50	25.50	1.59	1.46	1.50	2	0	0	0	0.79	0.00	5000	*	*	74	*
8-5-OC2-1.5	UT	47	1.00	0.0838	10.25	27.50	25.50	1.65	1.38	1.50	2	0.5	9	2	0.79	0.20	5000	*	*	141	*
8-5-XC0-1.5	UT	62	1.00	0.0838	10.25	27.50	25.50	1.50	1.50	1.50	2	0	0	0	0.79	0.00	4700	*	*	82	*
8-5-XC2-1.5	UT	62	1.00	0.0838	10.25	27.50	25.50	1.60	1.38	1.50	2	0.5	9	2	0.79	0.20	4700	*	*	148	*
11-5-OC0-3	UT	50	1.41	0.0797	18.13	31.50	28.05	3.25	2.88	2.75	2	0	0	0	1.56	0.00	5000	*	*	75	*
11-5-OC1-3	UT	50	1.41	0.0797	18.13	31.25	27.80	3.25	3.00	2.75	2	0.5	6	2	1.56	0.20	5000	*	*	104	*
11-5-OC2-3	UT	50	1.41	0.0797	18.13	31.25	27.80	3.25	3.00	2.75	2	0.5	12	2	1.56	0.20	5000	*	*	128	*
11-5-XC0-3	UT	67	1.41	0.0797	18.38	31.25	27.80	3.13	2.94	2.75	2	0	0	0	1.56	0.00	5400	*	*	84	*
11-5-XC1-3	UT	67	1.41	0.0797	18.25	31.25	27.80	3.13	2.94	2.75	2	0.5	6	2	1.56	0.20	5400	*	*	117	*
11-5-XC2-3	UT	67	1.41	0.0797	18.33	31.25	27.80	3.13	2.94	2.75	2	0.5	12	2	1.56	0.20	5400	*	*	141	*
5-5-OC0-3.4	UT	33	0.625	0.0767	13.00	12.00	10.94	1.00	1.00	0.75	4	0	0	0	0.31	0.00	5200	*	*	80	*
5-5-OC1-2.5	UT	18	0.625	0.0767	35.00	12.50	10.94	3.50	3.75	1.25	4	0	0	0	0.31	0.00	5200	*	*	91	*
5-5-OC2-1.25	UT	25	0.625	0.0767	35.00	12.25	10.69	3.50	3.75	1.25	4	0	0	0	0.31	0.00	5200	*	*	88	*
5-5-OC0-2	UT	15	0.625	0.0767	35.00	12.25	9.94	3.50	3.75	2.00	4	0	0	0	0.31	0.00	5700	*	*	110	*
5-5-XC0-2	UT	20	0.625	0.0767	35.00	12.25	9.94	3.50	3.75	2.00	4	0	0	0	0.31	0.00	5700	*	*	97	*
5-5-XC0-2	UT	20	0.625	0.0767	35.00	12.25	9.94	3.50	3.75	2.00	4	0	0	0	0.31	0.00	5700	*	*	120	*

Table A-1: Splice details for specimens tested at the University of Texas

TEST #	School	l_s in.	d_b in.	R_r	b^t in.	h^t in.	d^t in.	c_{so} in.	c_{sl} in.	c_b in.	N_b	d_{tr} in.	N_s	N_l	A_b in. ²	A_s in. ²	f_c psi	f_y ksi	f_{yt} ksi	f_{sc} ksi	f_{su} ksi
8-5-OC0-2.5	NCSU	31	1.00	0.0838	14	24	21.0	2.50	2.50	2.50	2	0	0	0	0.79	0.00	6000	*	*	95	*
8-5-OC2-2.5	NCSU	31	1.00	0.0838	14	24	21.0	2.50	2.50	2.50	2	0.5	8	2	0.79	0.20	6000	*	*	142	*
8-5-XC0-2.5	NCSU	41	1.00	0.0838	14	24	21.0	2.50	2.50	2.50	2	0	0	0	0.79	0.00	5800	*	*	107	*
8-8-OC0-1.5	NCSU	40	1.00	0.0838	10	24	22.0	1.50	1.50	1.50	2	0	0	0	0.79	0.00	8400	*	*	90	*
8-8-OC2-1.5	NCSU	40	1.00	0.0838	10	24	22.0	1.50	1.50	1.50	2	0.5	5	2	0.79	0.20	8400	*	*	151	*
8-8-XC0-1.5	NCSU	54	1.00	0.0838	10	24	22.0	1.50	1.50	1.50	2	0	0	0	0.79	0.00	10200	*	*	108	*
8-8-XC2-1.5	NCSU	54	1.00	0.0838	10	24	22.0	1.50	1.50	1.50	2	0.5	7	2	0.79	0.20	10200	*	*	151	*
11-8-OC0-3	NCSU	43	1.41	0.0797	18	24	20.3	3.00	3.00	3.00	2	0	0	0	1.56	0.00	6070	*	*	78	*
11-8-OC2-3	NCSU	43	1.41	0.0797	18	24	20.3	3.00	3.00	3.00	2	0.5	8	2	1.56	0.20	6070	*	*	116	*
11-8-XC0-3	NCSU	57	1.41	0.0797	18	24	20.3	3.00	3.00	3.00	2	0	0	0	1.56	0.00	8383	*	*	96	*
11-8-XC2-3	NCSU	57	1.41	0.0797	18	24	20.3	3.00	3.00	3.00	2	0.5	8	2	1.56	0.20	8383	*	*	128	*
11-5-OC0-2	NCSU	69	1.41	0.0797	14	36	33.3	2.00	2.00	2.00	2	0	0	0	1.56	0.00	5344	*	*	74	*
11-5-OC2-2	NCSU	69	1.41	0.0797	14	36	33.3	2.00	2.00	2.00	2	0.5	11	2	1.56	0.20	5344	*	*	132	*
11-5-OC3-2	NCSU	69	1.41	0.0797	14	36	33.3	2.00	2.00	2.00	2	0.5	23	2	1.56	0.20	5344	*	*	151	*
11-5-XC0-2	NCSU	91	1.41	0.0797	14	36	33.3	2.00	2.00	2.00	2	0	0	0	1.56	0.00	4058	*	*	72	*
11-5-XC2-2	NCSU	91	1.41	0.0797	14	36	33.3	2.00	2.00	2.00	2	0.5	11	2	1.56	0.20	4058	*	*	127	*
11-5-XC3-2	NCSU	91	1.41	0.0797	14	36	33.3	2.00	2.00	2.00	2	0.5	23	2	1.56	0.20	4058	*	*	155	*
8-5-OC0-1.5	KU	47	1.00	0.0838	14	30	28.1	1.48	3.60	1.40	2	0	0	0	0.79	0.00	5940	*	*	77	*
8-5-XC0-1.5	KU	63	1.00	0.0838	14	30	28.1	1.41	3.69	1.41	2	0	0	0	0.79	0.00	5940	*	*	89	*
8-5-OC2-1.5	KU	47	1.00	0.0838	14	30	28.1	1.40	3.58	1.40	2	0.5	8	2	0.79	0.20	6950	*	*	126	*

Table A-2: Splice details for specimens tested at North Carolina State University and the University of Kansas

Cross-section, reinforcement, and failure load details for specimens tested at the University of Texas are listed in Table A-3. In this table, c_t represents the clear cover above the compression reinforcement.

Specimen	f'_c (psi)	b (in)	h (in)	Spliced Tension Reinforcement			Compression Reinforcement			Failure Load (kip/ram)	Failure Stress (ksi)
				Bar Size (U.S.)	# of Bars	c_b (in)	Bar Size (U.S.)	# of Bars	c_t (in)		
8-8-OC0-1.5	8300	10.25	22.38	8	2	1.50	8	2	3.00	39.1	80
8-8-OC1-1.5	8300	10.13	23.25	8	2	1.50	8	2	3.00	63.0	123
8-8-OC2-1.5	8300	10.13	23.25	8	2	1.50	8	2	3.00	75.4	147
8-5-OC0*-1.5	5200	10.25	27.50	8	2	1.50	8	2	3.00	44.1	72
8-5-OC1*-1.5	5200	10.25	27.50	8	2	1.50	8	2	3.00	60.6	99
8-5-OC2*-1.5	5200	10.25	27.50	8	2	1.50	8	2	3.00	78.8	129
8-8-XC0-1.5	7800	10.25	27.50	8	2	1.50	8	2	3.00	53.0	86
8-8-XC1-1.5	7800	10.25	27.50	8	2	1.50	8	2	3.00	75.2	122
8-8-XC2-1.5	7800	10.25	27.50	8	2	1.50	8	2	3.00	89.5	144
8-5-OC0-1.5	5000	10.25	27.50	8	2	1.50	8	2	3.00	45.2	74
8-5-OC2-1.5	5000	10.25	27.50	8	2	1.50	8	2	3.00	85.9	141
8-5-XC0-1.5	4700	10.25	27.50	8	2	1.50	8	2	2.25	50.2	82
8-5-XC2-1.5	4700	10.25	27.50	8	2	1.50	8	2	2.25	92.2	148
11-5-OC0-3	5000	18.13	31.50	11	2	2.75	11	2	2.75	83.3	75
11-5-OC1-3	5000	18.13	31.25	11	2	2.75	11	2	2.75	115.0	104
11-5-OC2-3	5000	18.13	31.25	11	2	2.75	11	2	2.75	140.9	128
11-5-XC0-3	5400	18.38	31.25	11	2	2.75	11	2	2.75	92.2	84
11-5-XC1-3	5400	18.25	31.25	11	2	2.75	11	2	2.75	128.0	117
11-5-XC2-3	5400	18.33	31.25	11	2	2.75	11	2	2.75	154.6	141
5-5-OC0-3/4	5200	13.00	12.00	5	4	0.75	5	2	0.88	23.2	80
5-5-XC0-3/4	5200	13.00	12.00	5	4	0.75	5	2	1.50	26.0	91
5-5-OC0-1.25	5200	35.00	12.50	5	4	1.25	5	4	2.00	26.6	88
5-5-XC0-1.25	5200	35.00	12.25	5	4	1.25	5	4	2.00	32.5	110
5-5-OC0-2	5700	35.00	12.25	5	4	2.00	5	4	1.38	26.2	97
5-5-XC0-2	5700	35.00	12.25	5	4	2.00	5	4	1.50	32.8	120

Table A-3: Cross-section, reinforcement, and failure load details for specimens tested at the University of Texas

REFERENCES

- AASHTO, 2007, "AASHTO LRFD Bridge Design Specifications: Customary Units," 4th Ed., American Association of State Highway and Transportation Officials, Washington, D.C., 1518 pp.
- Ahlborn, T. and DenHartigh, T., 2002, "A Comparative Bond Study of MMFX Reinforcing Steel in Concrete," *Final Report*, CSD-2002-03, Michigan Technological University, Center for Structural Durability, Houghton, M.I., July, 24 pp.
- ACI Committee 318, 2005, "Building Code Requirements for Reinforced Concrete (ACI 318-05) and Commentary (ACI 318R-05)," American Concrete Institute, Farmington Hills, Mich., 430 pp.
- ACI Committee 408, 2003, "Bond and Development of Straight Reinforcing Bars in Tension (ACI 408R-03)," American Concrete Institute, Farmington Hills, Mich., 49 pp.
- ASTM C 39-04a, 2004, "Standard Method of Test for Compressive Strength of Cylindrical Concrete Specimens," ASTM International, West Conshohocken, Pa., 14 pp.
- Azizinamini, A.; Chisas, M.; and Ghosh, S. K., 1995, "Tension Development Length of Reinforcing Bars Embedded in High-Strength Concrete," *Engineering Structures*, V. 17, No. 7, pp. 512-522.
- Azizinamini, A.; Stark, M.; Roller, J. J.; and Ghosh, S. K., 1993, "Bond Performance of Reinforcing Bars Embedded in High-Strength Concrete," *ACI Structural Journal*, V. 90, No. 5, Sept.-Oct., pp. 554-561.
- Darwin, D.; Tholen, M. L.; Idun, E. K.; and Zuo, J., 1996a, "Splice Strength of High Relative Rib Area Reinforcing Bars," *ACI Structural Journal*, V. 93, No. 1, Jan.-Feb., pp. 95-107.
- Darwin, D.; Zuo, J.; Tholen, M. L.; and Idun, E. K., 1996b, "Development Length Criteria for Conventional and High Relative Rib Area Reinforcing Bars," *ACI Structural Journal*, V. 93, No. 3, May-June, pp. 347-359.
- Dawood, M.; Seliem, H.; Hassan, T.; and Rizkalla, S., 2004, "Design Guidelines for Concrete Beams Reinforced with MMFX Microcomposite Reinforcing Bars," *Proceedings of the International Conference on Future Vision and Challenges for Urban Development*, Cairo, Egypt, Dec. 20-22., 12 pp.

- Donnelly, K., 2007, "Behavior of Minimum Length Splices of High-Strength Reinforcement," *Thesis*, University of Texas, Dept. of Civil, Architectural, and Environmental Engineering, Austin, T.X.
- El-Hacha, R.; El-Agroudy, H.; and Rizkalla, S. H., 2006, "Bond Characteristics of High-Strength Steel Reinforcement," *ACI Structural Journal*, V. 103, No. 6, Nov.-Dec., pp. 771-782.
- El-Hacha, R and Rizkalla, S. H., 2002, "Fundamental Material Properties of MMFX Steel Bars," *Research Report*, RD-02/04, North Carolina State University, Constructed Facilities Laboratory, Raleigh, N.C., July, 62 pp.
- Esfahani, M. R. and Rangan, B. J., 1998, "Local Bond Strength of Reinforcing Bars in Normal Strength and High-Strength Concrete (HSC)," *ACI Structural Journal*, V. 95, No. 2, Mar.-Apr., pp. 96-106.
- Gergely, P. and Lutz, L. A., 1968, "Maximum Crack Width in Reinforced Concrete Members," *Causes, Mechanisms, and Control of Cracking in Concrete*, SP-20, American Concrete Institute, Farmington Hills, M.I., pp. 87-117.
- Hamad, B. S., and Itani, M. S., 1998, "Bond Strength of Reinforcement in High-Performance Concrete: The Role of Silica Fume, Casting Position, and Superplasticizer Dosage," *ACI Materials Journal*, V. 95, No. 5, Sept.-Oct., pp. 499-511.
- Maeda, M.; Otani, S.; and Aoyama, H., 1991, "Bond Splitting Strength in Reinforced Concrete Members," *Transactions of the Japan Concrete Institute*, V. 13, pp. 581-588.
- Mathey, R., and Watstein, D., 1961, "Investigation of Bond in Beam and Pull-Out Specimens with High-Yield-Strength Deformed Bars," *ACI JOURNAL, Proceedings* V. 57, No. 9, Mar., pp 1071-1090.
- MMFX Steel Corporation of America, 2004, *MMFX 2 Rebar – Product Guide Specification*, Charlotte, N.C. 10 pp.
- Orangun, C. O.; Jirsa, J. O.; and Breen, J. E., 1977, "Reevaluation of Test Data on Development Length and Splices," *ACI JOURNAL, Proceedings* V. 74, No. 3, Mar., pp. 114-122.
- Pay, A. C., 2005, "Bond Behavior of Unconfined Steel and Fiber Reinforced Polymer (FRP) Bar Splices in Concrete Beams," *Dissertation*, Purdue University, West Lafayette, I.N., Dec., 336 pp.

Sakurada, T.; Morohashi, N.; and Tanaka, R., 1993, "Effect of Transverse Reinforcement on Bond Splitting Strength of Lap Splices," *Transactions of the Japan Concrete Institute*, V. 15, pp. 573-580.

Zuo, J., and Darwin, D., 2000, "Splice Strength of Conventional and High Relative Rib Area Bars in Normal and High-Strength Concrete," *ACI Structural Journal*, V. 97, No. 4, July-Aug., pp 630-641.

VITA

Gregory Michael Glass, son of Larry Thomas Glass and Angela Battaglini Glass, was born in Panama City, Florida on February 12, 1983. Greg completed his high school education at Charlotte Catholic High School in Charlotte, North Carolina in June of 2001; and he entered Princeton University in September of the same year. He received a Bachelor of Science in Engineering in Civil and Environmental Engineering in May of 2005 from Princeton University. In August of 2005, Greg entered the Graduate School at the University of Texas at Austin to pursue a Master of Science in Engineering in Civil Engineering.

Permanent Address: 4901 Truscott Road
Charlotte, N.C. 28226

This thesis was typed by the author.